REPUBLIQUE ALGERIENNE DEMOGRATIQUE ET POPULAIRE
Ministère de l'Enseignement Supérieur et de la Recherche Scientifique
Université Abdelhamid Ibn Badis de Mostaganem
Faculté des Sciences et de la Technologie
Département de Génie Civil

THESE

Présentée en vue de l'obtention du diplôme de doctorat LMD

Spécialité : Génie civil

Option : Structures

PAR

BENNACEUR Djihad

Effets des propriétés physiques du sol sur le transfert d'énergie géothermique

Effects of soil physical properties on geothermal energy transfer

Soutenue le 22/06/2025 devant le jury composé de

Pr. BELAS Nadia	Présidente	UMAB Mostaganem
Pr. ARAB Ahmed	Examinateur	Univ. Hassiba Benbouali de Chlef
Pr. DELLA Noureddine	Examinateur	Univ. Hassiba Benbouali de Chlef
Pr. MEBROUKI Abdelkader	Examinateur	UMAB Mostaganem
Pr. LAREDJ Nadia	Directrice de thèse	UMAB Mostaganem
Pr. MISSOUM Hanifi	Co-directeur de thèse	UMAB Mostaganem

ANNÉE UNIVERSITAIRE: 2024/2025

Acknowledgment

Louanges à Allah, le Tout Miséricordieux, le Très Miséricordieux, qui m'a accordé la force et la patience nécessaires pour mener à bien cette thèse.

Je tiens à exprimer ma profonde gratitude à **Pr. LAREDJ Nadia**, ma directrice de thèse, ainsi qu'à **Pr. MISSOUM Hanifi**, mon co-directeur de thèse, pour leur encadrement rigoureux, leur disponibilité et leurs précieux conseils tout au long de ces années de recherche. Leur expertise et leurs encouragements ont été des piliers essentiels dans l'accomplissement de ce travail.

J'adresse mes sincères remerciements aux membres du jury pour l'honneur qu'ils me font en acceptant d'évaluer mon travail :

Pr. BELAS Nadia, présidente du jury, pour l'intérêt porté à cette recherche et les précieuses remarques qui contribueront à son enrichissement.

Pr. ARAB Ahmed, **Pr. DELLA Noureddine** et **Pr. MEBROUKI Abdelkader**, examinateurs, pour le temps consacré à l'évaluation de cette thèse, leurs critiques constructives et leur expertise qui me permettront d'améliorer ce travail.

Je tiens également à remercier chaleureusement **Pr. MALIKI Mustapha** pour son aide précieuse dans la simulation de ma thèse. Son expertise et sa disponibilité ont été d'une grande aide dans l'aboutissement de ce travail.

Un immense merci à mes collègues et amis, **Madame MOSTEFA Fouzia, Monsieur MEHELA Tewfik, Monsieur MEKAIDECHE Khalfallah et Monsieur Mahi Eddine Brahimi**, pour leur soutien moral indéfectible tout au long de cette aventure. Leur bienveillance et leur encouragement m'ont été d'un grand réconfort dans les moments de doute et de fatigue.

Enfin, **je remercie du fond du cœur ma famille**, qui a toujours été présente à mes côtés. Je tiens à exprimer ma profonde reconnaissance **à ma mère, mon père, ma sœur, et mes deux frères**, dont le soutien inébranlable m'a portée tout au long de ce parcours. Un remerciement tout particulier à **mon mari**, qui a été mon plus grand appui moral, toujours là pour m'encourager, me motiver et me donner la force d'avancer, même dans les moments les plus difficiles.

Summary

Figures list

Chapter I

Chapter II

Chapter III

Chapter IV

Chapter V

Table list

Chapter I

Chapter II

Chapter III

Chapter IV

Chapter V

List of Symbols

Symbols	Name
R_n	Net radiation, W/m^2
H	Sensible heat flux, W/m^2
G	Ground heat transfer, W/m^2
R_s	Shortwave radiation, W/m^2
E	Evapotranspiration rate
L	Latent heat of vaporization of water, J/kg
LE	Latent heat flux, W/m^2
a_l	The surface albedo
R_a	Longwave radiation, W/m^2
σ	Stefan-Boltzman constant, Wm^{-2}K^{-4}
ε	Emissivity of the surface
G_{SC}	The solar constant, 1367 W/m^2
dr	The relative distance between the Earth and the Sun
ω_S	The angle corresponding to sunset time
φ	Latitude, rad
δ_s	Solar declination, rad
T_{max}	Maximum temperature, K
T_{min}	Minimum temperature, K
T_a	Ambient temperature, K
T_s	Soil temperature, K
k_{Rs}	The correction coefficient, 0.18
r_a	The aerodynamic heat resistance, s/m
U_{Wind}	The wind speed at the elevation Z_m, m/s
h_c	The vegetation height ,m
Z_m	The height where the meteorological parameters are measured, m
Z_{om}	The roughness length for momentum transfer, m
Z_{oh}	The roughness length for vapor transfer, m
K	The von Karman constant
P	The precipitation rate, mm/s
E_P	The evaporation potential, mm/s
Δ	The rate of change of the saturation vapor pressure curve, kpa/K
e_s	The saturation vapor pressure, kpa
e_a	The actual vapor pressure, kpa

δ	The psychrometric constant, kpa/K
r_c	The canopy resistance, s/m
P_{at}	Atmospheric pressure, Pa
r_{mw}	The molecular weight of water vapor relative to dry air
r_l	The stomatal resistance of a single leaf, s/m
LAI	The leaf area index
$C(h)$	The specific moisture capacity
h	The suction head, m
$K(h)$	The unsaturated hydraulic conductivity, m/s
K_s	The saturation hydraulic conductivity, m/s
S_e	The effective degree of saturation
θ	The volumetric soil water content, m^3/m^3
θ_r	The residual water contents, m^3/m^3
θ_s	The saturated water contents, m^3/m^3
α	Van Genuchten empirical shape parameter, m^{-1}
$n_1 - m$ - l	Van Genuchten empirical shape parameter
ρ_s	The soil density, kg/m^3
ρ_w	The water density, kg/m^3
ρ_d	The soil dry density, kg/m^3
ρ_a	The density of the air, kg/m^3
$c_{p\text{-}w}$	The specific heat capacity of water, $Jkg^{-1}K^{-1}$
$c_{p\text{-}s}$	The specific heat capacity of soil, $Jkg^{-1}K^{-1}$
$c_{p\text{-}a}$	The specific heat capacity of the air, $Jkg^{-1}K^{-1}$
u_w	The soil water velocity, m/s
k_s	The soil thermal conductivity, $Wm^{-1}K^{-1}$
C_v	The soil volumetric heat capacity, Jm^3K^1
Q_s	The soil heat source, W/m^3

Abstract

Geothermal energy is a promising renewable resource, but its efficiency depends on the thermal properties of the soil. This study examines heat transfer in unsaturated soils, focusing on soil type, porosity, density, and salinity, using a numerical hydrothermal model for the Oran and Adrar regions of Algeria. The results show that clay-rich soils with low porosity and high density retain heat better, making them ideal for geothermal applications. Salinity also plays a role, with moderate salinity (C = 0.1 M) improving thermal performance in sandy soils, while higher salinity (C = 0.2 M) enhances heat retention in sandy loam.

Another key finding is that soil temperature stabilizes at shallow depths (~8m), except when an external heat source is present. These observations are crucial for geothermal transfer, as selecting the ideal soil characteristics can increase the effectiveness of heat extraction. Future research should refine numerical models for heat exchangers, incorporate water vapor transport into heat transfer simulations, and validate findings with experimental data. This study provides valuable guidance for optimizing geothermal energy systems, with practical applications in renewable energy, climate adaptation, and sustainable construction.

Keywords

Geothermal energy, heat transfer, soil-atmosphere interaction, thermal conductivity, porosity, salinity.

Résumé

L'énergie géothermique est une ressource renouvelable prometteuse, mais son efficacité dépend des propriétés thermiques du sol. Cette étude examine le transfert de chaleur dans les sols non saturés, en se concentrant sur le type de sol, la porosité, la densité et la salinité, en utilisant un modèle hydrothermique numérique pour les régions d'Oran et d'Adrar en Algérie. Les résultats montrent que les sols riches en argile ayant une faible porosité et une densité élevée retiennent mieux la chaleur, ce qui les rend idéaux pour les applications géothermiques. La salinité joue également un rôle majeur, une salinité modérée (C = 0,1 M) améliore la performance thermique des sols sableux, tandis qu'une salinité plus élevée (C = 0,2 M) améliore la rétention de la chaleur dans les sablo-limoneux.

Une autre observation notable est que la température du sol s'équilibre à une faible profondeur (~8m), à moins qu'il n'y ait une source de chaleur extérieure. Ces observations sont cruciales pour le transfert géothermique, car le choix des propriétés idéales du sol peut augmenter l'efficacité de l'extraction de la chaleur. Les futures recherches devraient affiner les modèles numériques pour les échangeurs de chaleur, intégrer le transfert de vapeur d'eau dans les simulations du transfert de chaleur et valider les résultats avec des données expérimentales. Cette recherche offre des orientations utiles pour l'optimisation des systèmes géothermiques, avec des mises en œuvre concrètes dans les secteurs de l'énergie renouvelable, de l'adaptation climatique et de l'habitat durable.

Mots-clés

Énergie géothermique, transfert de chaleur, interaction sol-atmosphère, conductivité thermique, porosité, salinité.

ملخص

تُعد الطاقة الحرارية الأرضية موردًا متجددًا واعدًا، لكن كفاءتها تعتمد على الخصائص الحرارية للتربة. تبحث هذه الدراسة في انتقال الحرارة في التربة غير المشبعة، مع التركيز على نوع التربة ومساميتها وكثافتها وملوحتها، باستخدام نموذج عددي حراري مائي لمنطقتي وهران وأدرار في الجزائر. أظهرت النتائج أن التربة الطينية الغنية بالطين ذات المسامية المنخفضة والكثافة العالية تحتفظ بالحرارة بشكل أفضل، مما يجعلها مثالية لتطبيقات الطاقة الحرارية الأرضية. تلعب الملوحة دورا هاما حيت الملوحة المعتدلة ذات تركيز 0.1م تعمل على تحسين الأداء الحراري للتربة الرملية بينما الملوحة العالية ذات تركيز 0.2م تعمل على احتباس الحرارة في التربة الطينية.

ومن النتائج الرئيسية الأخرى أن درجة حرارة التربة تستقر عند عمق سطحي (حوالي 8 أمتار)، إلا في حالة وجود مصدر حراري خارجي. وتعتبر هذه الملاحظات حاسمة بالنسبة لنقل الطاقة الحرارية الأرضية، حيث أن اختيار خصائص التربة المثالية يمكن أن يزيد من فعالية استخلاص الحرارة. يجب أن تعمل الأبحاث المستقبلية على تحسين النماذج العددية للمبادلات الحرارية، ودمج نقل بخار الماء في عمليات محاكاة نقل الحرارة، والتحقق من صحة النتائج مع البيانات التجريبية. توفر هذه الدراسة إرشادات قيمة لتحسين أنظمة الطاقة الحرارية الأرضية، مع تطبيقات عملية في مجال الطاقة المتجددة والتكيف مع المناخ والبناء المستدام.

الكلمات المفتاحية

الطاقة الحرارية الأرضية، انتقال الحرارة، التفاعل بين التربة والغلاف الجوي، الناقلية الحرارية، المسامية، الملوحة.

Introduction

Energy is necessary for human activities, including economic and social development, since society development depends on the growing fulfillment of numerous needs, including food, education, housing, recreation, health, and transportation. However, most of the energy resources are from fossil fuels, with finite reserves and hence being depletable. The global energy situation has serious issues like affordability, energy security, and reducing carbon emissions. The crisis in Ukraine has pushed the issue of the depletion of fossil fuels to the center stage [1]. Rising living standards, industrialization, and a growing population are driving energy demand to historic highs [2]. The International Energy Agency projects that worldwide energy demand will increase by 50% by 2050 [3]. Despite the COVID-19 epidemic temporarily decreasing demand, the IEA predicts it will recover by 2023 [4].

Algeria's building sector is energy intensive. According to the National Agency for the Promotion and Rationalization of the Use of Energy (APRUE), it consumes 41% of total energy, surpassing agriculture with 33%, industry with 19%, and transportation with 7% [5]. Since gaining independence, Algeria has prioritized the development of its energy sector, leveraging its significant fossil fuel resources. By 2015, the country ranked as the 18th-largest oil producer, the 10th-largest natural gas producer, and the 6th-largest gas exporter globally. The hydrocarbon sector remains the backbone of Algeria's economy, contributing over 96% of export revenues, 30% of GDP, and 60% of budget revenues. However, rising domestic energy demand, the risk of resource depletion, and global warming concerns have brought to the fore the need to diversify energy sources [6]. These interconnected problems highlight the pressing need for innovative and sustainable energy strategies, including a substantial shift towards renewable energy sources, in order to secure a cleaner, more resilient energy future. Furthermore, the increasing demand in energy is placing a great deal of strain on the world's energy resources, many of which are nonrenewable and harmful to the environment.

Renewable energy offers promising solutions. This type of energy comes from natural resources that regenerate at a faster rate than they are consumed. These sources include solar, wind, hydro, geothermal and biomass (wood, biofuels, etc.). Geothermal energy is a promising and environmentally friendly energy source, harnessing natural heat from Earth's layered structure. The Earth's magmatic layer below the crust generates most heat, which is transported to the surface through crustal plate movement. Geothermal energy can be used for electricity, cooling, heating, or industrial processes, often in high geothermal activity areas.

Geothermal energy represents a promising source of renewable energy for Algeria, although it is still under-exploited. Algeria has vast geothermal potential, with over 200 thermal springs distributed mainly in the north of the country, including six major geothermal regions. Research was conducted to assess the geothermal potential in southern Algeria [7]. It evaluates the resources available in the Sahara region, particularly in sedimentary basins of stable continental zones. The research creates detailed maps of geothermal gradients and heat flow across different areas, identifying two distinct geothermal zones. In order to promote the growth of geothermal energy as a renewable resource in Algeria and Egypt, another study [8] intends to present a thorough analysis of geothermal resources in North Africa. Other researchers [9] have investigated Algeria's geothermal energy potential as a renewable energy source, emphasizing how crucial geophysics is to comprehend and utilize these resources. Additionally, others [10] sought to suggest useful uses for geothermal energy, like district heating and greenhouse heating using low-energy geothermal methods, especially through the Eastern Sahara's Continental Intercalative aquifer.

Despite the efforts of many researchers, very little research has been done on geothermal transfer in unsaturated soils. The purpose of this study is to understand how different soil properties affect geothermal energy transfer and how we can use this knowledge to improve energy efficiency. Since soil plays a key role in storing and transferring heat, this research looks at how factors like soil layers, type, salinity, porosity, and density influence its ability to retain and transfer heat. By studying these aspects, we can better understand how heat flows through the ground and how soil conditions impact geothermal energy systems. This knowledge is especially useful for optimizing renewable energy applications, improving thermal management in construction, and even helping with climate modeling.

This study is subdivided into five chapters, the first chapter introduces geothermal energy as an environmental and sustainable resource aimed at various applications, including heating, electricity generation, and hot water production. Comparison with fossil fuels highlights its advantages, such as environmental and economic worthiness. Still, the disadvantages of high initial investment and the necessity of complete expertise are other additional challenges that have been alluded to. With proper infrastructure development, professional capacity enhancement, and extensive geothermal exploration, Algeria's under-exploited geothermal resources can be central to the country's energy diversification strategy.

The second chapter explores a description and classification of soils. Particular focus is placed on unsaturated soils and how they affect geothermal performance. Furthermore, it provides a

detailed explanation of the physical properties that can affect geothermal transfer. In addition, a detailed section is deduced to the thermal properties, including thermal conductivity, diffusivity, and volumetric heat capacity. Another section provides the influence of physical properties on the thermal ones. The chapter also includes theoretical equations and a literature review to understand past research in this area comprehensively.

The Third chapter provides a comprehensive description of heat transfer phenomena. It explains the fundamental concepts of thermal energy, heat and temperature, with a special focus on the temperature gradient's role in causing heat flow. The governing equation, founded on the conservation principle, were presented to consider thermal and hydraulic transfer in the soil. Empirical models, such as the Richards equation and the van Genuchten-Mualem model, were also introduced to facilitate numerical analysis of moisture transport in unsaturated soils.

The fourth chapter explores the soil-atmospheric interactions and their impact on heat and moisture transfer. It addresses critical heat fluxes such as net radiation, sensible, latent and ground heat fluxes and the governing equation of the moisture heat and solute transfer under unsaturated soils. The meteorological data and the parameter chosen for this study are widely discussed. The chapter ended by a numerical modelling strategy to simulate hydric and thermal behavior of the soil to determine the soil temperature and the Fluxes of the soil-atmospheric interactions, furthermore a validation of the model is provided for the reliability and applicability to real-life conditions.

Finally, the fifth chapter explores the results obtained from the numerical model applied to the four aspects of the research, including the influence of multilayer soil, soil type, salinity, and selected physical properties. This chapter offers a detailed discussion of the results and draws conclusions on the use of geothermal energy in Algeria, taking into account the factors analyzed in the four previous sections.

Chapter I

Geothermal Energy

I.1. Introduction

The global energy landscape is at a critical juncture, facing profound challenges and uncertainties, intensified by the war in Ukraine. This conflict has brought attention to important issues like affordability, energy security, and the urgent need to reduce carbon emissions [1]. Progress has been slow, and carbon emissions are still rising, even though reaching the Paris climate goals calls for swift and decisive action to speed up decarbonization. The urgency of this situation is further underscored by the fact that fossil fuels, especially oil and gas, are becoming less and less available; estimates suggest there will be less than 60 years of viable reserves, barring the discovery of new deposits [11].

Meanwhile, rising living standards, industrialization, and population growth are pushing energy demand to previously unheard-of heights [2]. Global energy needs could increase by about 50% by 2050 if current trends continue, according to the International Energy Agency (IEA) [3]. This projection aligns closely with the data presented in Figure I. 1, which illustrates the global population's historical and projected future growth and corresponding increases in total and per capita energy consumption.

Although the COVID-19 pandemic temporarily curbed energy consumption dropping global demand by 3.8% in early 2020 compared to the same period in 2019, the IEA expects demand to rebound to pre-pandemic levels by 2023, assuming the virus was controlled by 2021 [4].

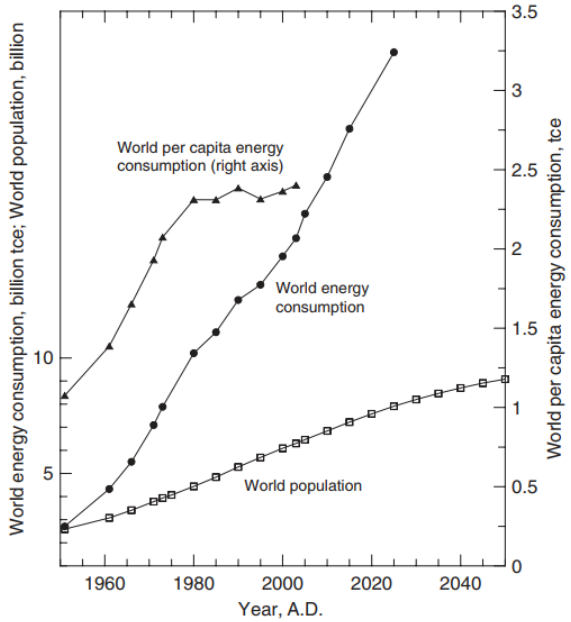

Figure I. 1. Evolution of world energy consumption, world population and per capita energy consumption (1940-2050) *[2]*

The global energy demand, mainly dominated by fossil fuels, has also raised concerns about sustainability and environmental degradation. Fossil fuels now account for over 80% of total energy consumption in 2023 and non-OECD countries alone are set to have their energy demand rise by 84% by 2035 [12]. The demand for alternative sources of energy has never been more urgent. Such a transition is very relevant to energy-intensive sectors such as Algeria's construction sector, which alone consumes 41% of the country's energy, beating agriculture with 33%, industry with 19% and transport with 7% [5].

In order to ensure a cleaner, more resilient energy future, these interrelated issues underline the urgent need for creative and sustainable energy strategies, including a significant shift towards renewable energy sources. Existing energy resources, many of which are non-renewable and detrimental to the environment, are under tremendous strain due to this growing demand. Renewable energy sources have become crucial substitutes to meet the expanding energy demands while addressing environmental issues. Renewable energy sources, including solar, wind, hydroelectric, and geothermal energy are naturally replenished and emit little to no greenhouse gases, in contrast to fossil fuels. Adopting them is essential to reducing the effects of climate change and moving toward a low-carbon future.

Among all the renewable sources, geothermal energy is the one chosen in this study, a renewable and sustainable energy source, harnesses the heat of the earth's interior. This natural resource is used to generate electricity, heat buildings, and, in a particularly innovative way, heat agricultural greenhouses. In agriculture, it is an efficient and environmentally friendly solution that not only improves crop production but also significantly reduces the carbon footprint, offering hope for a more sustainable future. A key element of geothermal systems is the heat exchanger, designed to transfer heat from the ground to the greenhouses with unparalleled efficiency. These geothermal heat exchangers are specifically engineered to maximize heat transfer efficiency and provide optimal temperature control within the greenhouse. Since nations are striving to balance economic progress with the conservation of environment, geothermal energy investment represents an appropriate approach to meeting the growing demand of energy while diminishing the impacts of climate change [13]. The working principles of geothermal energy are thoroughly examined in this chapter.

I.2. Geothermal Energy

Geothermal energy is one of the most promising and environmentally friendly forms of energy. Earth's layered structure includes a 30 km crust, 70 km mantle, and 3,400 km core radius (Figure

I. 2). A magmatic layer below the crust supplies most heat generated by radioactive decay. This heat is transported to the surface due to crustal plate movement, causing high temperature and pressure conditions. The lighter transported mantle moves upwards, heating rocks and water at 25°C/km. Earth has enough geothermal energy to last 4-5 billion years, with heat stored in the first 10 km of the Earth's surface.

Geothermal energy is the science and technique of harnessing natural heat from deep within the Earth to produce energy. This energy can be used as electricity through geothermal power plants or as heat for cooling, heating, or industrial processes. It is based on using the Earth's natural thermal gradients, often in areas of high geothermal activity, such as near volcanoes, hot springs, or geological faults.

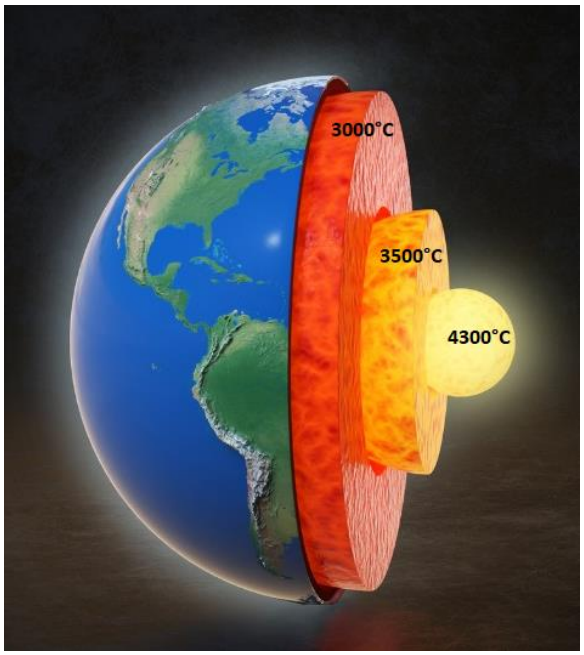

Figure I. 2. Earth's cross-section displaying terrestrial layers [14]

I.3. Geothermal gradient

The geothermal gradient refers to the rise in rock temperature with depth. Depending on the strata crossed, the gradient fluctuates. There are significant regional variations in the earth's crust's geothermal gradient. While the average temperature is about 3°C per 100 meters, some places, like Larderello (Italy) have temperatures above 100°C per 100 meters. In contrast, other areas, like Padua (Italy) have temperatures as low as 1°C per 100 meters [7]. Figure I. 3 shows an example of the geothermal gradient in the Gulf of Mexico basin, where the sediments are mainly swelling clays [2].

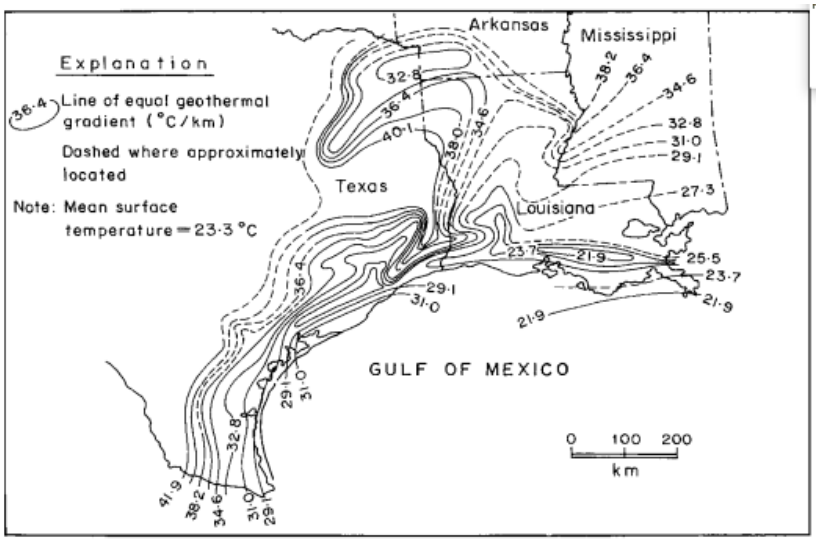

Figure I. 3. U.S. Gulf Coast Geothermal Gradients *[2]*

I.4. The Use of Geothermal Energy historically

I.4.1. Early Utilization of Geothermal Energy

- **Historical Use by Indigenous Peoples**

North American Indians utilized geothermal springs for therapeutic bathing and healing, with evidence of such practices dating back thousands of years. Hot springs in South Dakota were significant to tribes like the Sioux and Cheyenne.

- **Culinary Applications**

The Fishing Cone Geyser in Yellowstone Lake was used by fishermen to cook fish, showcasing practical uses of geothermal energy in food preparation.

- **Roman and Ancient Cultures**

The Romans widely utilized thermal springs for bathing and therapeutic purposes, developing spas around the natural features more than 2000 years ago. They believed in the water's healing powers.

- **Global Practices**

Other cultures also learned to use hot springs for cooking and bathing, including the Japanese, the Turks, and the Maori. These historical usages were not unique but common for many civilizations.

- **Modern Applications**

Today, geothermal energy is harnessed for heating and cooling, with heat pumps employed to utilize hot water from geothermal sources [15].

I.4.2. Early Developments

Geothermal energy began in the mid-19th century when thermodynamics advanced enough to convert hot steam into mechanical and electrical energy efficiently.

- **Larderello, Italy**

The Larderello region is pivotal in geothermal history, where the first geothermal energy conversion plant was established in 1827 by Francesco Larderel. This plant initially produced heat for boron extraction and later evolved into electrical power generation by 1904.

- **Expansion in Iceland**

In the 1920s, Reykjavik, Iceland, began large-scale geothermal heating, leading to the current situation where geothermal energy supplies 53% of the country's primary energy.

- **Global Growth**

Following Italy and Iceland, countries like New Zealand and the USA developed geothermal plants in the mid-20th century, the Geysers in California grew to be the world's most extensive geothermal installation.

- **Challenges and Setback**

Some installations in nations like Greece and Argentina have been shut down due to economic conditions and environmental regulations that have made geothermal energy less profitable.

- **Recent Developments**

Geothermal energy production in Germany increased in the early 2000s, indicating a renewed interest in renewable energy sources as fossil fuel prices fluctuated [15].

I.5. Application of geothermal energy

Geothermal energy can be used for various purposes depending on the subterranean reservoir's features. These reservoirs vary in temperature, depth, and geological context, enabling them to be adapted to specific needs, whether for power generation, heating, or other uses.

- Geothermal energy with high energy content is defined by temperatures above 150°C. The primary locations for this kind of deposit are seismic and volcanic areas near

tectonic plate borders. Its primary purpose is to produce electricity. To do this, steam from the geothermal reservoir is directed toward a turbine, which is then connected to an alternator.

- Geothermal energy with low energy uses temperatures ranging from 30°C to 150°C. These deposits are primarily found in large sedimentary basins and are typically found in permeable, water-filled formations at average depths of 1,000 to 2,500 meters. District heating and greenhouse heating are its primary applications.

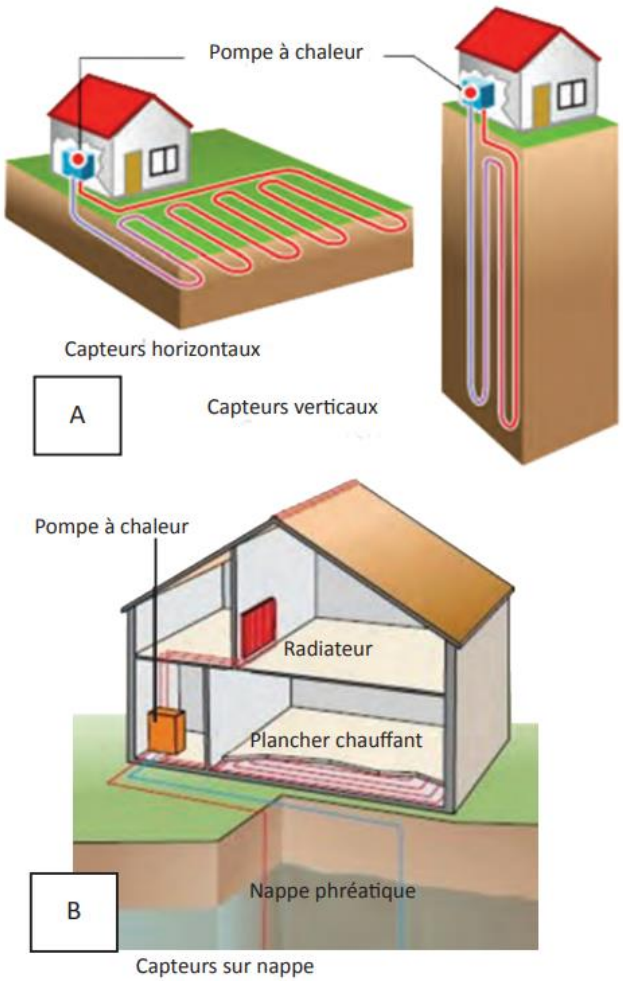

Figure I. 4. Very low-energy geothermal energy [16]

- Very low-energy geothermal energy is found at shallow depths, notably groundwater, where temperatures vary between 10°C and 30°C. Applications for it include horticulture, agricultural drying, fish farming and for the heating and the cooling of the buildings. Figure I. 4 illustrates two types of geothermal systems that heat buildings using a heat pump. In system A, horizontal collectors, installed at shallow depth, or vertical collectors, drilled at depth, capture heat from the ground. System B uses a water

table as a heat source, drawing thermal energy directly from the groundwater. In both systems, the heat pump will gather the heat from the collectors, raising the temperature and distributing it via radiators or underfloor heating, resulting in ideal thermal comfort while utilizing renewable energy.

- HDR (Hot Dry Rock) geothermal energy is a technology developed to exploit dry rock at depths (less than 6 km), such as granite. This technique injects cold water into boreholes or injection wells at high pressure. A production borehole allows the heat to be recovered after the water, which has been heated by contact with the rock, rises to the surface [17].

From industrial energy production to home heating and cooling, Figure I. 5 depicts the applications for each level.

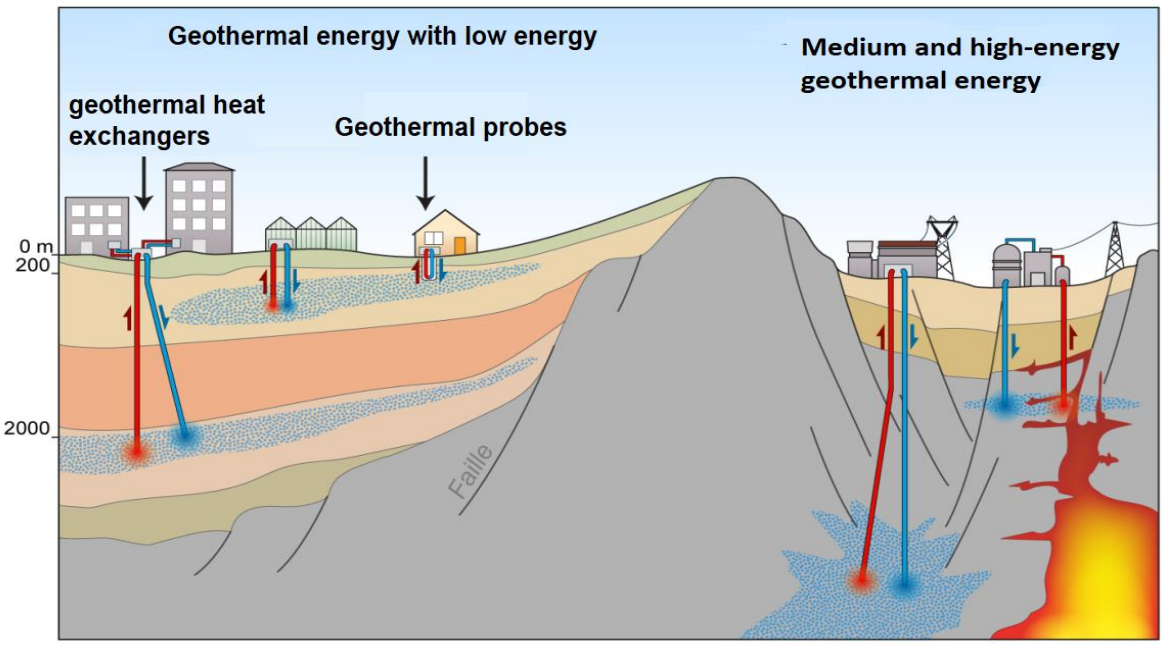

Figure I. 5. Types of geothermal energy and their applications [18]

The Lindal diagram, introduced by Icelandic engineer Baldur Lindal [19], illustrates the temperature ranges suitable for various direct-use applications as mentioned in Figure I. 6. Agricultural and aquacultural activities typically require the lowest temperatures, ranging from 25°C to 90°C, but issues such as arsenic contamination and dissolved gases like boron often necessitate the use of heat exchangers to protect plants and animals. Space heating commonly operates between 50°C to 100°C, though temperatures as low as 40°C may suffice in marginal cases, with ground-source heat pumps extending usability down to 4°C. Cooling systems and industrial processes generally demand temperatures exceeding 100°C.

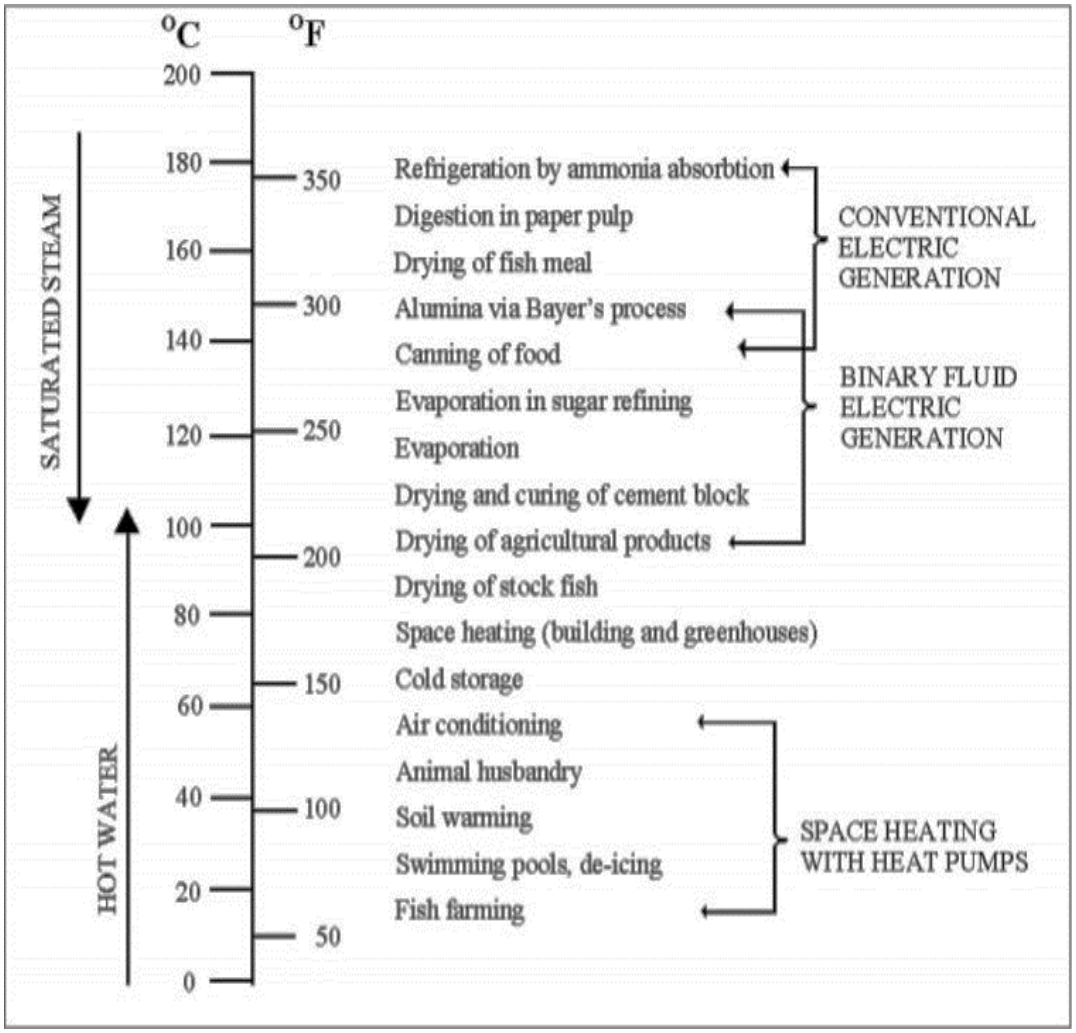

Figure I. 6. Lindal Diagram *[19]*

The various thermal regeneration techniques are shown in Figure I.7, separated into two primary groups: artificial and enhanced natural regeneration. The first category includes cooling methods like fluid coolers, cooling towers, cooling ponds, and surface heat ejectors, mainly used in cooling-dominated systems. It is based on elements like field geometry and operation. Conversely, artificial regeneration includes several strategies, including solar thermal collectors like evacuated tube collectors (ETC) and flat plate collectors, as well as PVT (Photovoltaic-Thermal) systems, which can be either glazed or unglazed. Within this category, which can be further separated into active and passive approaches, are space heating, waste heat, space cooling, and DHW utilization techniques. Lastly, other complementary methods that help with thermal management include the use of air and garden ponds. This classification summarizes how essential cooling, dissipation, and heat storage systems are for optimizing energy performance in multiple fields, such as civil and agricultural engineering [20].

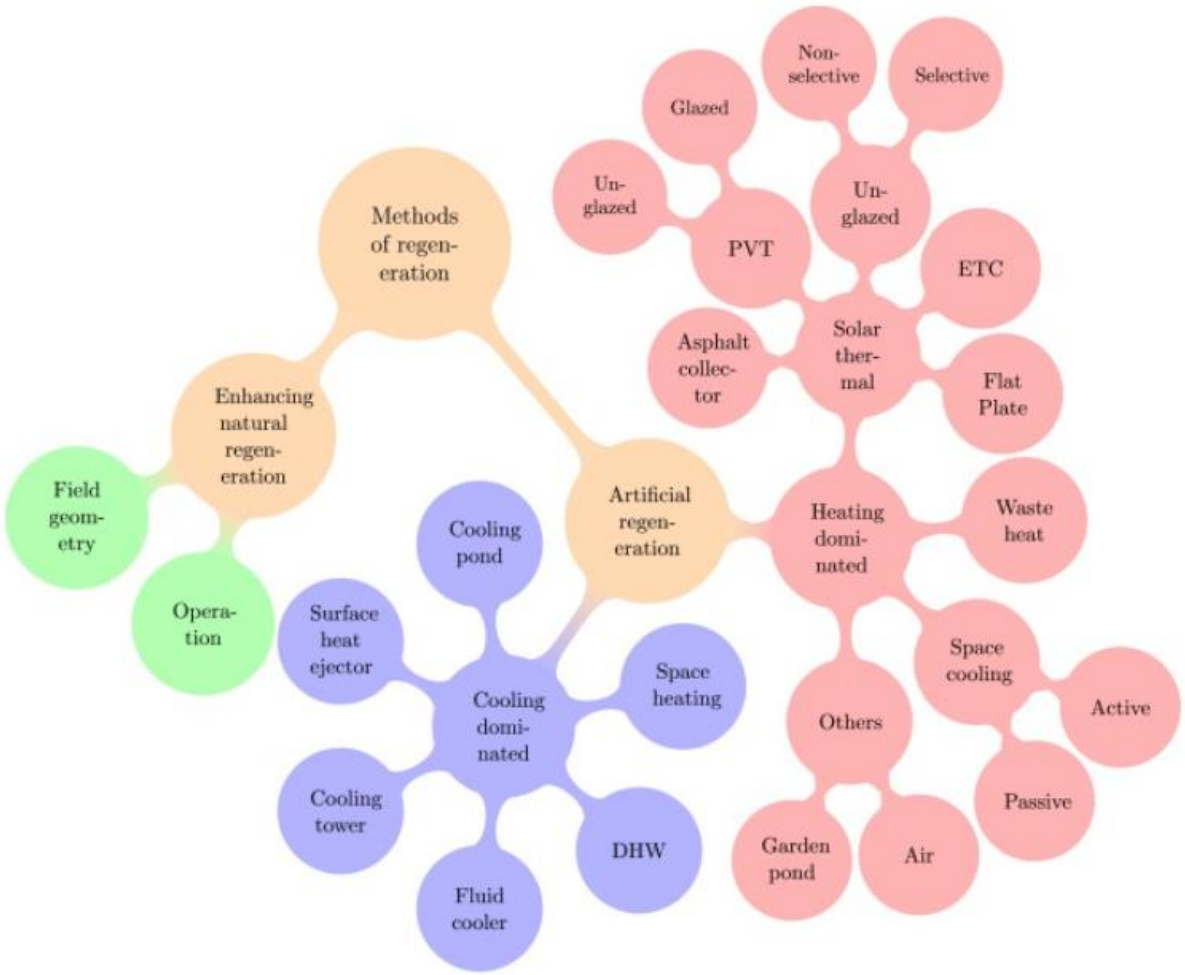

Figure I. 7. Classification of Thermal Regeneration Methods [20]

I.6. Geothermal energy worldwide

The global energy mix varies significantly depending on each nation's natural resources, energy policies, and economic priorities. While some people prefer fossil fuels, others get their energy from nuclear or renewable sources.

Figure I. 8 shows the breakdown of energy consumption per capita (in kWh) across several countries based on the three primary energy sources: nuclear, renewable energy, and fossil fuels. It shows that Canada and the USA have the highest consumption, dominated by fossil fuels, while Canada has a notable contribution from renewables. Australia has a balanced use of fossil fuels and renewables, and Sweden stands out for its combination of renewables and nuclear power. However, nations like Brazil and India have far lower overall consumption, with India depending primarily on fossil fuels and Brazil on renewable energy. This diversity reflects the various energy priorities and how they affect the sustainability of the environment.

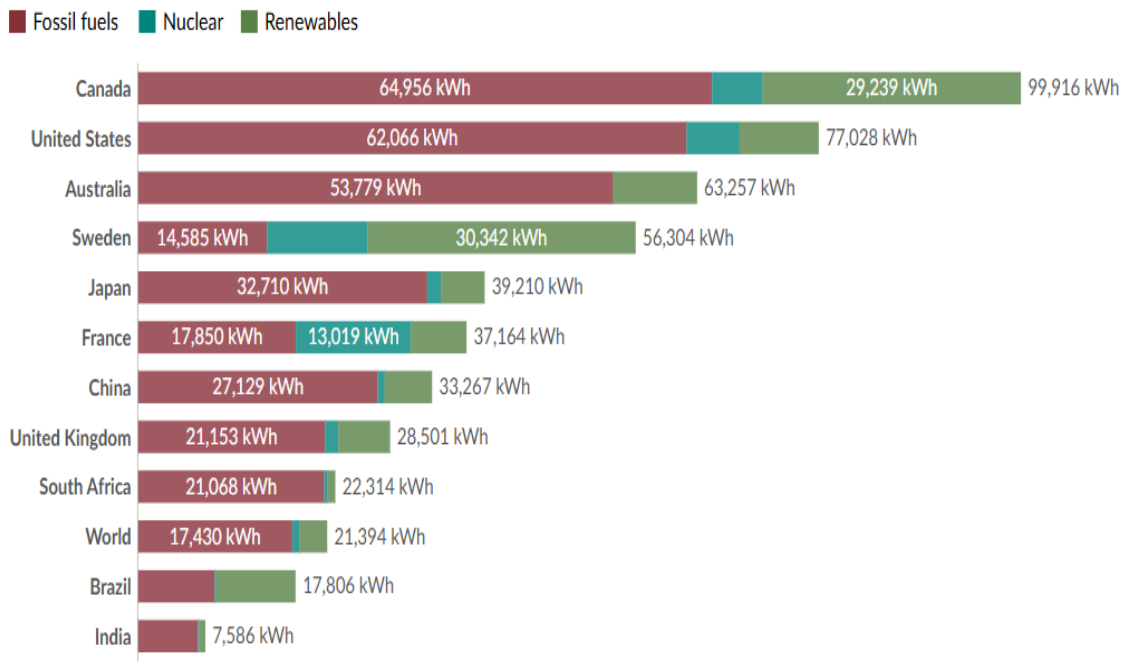

Figure I. 8. Energy consumption per capita by energy source across various nations (2023) [21]

Geothermal energy can be found anywhere in the world, though its potential for use varies from place to place [22]. Typically, favorable regions are found at active continental margins as illustrated in Figure I. 9.

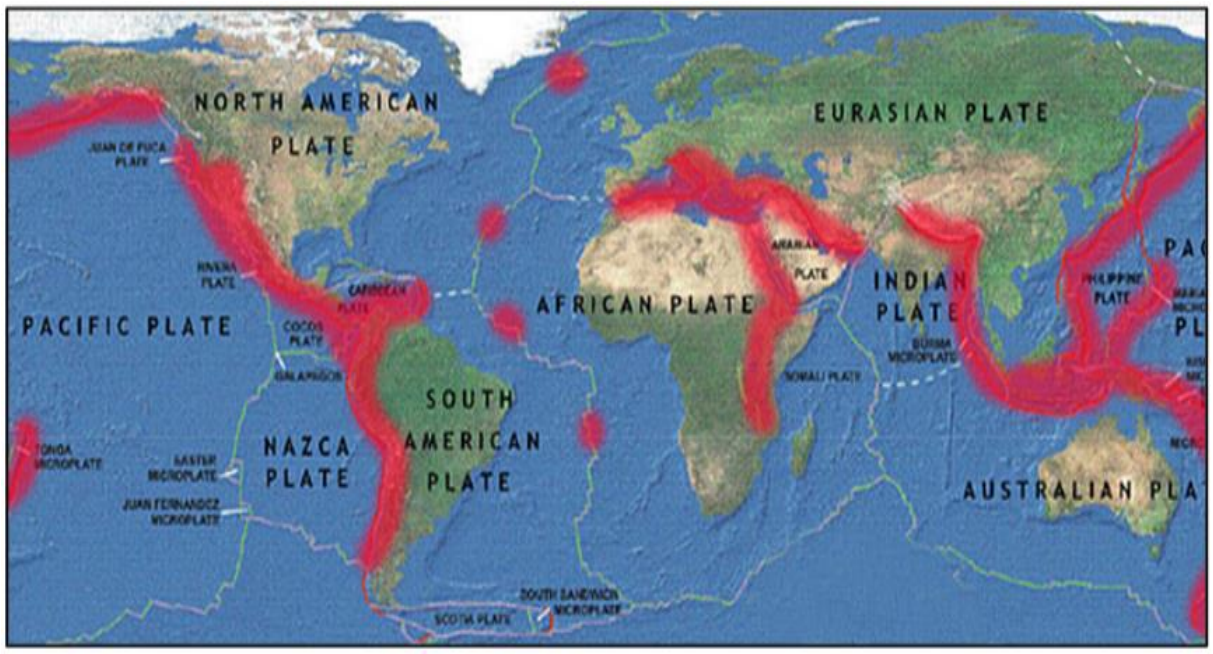

Figure I. 9. Areas with high geothermal potential and continental plates [22]

Depending on the location, these uses range from industrial or agricultural purposes to space heating in cold climates. Certain countries, like China, Sweden, and the United States, are

notable for the size of their infrastructures and the effectiveness of their exploitation. Table I. 1 lists the major nations that directly use geothermal energy, with uses differing depending on the region and economic climate

Table I. 1. The top nations for direct use of geothermal energy [23]

Country	TJ/yr	GWh/yr	MWt	Capacity Factor	Principal Use
China	45373	12605	3687	0.39	Bathing
Sweden	36000	10000	3840	0.30	Heat Pumps
United States	31239	8678	7817	0.13	Heat Pumps
Turkey	24840	6900	1495	0.53	Bathing/Heating
Iceland	24500	6806	1844	0.42	District Heating
Japan	10301	2862	822	0.40	Bathing
Italy	7554	2098	607	0.39	Bathing/Spas
Hungary	7940	2206	694	0.36	Bathing/Spas
New Zealand	7086	1968	308	0.73	Industrial
Brazil	6622	1840	360	0.58	Bathing/Spa

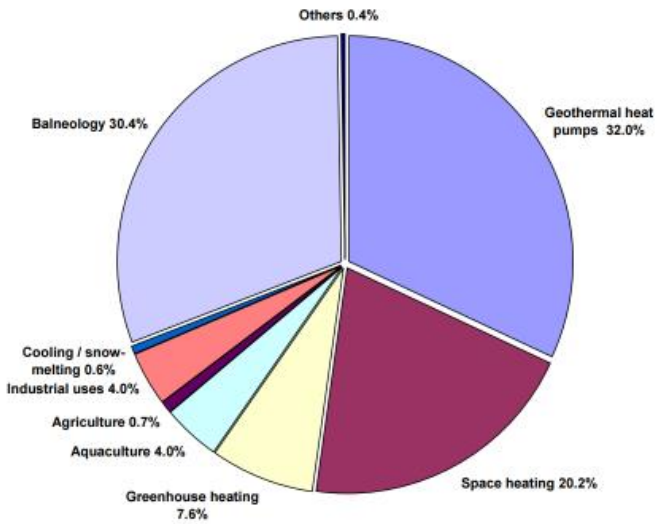

Figure I. 10. Global installed capacity distribution (MWt) [23]

Figure I. 10 completes this analysis by showing that the most significant percentage (32%) is occupied by geothermal heat pumps, highlighting their essential contribution to building

heating and cooling. These systems are a well-liked option in nations looking to meet energy sustainability goals because of their exceptional energy efficiency and capacity to lower greenhouse gas emissions. The second most significant use, with 30.4%, is balneology. This indicates a strong interest in spas, thermal activities, and other applications linked to health and well-being, especially in areas where geothermal sources are readily available

The significance of geothermal energy in supplying heat in cold climates is demonstrated by the fact that space heating comes in third with 20.2%. This use, which frequently complements heat pumps, can involve more basic systems directly using the earth's natural heat source. Specialized uses, like aquaculture (4%) and greenhouse heating (7.6%), demonstrate how this resource can be explicitly used to support fish farming and agriculture. Although their share is still relatively small, industrial (4%) and agricultural (0.7%) applications demonstrate how geothermal energy can be tailored to more complex requirements. Lastly, less common uses like "other" applications (0.4%) and cooling and snow removal (0.6%) show that some exploitation areas are still in their infancy. This highlights unrealized potential, especially in industries where geothermal energy has the potential to displace more polluting sources. To sum up, this graphic illustrates the variety of geothermal energy applications, focusing on wellness and heating applications, but it also presents growth prospects in untapped or underutilized markets. The benefits of this renewable energy source are balanced with the local community's needs.

I.7. Geothermal energy In Algeria

Algeria is the largest country in North Africa (Figure I. 11), with the Mediterranean Sea to the north and the Sahara Desert to the south. This large area has a remarkably diverse range of climates and topography. The country's north, dominated by the Mediterranean coast and the Atlas Mountains, experiences hot, dry summers and mild, rainy winters. Most people live in this area, which is rich in agricultural land and is where cities like Algiers, Oran, and Constantine are located. On the other hand, the south, which comprises about 80% of the nation, has a harsh desert climate with scorching summers and little precipitation. Although the vast and magnificent Algerian Sahara is home to many oases and unusual rock formations, it is not heavily populated, with most communities residing in oasis towns like Tamanrasset and Ghardaïa. Algeria has many natural and cultural aspects, as evidenced by the diverse lifestyles and landscapes reflected in this north-south contrast and climatic differences.

Despite having an abundance of natural resources, Algeria primarily depends on fossil fuels to meet its energy needs. With substantial reserves, mainly in the Sahara, the nation is one of the world's top producers and exporters of natural gas. The primary domestic energy source for heating and power generation is natural gas, but oil exports contribute significantly to the national economy.

With more than 3,000 hours of sunshine annually, Algeria is starting to investigate renewable energy sources, especially solar power, because of its great potential. Reducing reliance on hydrocarbons and diversifying the energy mix are the goals of projects like photovoltaic parks and hybrid solar power plants that are progressively coming into existence. The nation also has the potential for geothermal energy because of its many thermal springs, especially in the north and some of the Sahara. This resource is still underutilized, but it has the potential to be very important for local uses like heating and balneology.

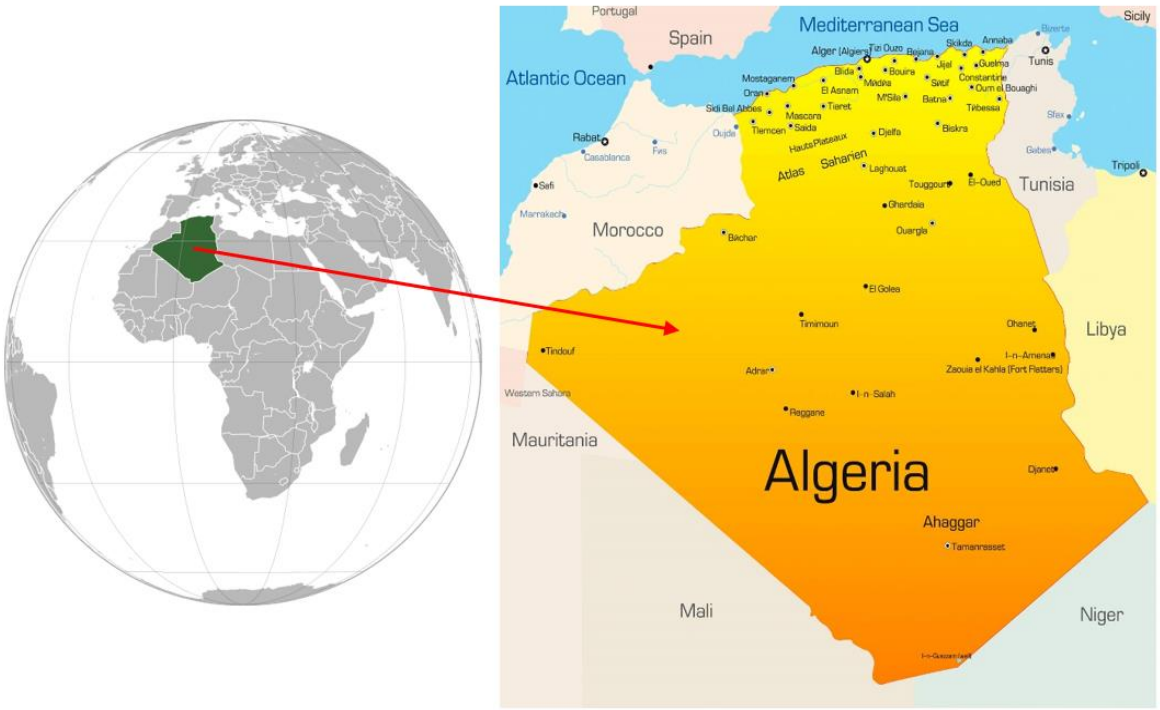

Figure I. 11. Location of Algeria *[24, 25]*

Despite Algeria's dependence on fossil fuels, Figure I. 12 clearly explains how the country is building up its capacity for renewable energy from 2014 to 2023. It has also grown steadily since 2014 until it reached nearly 650GW in 2018 and stabilized up to 2023. This growth trend indicates an effort toward diversifying energy sources, which considers increased renewable energy sources, such as solar and wind power. These indeed illustrate the will of Algeria to reduce its dependence on hydrocarbons by using its favorable climate, essentially its abundant

sunshine. Coupled with the nation's untapped geothermal energy potential, this transition to renewable energy marks one of the significant steps in the country's energy transition. These initiatives are part of a more significant push to boost long-term sustainability, meet rising energy demand, and aid in the fight against climate change.

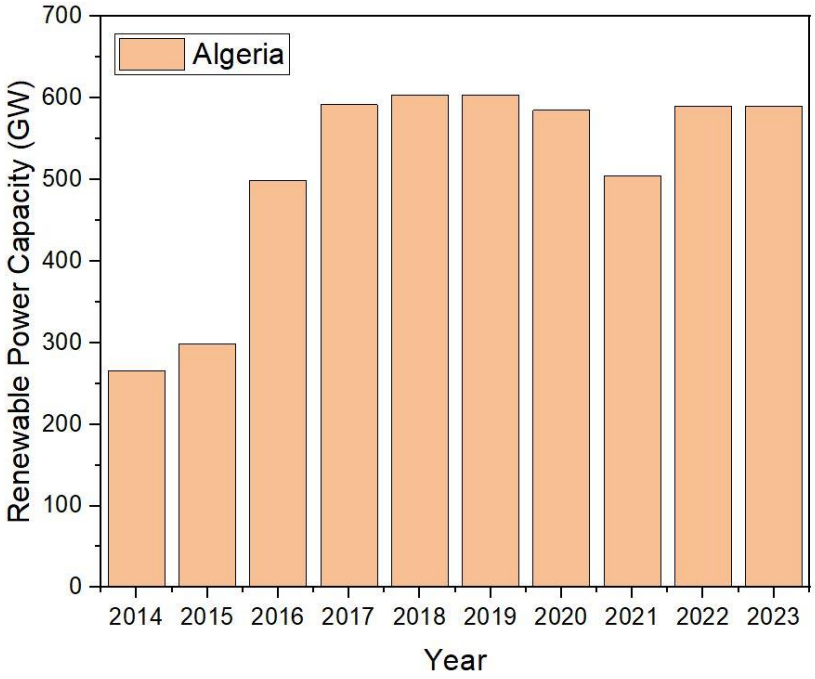

Figure I. 12. Renewable Energy Capacity in Algeria (2014-2023) [26]

I.7.1. Why make geothermal energy investments in Algeria?

Algeria's geological characteristics and wealth of natural resources make it a promising country for geothermal energy. With high temperatures appropriate for geothermal exploitation, more than 200 thermal springs have been found, including prominent locations like Hammam Chellala (98°C in Guelma), Hammam Boutaleb (52°C in Sétif), and Hammam Bouhanifia (66°C in Mascara). Furthermore, three regions with a strong geothermal gradient have been identified: Kabylie in the center-north, Oran in the northwest, and Constantine in the northeast, as represented in Figure I. 13 and Table 2. These areas suggest easier access to terrestrial heat and reduced extraction costs. As thermal springs are spread over a wider geographical area, several sites for developing energy projects are offered to address varying local needs [7]

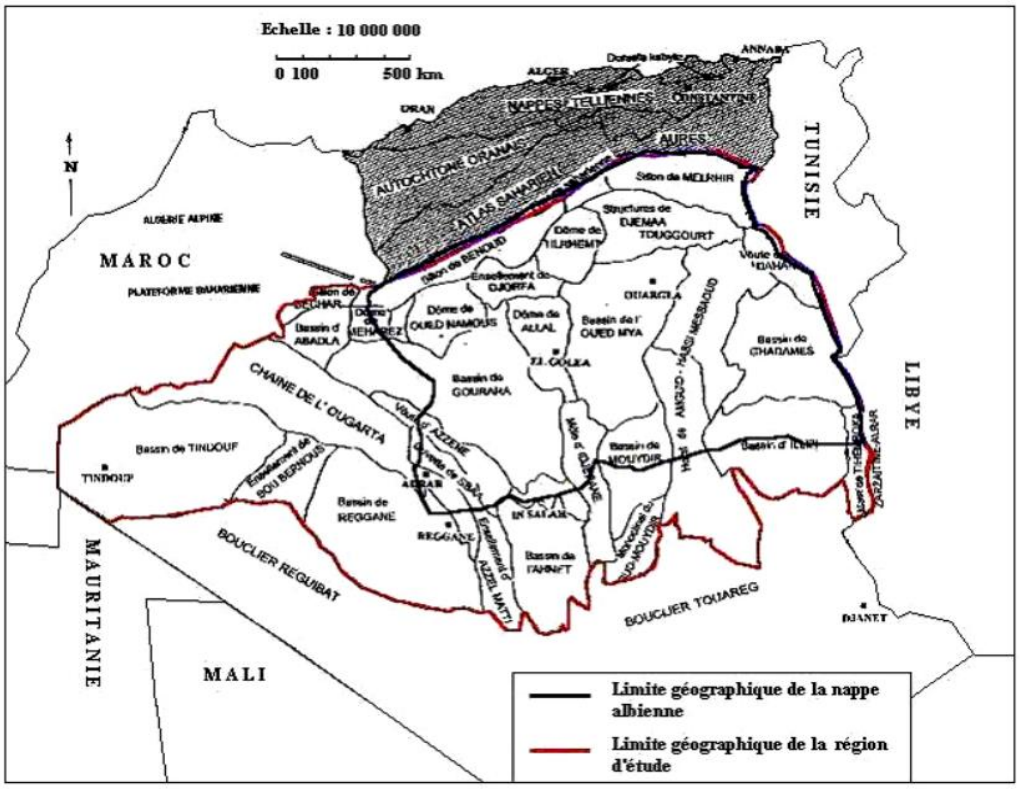

Figure I. 13. Geographical limit of the Albian nappe [7]

Table I. 2.Temperature of a few Northern Algerian thermal springs [7]

Thermal Sources	Location	Temperature (°C)
H. Chellala	Guelma	98.0
H. Bou Hadjar	Aïn Témouchent	66.5
H. Bouhanifia	Mascara	66.0
H. Boutaleb	Sétif	52.0
H. Essalihine	Khenchela	70.0
H. Salhine	Skikda	55.0
H. Sidi Bou Abdellah	Relizane	51.0
H. Delaa	M'sila	42.0

Furthermore, geothermal energy is an opportunity to give the country a diversity of energies while benefiting from the reliance on renewable and sustainable energy sources and reducing

the country's dependence on fossil fuels. Beyond producing electricity, potential uses include direct home heating, industry, agriculture (including heating greenhouses), and the growth of the already-established spa tourism industry. As a result, geothermal energy is a viable and strategic resource for Algeria's energy needs as part of a sustainable energy transition.

I.8. Geothermal Development Challenges

Geothermal energy development presents several difficulties, including social, economic, and environmental effects. Careful management is necessary to maximize positive and minimize adverse effects for ecosystems and communities. An examination of the impact by theme is provided below [27]:

- Poverty

Exploiting energy resources can increase per capita income and salaries while promoting social development initiatives. It also enables access to affordable energy, improved living conditions, better food security, and increased access to drinking water. However, these benefits can be offset by rising property prices and the displacement of communities.

- Health

In terms of health, these activities can improve medical and sanitary infrastructures, reduce indoor pollution, and offer therapeutic uses. However, they can also lead to odor nuisance, toxic gas emissions, water contamination, and increased noise pollution.

- Education

Positive impacts include the development of educational infrastructures and improved school attendance. However, sudden or unexpected cultural changes can disrupt existing systems.

- Natural hazards

These projects can reduce specific natural hazards but also entail dangers such as artificial earthquakes, land subsidence, and hydrothermal eruptions.

- Atmosphere

Energy exploitation can limit greenhouse gas emissions from other energy sources. On the other hand, it can also produce greenhouse gases, H_2S emissions, and other toxic gases.

- Soil

Land use remains relatively low compared to other energy sources, which is advantageous. However, this can lead to loss of natural habitat, soil compaction, and conflicts of use with different activities.

- Forests

These resources can replace traditional biomass but at the cost of negative impacts such as deforestation and the destruction of forest ecosystems.

- Freshwater

Compared with other energy sources, mining has the advantage of consuming little water over its life cycle. Despite this, it can conflict with other water uses and cause contamination of aquifers and other water bodies.

- Biodiversity

Despite the overt enhancements in terms of energy security, these practices might disrupt the natural habitats and damage rare ecosystems.

- Economic development

These activities provide more energy security, reduced reliance on weather, more effective operations, and numerous other direct and indirect financial advantages. However, they generate few long-term, sustainable jobs.

- Consumption and production

Utilizing waste heat has advantages, but drawbacks include the potential for environmental contamination, overuse of resources, and the high cost of some equipment, like turbines.

I.9. Advantages and disadvantages of geothermal energy

I.9.1. Advantages of geothermal energy

Geothermal energy presents a range of notable advantages that make it an appealing option for both residential and commercial use. Its sustainability and reliability are among its strongest benefits, offering a consistent energy source regardless of external weather conditions. This makes it particularly ideal for continuous energy production year-round. Additionally, geothermal systems contribute to reducing the overall environmental impact by minimizing greenhouse gas emissions, which is crucial in the ongoing battle against global warming. The

energy savings are another significant advantage—geothermal heat pumps can lower heating bills by 30-60%, allowing for a relatively quick return on investment. The versatility of geothermal energy also stands out, as it can be used for both heating and cooling, making it a practical choice for a wide variety of applications. Furthermore, geothermal energy systems are space-efficient; they require less land area compared to solar or wind farms, and the ground can be used for other purposes once the necessary collectors are installed underground. In terms of maintenance, geothermal systems are durable, with low maintenance needs and a long service life, making them a low-maintenance option in the long run.

I.9.2. Disadvantages of geothermal energy

Despite these numerous benefits, there are several disadvantages to consider. One of the primary drawbacks is the high initial cost of installation, which can discourage potential adopters despite the long-term savings. Geographical limitations also affect the viability of geothermal energy; regions with little geothermal activity are less suitable for harnessing this energy, and efficiency can vary based on location. Additionally, the collectors used in geothermal systems have a limited lifespan, typically requiring replacement every 20 to 25 years. Finally, geothermal energy systems require a high level of technical expertise for installation, and the process often necessitates detailed studies and professional assessment to ensure proper implementation.

I.10. Conclusion

Geothermal energy is one of the few sustainable energy sources that combine low greenhouse gas emissions with long-term savings. It can be used for heating, hot water production, and electricity generation. Although it requires considerable initial investment and specialized knowledge, its environmental and economic benefits make it a suitable alternative to fossil fuels. The geothermal aspect in Algeria remains largely unexplored especially in very active geological regions, the Sahara is a promising renewable energy vector for the country's diversification. In this way, Algeria could use that natural resource to cut dependency on hydrocarbons and heat toward a more sustainable future by developing infrastructure, training professionals, and conducting extensive geothermal investigations.

Chapter II

Soil physical and chemical properties

II. 1. Introduction

As explained in the first chapter, geothermal energy uses the heat that exists in the earth to generate energy for multiple uses such as power generation or heating. One of the main factors influencing this technology's effectiveness is the ground's physical properties, which directly affect the subsoil's ability to store and transfer heat. Among these properties, thermal conductivity, thermal diffusivity, heat capacity and porosity play a key role in the performance of geothermal systems. These properties change depending on the density, moisture content, and mineralogical composition of the soil, as well as the presence of fractures or interstitial fluids. Therefore, it is essential to comprehend how soil physical characteristics affect geothermal installation sizing and efficiency to ensure high-performance, sustainable exploitation of this renewable energy source.

This chapter will discuss the physical, thermal, and chemical properties of soils, focusing on unsaturated soils. Each parameter will be thoroughly detailed and explained, including its corresponding equation. A dedicated section will also review relevant literature, highlighting previous research and findings in this field.

II. 2. Soil description

Soil is an unconsolidated layer of mineral or organic matter influenced by environmental factors such as climate, living organisms, and topography. It typically comprises multiple horizons and has different physical, chemical, biological, and morphological characteristics. Specific horizons are absent in particular environments, like deserts, and vary depending on the soil type. Soil is a solid grain matrix connected by air or water pores.

A typical soil profile with five different horizons is depicted in Figure II. 1. At the surface, the O horizon is a layer rich in decomposing organic matter, forming humus. Just below, the A horizon, known as topsoil, contains organic and mineral matter essential for plant growth. The B horizon, or subsoil, is characterized by an accumulation of minerals leached from the upper layers, such as clay and iron. Deeper down, the C horizon is a transition zone where the weathered bedrock retains some original characteristics. Finally, the R horizon at the base corresponds to compact bedrock. This profile shows the soil stratification, influenced by environmental and biological processes [28].

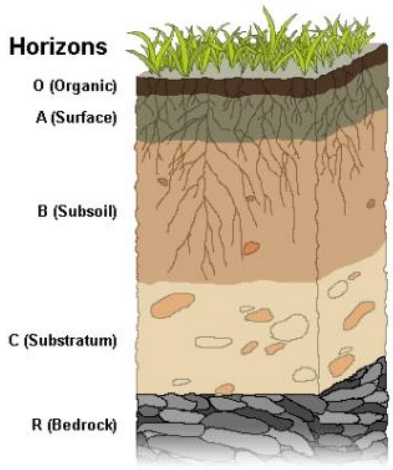

Figure II. 1. The different horizons of a soil profile [28]

II. 3. Characteristic values

Soil is considered to be an assembly of independent solid grains of varying sizes. As seen in Figure II.2, the voids, or interstitial spaces, between these grains can be filled with either water or air. The amount of water in these cavities determines the soil's moisture status [29]:

- Dry soil: all the voids are filled with air; there is no water.
- Unsaturated soil: air fills the voids, while water occupies part of them.
- Saturated soil: all voids are completely filled with water, with no space for air.

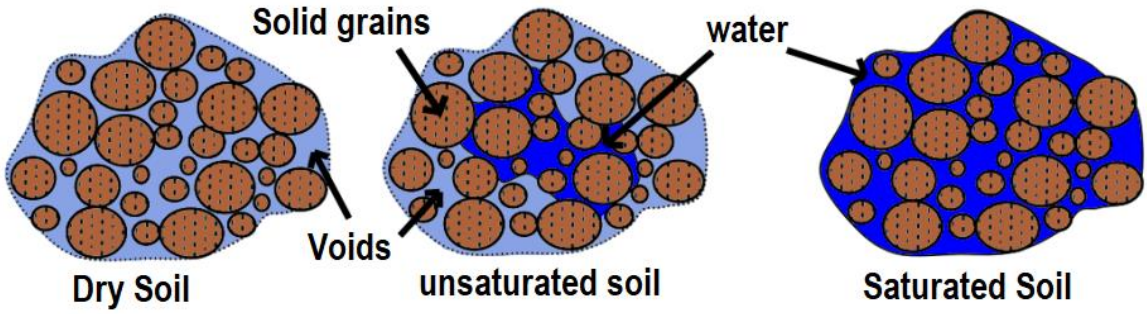

Figure II. 2. A schematic of soil states [29]

The representation of volume includes the space occupied by solid grains (V_s), as well as the empty voids (V_v) that contain air (V_a) and water (V_w). All these components together form a total volume (V) as represented in Figure II.3. The representation also allows for some vital parameters to be derived such as total porosity (n), water content (θ) and degree of saturation (S_r).

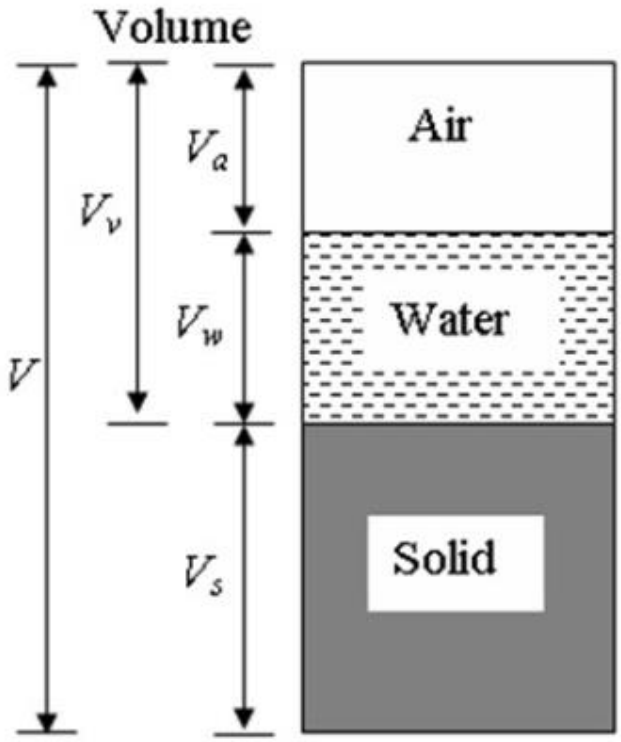

Figure II. 3. Volume distribution in soil: air, water and solids *[30]*

II.3.1. Soil classification

Soil classification methods are based on several key elements. Firstly, they are based on specific soil properties, such as texture, depth and drainage, rather than environmental criteria. Secondly, the origin of the soil and its link with the bedrock are essential, as early classifications relied mainly on geology to understand their composition. While more recent methods focus on soil properties, older ones considered elements such as climate and vegetation to identify large-scale soil types. Agriculture also plays an important role in classification, as natural vegetation and cultivation conditions are analyzed to assess land potential. Finally, in the past, soils were often classified according to simple criteria such as color or texture before more precise systems integrating several parameters were adopted. Today, these different aspects make it possible to refine soil classification by combining scientific knowledge with practical needs [31].

II.3.2. USDA classification of textural soil

The USDA textural triangle is shown in Figure II.4. A soil sample is categorized into one of the twelve soil texture classes based on the proportions of sand, silt, and clay, shown along each of the three axes. The eight subclasses within the sand and loamy sand categories offer a level of granularity that may, in certain instances, exceed what can be reliably assessed by field methods. Only distinctions that are pertinent to utilization and management, and that can be reliably

identified in the field, should be employed when texture determinations depend just on field estimations [32].

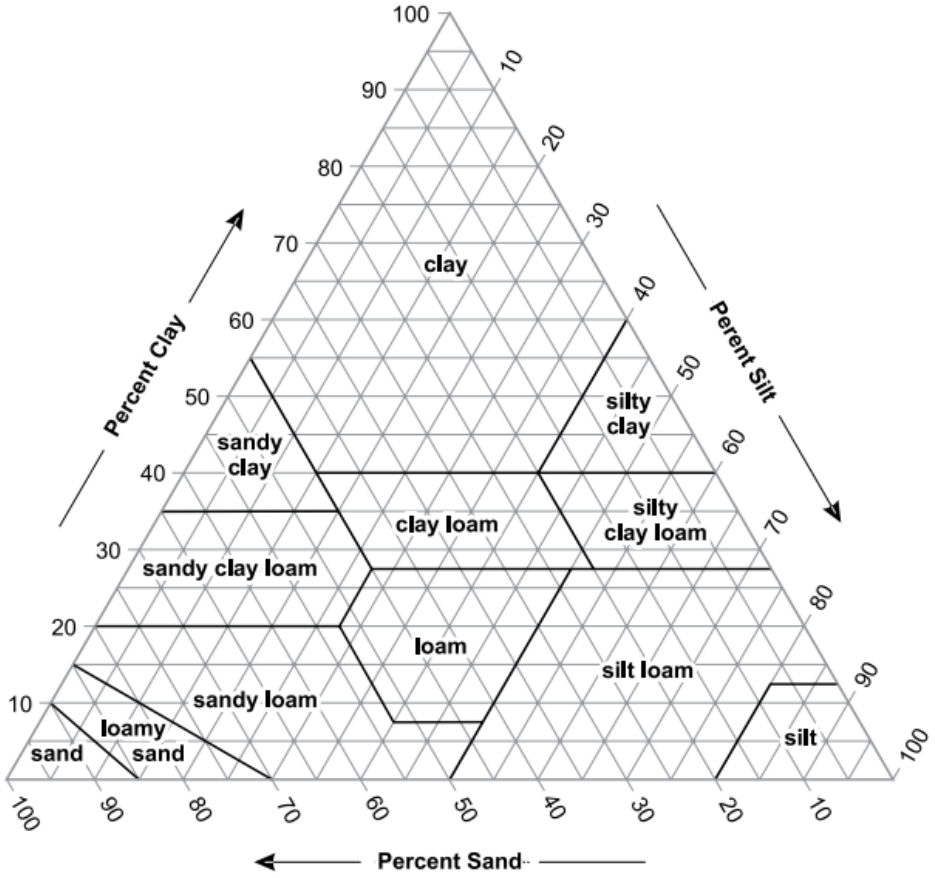

Figure II. 4. Textural soil classification by the USDA [32]

II.3.3. Moreno-Maroto and Azcarate's texture-plasticity classification chart

Figure II.5 displays the texture-plasticity classification graph Moreno-Maroto and Azcarate developed, demonstrating the relationship between a soil's texture and plasticity. At the bottom, the horizontal axis represents the proportion of sand. On the left, the vertical axis indicates the soil's plasticity, i.e. its capacity to deform under the effect of water. The soil becomes more plastic as it moves up the graph, indicating improved water retention and cohesiveness. On the other hand, the soil gets sandier and less plastic as it moves farther to the right. Different soil types, such as the highly plastic clay at the top and the nearly non-plastic sand at the bottom right, can be found. Loam and silt are examples of intermediate soils. This type of classification is essential in engineering, particularly for determining whether the soil is stable and suitable for construction and for applying Heat ground exchangers [33, 34].

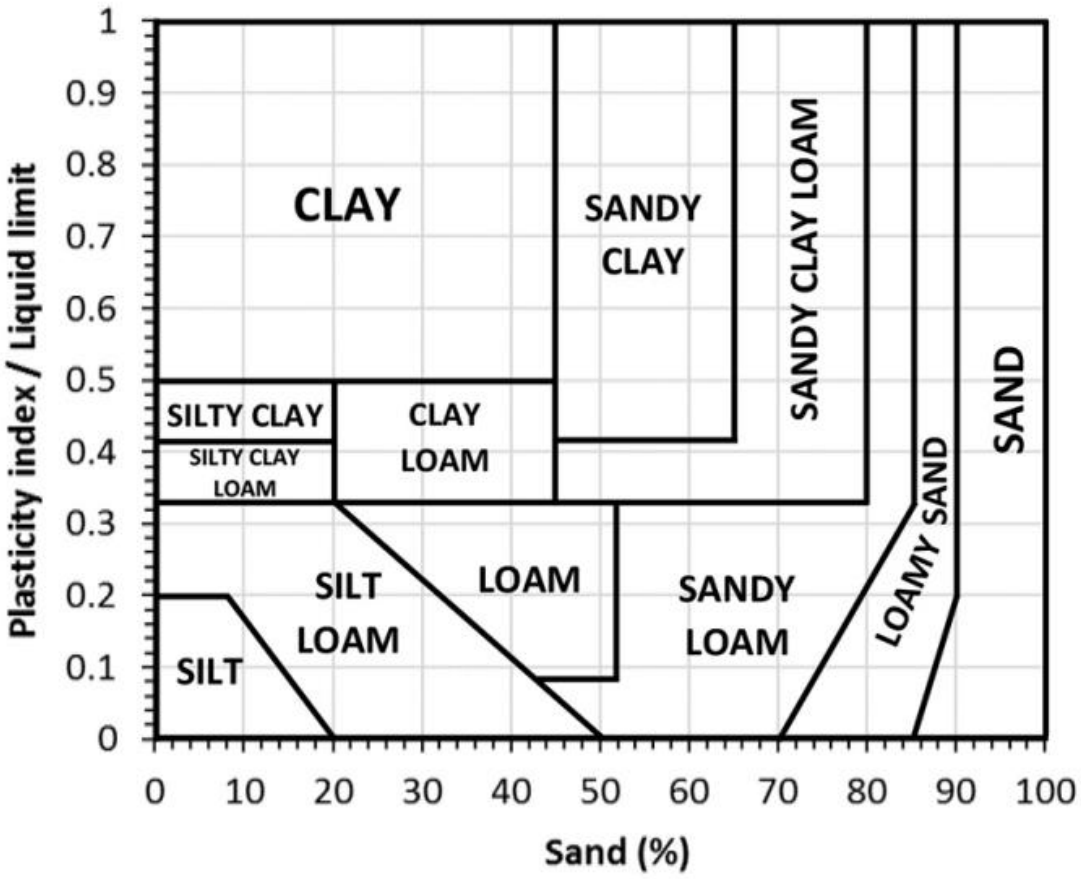

Figure II. 5. The texture-plasticity classification by Moreno-Maroto and Azcarate *[33, 34]*

II.3.4. L.C.P.C classification

The LCPC classification is based on the granulometry results and the fine fraction's plasticity characteristics (Atterberg). Soils are designated by the name of the predominant granulometric portion, qualified by an adjective relating to the secondary portions. There are three main types of soil: granular soils, where more than 50% of the elements by weight are greater than 80 µm; fine soils, where more than 50% of the elements by weight are less than 80 µm; and organic soils, where the organic matter content exceeds 10% [35].

- **Fine soils**

The classification of fine soils is based on plasticity criteria linked to Atterberg limits and is specified in the plasticity diagram (Figure II.6). Depending on the position of the representative point in this diagram, whose x-axis corresponds to the liquidity limit and y-axis to the plasticity index, four main categories can be distinguished: highly plastic loams, loams with low plasticity, highly plastic clays and clays with low plasticity.

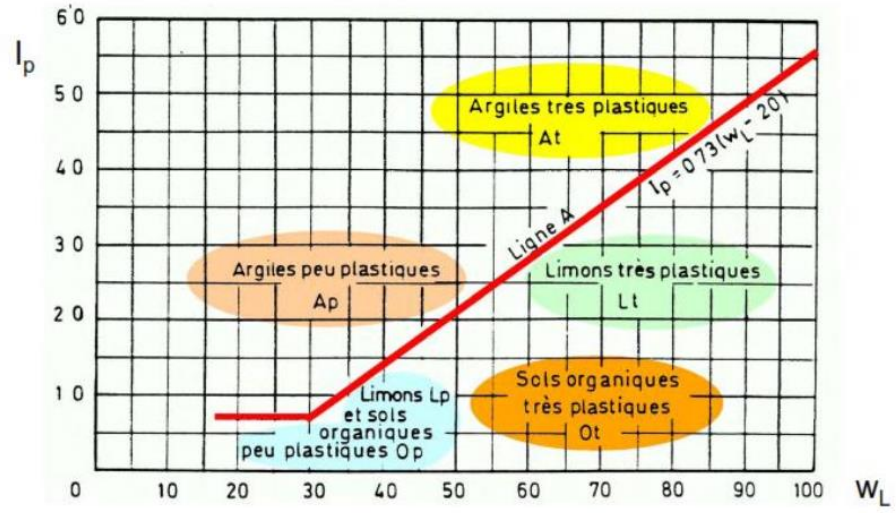

Figure II. 6. Fine soil classification using the L.C.P.C plasticity diagram [35].

- **Granular soils**

Granular soils are categorized based on Atterberg limits and grain size. This is detailed in Figure II.7 below.

Définitions			Symboles	Conditions	Désignation géotechnique
GRAVES	Plus de 50 % des éléments > 0,08 mm ont un diamètre > 2 mm	moins de 5 % d'éléments < 0,08 mm	Gb	$C_u = \frac{D_{60}}{D_{10}} > 4$ (*) et $C_c = \frac{(D_{30})^2}{D_{10} \times D_{60}}$ compris entre 1 et 3	grave propre bien graduée
			Gm	Une des conditions de Gb non satisfaite	grave propre mal graduée
		plus de 12 % d'éléments < 0,08 mm	GL	Limite d'Atterberg au-dessous de la ligne A (fig. 2)	grave limoneuse
			GA	Limite d'Atterberg au-dessus de la ligne A	grave argileuse
SABLES	Plus de 50 % des éléments > 0,08 mm ont un diamètre < 2 mm	moins de 5 % d'éléments < 0,08 mm	Sb	$C_u = \frac{D_{60}}{D_{10}} > 6$ et $C_c = \frac{(D_{30})^2}{D_{10} \times D_{60}}$ compris entre 1 et 3	sable propre bien gradué
			Sm	Une des conditions de Sb non satisfaite	sable propre mal gradué
		plus de 12 % d'éléments < 0,08 mm	SL	Limite d'Atterberg au-dessous de la ligne A	sable limoneux
			SA	Limite d'Atterberg au-dessus de la ligne A	sable argileux

Figure II. 7. Granular soil classification based on L.C.P.C [35].

II. 4. Physical Properties

II.4.1. Porosity

Soil porosity refers to the proportion of a soil's volume that is not occupied by solid particles. It plays a crucial role in determining how well the soil can hold and move water and air, both essential for healthy plant growth and overall soil function [36]. It can be calculated using the following equation

$$n[\%] = \frac{V_v}{V_t} \times 100 \quad \text{(II.1)}$$

Because soil isn't a continuous, solid mass, it naturally contains voids that vary in size. These voids fall into two categories: macropores, which allow for quick drainage and aeration, and micropores, which retain water for plant use. Together, these make up the total porosity of the soil.

To put it more clearly, the top layers of natural soil usually have between 40% and 70% porosity [37], which means that almost half of their volume is composed of tiny spaces that are either filled with water or air. In contrast, dense rocks, such as granite, have a very low porosity of about 1%, which makes them nearly solid and stops water from penetrating.

Porosity is essential for soil fertility. It impacts the amount of air that can circulate underground, the soil's ability to retain water and the ease with which plant roots can spread. Ideal conditions for plant growth and beneficial microbial activity are created when porosity is balanced so roots receive the oxygen they require, and the soil retains just the right amount of moisture [38].

A mechanical method of measuring total soil porosity was studied [37]. This method involved placing a soil sample in a regulated cell, adjusting its volume with a piston, and analyzing changes in gas phase pressure to determine porosity. Their study, which included five distinct soil samples, demonstrated a strong correlation between theoretical predictions and experimental results and confirmed the reliability of the method. This approach offers a precise way to assess a soil's suitability for construction and agricultural productivity.

Some research has been carried out [36] using the Concentration Conductivity Measurement (CCM) technique, which uses electrical conductivity to assess porosity and formation factors non-destructively. Experiments conducted on a range of granular materials, such as sand and glass beads, have shown that CCM produces incredibly accurate results consistent with existing models and the literature. Unlike conventional methods, CCM is more direct, less affected by

interference and requires simpler equipment, making it a practical choice for geotechnical studies. This method offers a reliable and efficient means of establishing porosity profiles, thus promoting soil mechanics and geotechnical engineering research.

Studies have been carried out [39] to categorize porosity according to material type, as represented in Table II.1.

Table II. 1. Typical values of soil porosity *[39]*

Soil Type		Porosity Range
Uniform materials	Equal spheres (theoretical values)	$0.26 < n < 0.48$
	Clean, uniform sand (fine or medium)	$0.29 < n < 0.50$
	Uniform, inorganic silt	$0.29 < n < 0.52$
Well-graded materials	Silty sand	$0.23 < n < 0.47$
	Clean, fine to coarse sand	$0.17 < n < 0.49$
	Micaceous sand	$0.29 < n < 0.55$
	Silty sand and gravel	$0.12 < n < 0.46$
Mixed soils	Sandy or silty clay	$0.20 < n < 0.64$
	Skip-graded silty clay with stones or rock fragments	$0.17 < n < 0.50$
	Well-graded gravel, sand, silt and clay mixture	$0.11 < n < 0.41$
Clay soils	Clay (30% - 50% clay sizes)	$0.33 < n < 0.71$
	Colloidal clay (0.002 mm > 50%)	$0.37 < n < 0.92$
Organic soils	Organic silt	$0.35 < n < 0.75$
	Organic clay (30% - 50% clay sizes)	$0.41 < n < 0.81$

II.4.2. Soil water content

Soil water content refers to the amount of water held in the soil, usually expressed as a percentage of its total weight or volume. It plays a crucial role in plant growth, soil stability,

and overall water movement in the environment. Measuring it accurately is essential for agriculture, forestry, and hydrology, with methods ranging from simple weighing techniques to advanced sensors and satellite monitoring [40]. The equation that follows can be used to calculate it.

$$\theta[\%] = \frac{W_w}{W_s} \times 100 \quad \text{(II.2)}$$

W_w and W_s refers to the weight of water and solid particles respectively.

The method used to determine the water content of the soil has undergone significant change in the past 20 years. More sophisticated technology is now used instead of outdated techniques like weighing soil samples or employing neutron probes. Today's instruments include ground-penetrating radar (GPR), capacitance sensors, time-domain reflectometry (TDR), and even satellite-based systems. With the help of these contemporary methods, measurements are now more precise and effective than ever before because water reacts to electrical signals differently than other soil constituents [40].

The amount of water in the soil has a major effect on geothermal transfer, affecting ice formation and heat transfer efficiency [41]. According to studies, higher soil water content causes the pipe outlet temperature to rise and the amount of ice that forms in the soil to decrease [41]. The ability to dissipate heat is influenced by water content; higher levels improve efficiency [42]. The amount of water in the soil has an impact on its thermal characteristics as well; dry soils with air-filled pores have low heat conductivity [43]. Furthermore, heat pumps operating hours and electricity consumption can be decreased when moisture levels in various soil types rise [44]. In general, controlling soil moisture is essential to maximizing ground-source heat pump system performance.

II.4.3. Soil Density

Soil density is the relationship between the mass and volume of a dry soil sample. It shows how concentrated and compact the mineral components are. The soil density can be calculated using the following Equation.

$$\rho = \frac{Mass}{Volume} \quad \text{(II.3)}$$

As with solid materials, the density of fluids changes with temperature [45]. Changes in density can affect heat and mass transfer through conduction and convection. Energy Geostructures

analysis and design may consider such a parameter [39]. The higher the density of the soil, the more its thermal conductivity, enhancing the soil's ability to conduct heat [46]. This is because closely compacted mineral grains reduce porosity, improving heat conduction. Variations in soil density affect temperature predictions, with denser soils showing a decreasing temperature trajectory over time [47]. Soil density plays a vital role in predicting the longevity, long-term performance, and environmental impact of geothermal systems [48]. In various types of soils, a different relation exists between density and thermal properties [46].

A crucial part of geotechnical engineering is determining the density of soils. Various approaches are used depending on the kind of soil, the field or lab environment, and the equipment available. One common technique is the Core Cutter Method, which involves removing a known-volume sample of soil using a cylindrical core cutter and weighing it to determine its density. Another popular method for determining in-situ density is the Sand Replacement Method (also known as the Sand Cone Test), which measures the volume and weight of excavated soil by replacing it with calibrated sand. The Water Displacement Method uses Archimedes' principle to calculate the soil volume by immersing it in water; it can be used for cohesive soils or samples with irregular shapes. The nuclear density gauge method involves calibration, too; however, this test can measure rapidly in a non-destructive way using gamma radiation. Moreover, the Compaction or Proctor tests obtain optimum moisture content, providing maximum dry density. Contrarily, in the Core Drilling Method, weight and volume are directly measured with the help of cylindrical cores. Each method has associated formulae, such as bulk density and dry density [49].

II.4.4. Saturation level

The percentage of a soil's void volume that is occupied by water is known as the saturation level (S_r) [50, 51]. It is a dimensionless parameter that is frequently given a percentage value [51]. At 100% saturation, all the voids in the soil are filled with water, making the soil said to be saturated. The saturation level can be calculated using the following formula:

$$S_r = \frac{V_v}{V_w} \tag{II.4}$$

The saturation level affects the heat transfer processes in the rock or soil, which has a major impact on geothermal applications [52]. In saturated porous media, heat transfer occurs through convection, conduction, and thermal dispersion, with hydraulic conductivity and effective

porosity governing convection, while thermal conductivity and specific heat capacity dictate thermal conduction and heat exchange between the solid matrix and fluid [52].

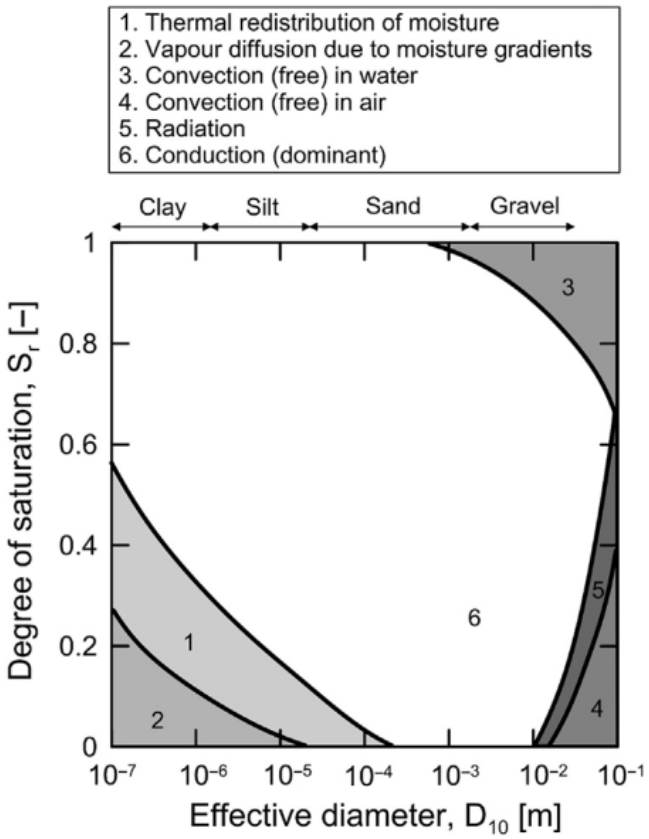

Figure II. 8. Modes of heat transfer in soils based on saturation level, and effective particle diameter *[39]*

The impact of the degree of saturation and effective soil particle diameter (D_{10}) on the primary heat transfer mechanisms is depicted in Figure II.8. Heat transfer is primarily controlled by the thermal redistribution of moisture and vapor diffusion due to moisture gradients in fine, poorly saturated soils like clay and silt. On the other hand, free convection in water takes over coarse, saturated soils like sand and gravel, promoting heat transfer through fluid movement. Free air convection and radiation become more significant in dry, coarse-textured soils. But in most cases, the thermal conduction mechanism remains predominant, at least for moderately saturated soils where neither vapor diffusion nor convection is important. The nature of soil and it moisture content hence become vital factors in the design and efficiency of the underground heat exchange systems, which makes the above observations highly relevant to geothermal energy [39, 53].

There are various methods for determining the level of saturation in soil, and each has advantages and disadvantages of its own. The most popular and conventional approach is

gathering small soil samples and weighing them both before and after drying to calculate the moisture content. Despite being simple and popular, this method takes a lot of time and cannot be used repeatedly in the same spot without uprooting the soil. Digital image processing is a more sophisticated option that examines variations in soil color as moisture levels change. This approach is more effective for field applications since it can be used to evaluate broader regions instead of just particular locations. Direct measurements of the saturation level can also be obtained using other methods, such as electrical resistivity, neutron moderation, and gamma-ray densitometry. Still, they need specific tools and meticulous calibration. Another indirect method uses the soil water characteristic curve, which calculates saturation by examining the connection between soil suction and water content, which is usually measured using tensiometers. Furthermore, dielectric-based techniques that measure moisture levels using electromagnetic signals include frequency domain reflectometry (FDR) and time domain reflectometry (TDR). Factors such as cost, accuracy, and whether repeated measurements over time are required to determine the best approach [54].

II. 5. Thermal properties

II.5.1. Thermal Conductivity

Thermal conductivity (k_s) is the amount of heat (in watts) that flows through a material that is one meter thick and one square meter in area when its two faces have a temperature differential of one K. The unit of measurement is W/m.K. The material is more insulating if the value is lower. When a material's thermal conductivity is less than 0.065 W/m.K., it is considered insulating [55]. Figure II.9 illustrates the Thermal conductivity of several materials of construction.

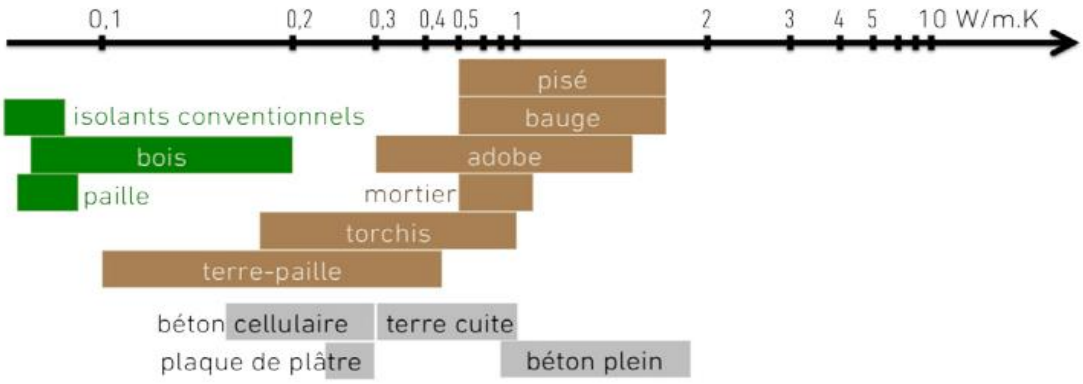

Figure II. 9. thermal conductivity of a few materials [55]

Soils' composition, water content, and structure are the primary determinants of their thermal conductivity. The thermal conductivity value for each type of soil is displayed in the following table, which also highlights some materials of the energy Geostructures.

Table II. 2. Thermal conductivity of materials used in energy Geostructures [56]

Materials	Thermal conductivity	
	Dry	Saturated
Clay	0.4-1.0	0.9-2.3
Silt	0.4-1.0	0.9-2.3
sand	0.3-0.8	1.7-5.0
Gravel	0.4-0.5	1.8
Peat	0.2-0.7	
Claystone / Siltstone	1.1-3.5	
Sandstone	1.3-5.1	
Quartzite	3.6-6.6	
Marl	1.5-3.5	
Limestone	2.5-4.0	
Argillaceous schists	1.5-2.1	
Metaquartzite	5.8	
Marble	1.3-3.1	
Gneiss	1.9-4.0	
Rhyolithe	3.1-3.4	
Granite	2.1-4.1	
Concrete	0.9-2.0	
Steel	14-60	

Soil thermal conductivity is a significant parameter with many uses, including modeling land-surface water and energy interactions, as well as calculating geothermal energy [57]. A wide range of factors impact soil thermal conductivity Compositional factors encompass mineral composition, particle size, shape, and gradation, environmental parameters comprise water content, density, and temperature. Additional factors involve the properties of soil components,

ions, salts, additives, and hysteresis effects [58]. Several studies have proposed various approaches for evaluating soil thermal conductivity some of them are listed bellow

a) Kersten 1949 model

The thermal conductivities of nineteen distinct soil types were compared by Kersten [59] using a single thermal probe. The soils of the different types included five gravels and sands, six sandy and clayey soils, seven crashed stones and mineral soils, and one organic soil. Temperature, density, water content, saturation level, soil texture, and mineralogy were the parameters which were considered to study the soil thermal conductivity. The equations obtained from this model are as follows

1- Unfrozen silts and clay soils

$$k_s = 0.1442[0.9\log(\theta) - 0.2]10^{0.6243\gamma_d} \quad \text{(II.5)}$$

2- Unfrozen sandy soils

$$k_s = 0.1442[0.7\log(\theta) + 0.4]10^{0.6243\gamma_d} \quad \text{(II.6)}$$

Where γ_d and θ are the dry density of soil (kg/m^3) and the water content (%) respectively [58].

b) de Vries (1963) model

The Maxwell equation for electrical conductivity of a mixture of granular materials dispersed in a continuous fluid served as the basis for the de Vries (1963) model [60]. According to de Vries (1963), soil comprises ellipsoidal soil particles and a continuous medium of water or air. The following formula is used to estimate the thermal conductivity of soil.

$$k_s = \frac{f_0\lambda_0 \sum_{n=1}^{N} k_n f_n \lambda_n}{f_0 + \sum_{n=1}^{N} k_n f_n} \quad \text{(II.7)}$$

Here, N represents the number of different types of ellipsoidal particles, while $f_0$and f_n denote the volume fractions of the continuous medium and the ellipsoidal particles, respectively. Similarly, λ_0 and λ_n correspond to the thermal conductivities of the continuous medium and the ellipsoidal particles, respectively.

c) Johansen 1974

Johansen [61] developed the normalized thermal conductivity $k_r$commonly known as the Kersten number. He suggested employing the k_r-S_r relationship to reflect the impact of soil type, porosity, moisture content, and mineralogy on thermal conductivity. a relationship

between k_s and k_r for unsaturated soils was established, based on the k_s values at both dry and saturated states

$$\begin{cases} k_s = (k_{sat} - k_{dry})k_r + k_{dry} \\ k_r = \dfrac{k - k_{dry}}{k_{sat} - k_{dry}} \end{cases} \quad \text{(II.8)}$$

1- Median and fine sands

$$k_r = 0.7\log(S_r) + 1 \quad \text{(II.9)}$$

2- Fine soils

$$k_r = \log(S_r) + 1 \quad \text{(II.10)}$$

3- Frozen fine sand and fine soils

$$k_r = S_r \quad \text{(II.11)}$$

Where S_r is the saturation degree

The thermal conductivities of soil under fully saturated and dry conditions are represented by k_{sat} and k_{dry}, respectively ($Wm^{-1}K^{-1}$).

$$k_{sat} = k_w^n k_{sol}^{1-n} \quad \text{(II.12)}$$

k_w *and* k_{sol} are the thermal conductivity of water and solid respectively ($Wm^{-1}K^{-1}$).

$$k_{dry} = \frac{0.137\gamma_d + 64.7}{2650 - 0.947\gamma_d} \quad \text{(II.13)}$$

The thermal conductivity model provided by Johansen is as follows:

$$k_s = \left(k_w^n k_{sol}^{1-n} - \frac{0.137\gamma_d + 64.7}{2650 - 0.947\gamma_d}\right)k_r + \frac{0.137\gamma_d + 64.7}{2650 - 0.947\gamma_d} \quad \text{(II.14)}$$

d) Donazzi 1979

The exponential function below was used by Donazzi [62] to describe the relationship between thermal resistivity ρ which is the inverse of thermal conductivity and porosity n and saturation degree S_r [63].

$$\rho = \rho_{wat}^n \rho_0^{1-n} \exp\left(3.08(1 - S_r)n\right) \quad \text{(II.15)}$$

Where ρ_{wat} is the water thermal resistivity (ρ_{wat} = 1.7 mK/W) and ρ_0 is the thermal resistivity of bulk material (m K/W)

e) Farouki–de Vries model (1981, 1982)

The de Vries (1963) model can describe frozen soil. To estimate the k_s of moist unfrozen and frozen soil, Farouki (1981, 1982) used liquid water as the continuous medium and treated soil minerals as uniform particles in the de Vries (1963) model (henceforth referred to as the Farouki–de Vries model) [60]

f) Chung & Horton 1987

Chung and Horton [64] described a simple empirical equation for thermal conductivity as a function of water content.

$$k_s = b_1 + b_2\theta + b_3\theta^{0.5} \quad \text{(II.16)}$$

where b_1, $b_2$and $b_3$are empirical parameters giving in W/m/K as mentioned above in the Table.

Table II. 3. Empirical Parameters of Eq. (II.15) *[64]*

Parameter	Clay	Loam	sand
b_1	-0.197	0.243	0.228
b_2	-0.962	0.393	-2.406
b_3	2.521	1.534	4.909

g) Coté and Konrad 2005

Based on the normalized thermal conductivity concept, Coté and Konrad [65] created a generalized thermal conductivity model for various soil types.

$$\begin{cases} k_s = (k_{sat} - k_{dry})k_r + k_{dry} \\ k_{dry} = \chi \times 10^{-\eta n} \\ k_r = \dfrac{\kappa S_r}{1 + (\kappa - 1)S_r} \end{cases} \quad \text{(II.17)}$$

For unfrozen soils $$k_{sat} = k_s^{1-n} \times 0.6^n \quad \text{(II.18)}$$

Tables II.3 and II.4 show the values of κ for certain soils and the χ and η values, respectively.

Table II. 4. κ values *[65]*

Unfrozen soils	κ
Gravel and coarse sands	4.60
Medium and fine sands	3.55
Silty and clayey soils	1.90

Table II. 5. χ and η values *[65]*

materials	χ	η
Cracked Rocks and gravels	1.70	1.80
Natural mineral soils	0.75	1.20
Organic fibrous soils (peat)	0.30	0.87

h) Lu et al. 2007

Lu and al. [66] conducted a series of indoor thermal conductivity tests on 12 kinds of natural soils using a Thermo-TDR probe under different property and moisture content conditions. Based on Johansen's [61] prediction model, a thermal conductivity prediction model was developed, expressed in the following formula:

$$k_s = [k_w^n k_{sol}^{1-n} - (b - an)]exp\left[\alpha_1(1 - S_r^{\alpha_1 - 1.33})\right] + (b - an) \quad \text{(II.19)}$$

Where *a* and *b* are parameters used for determining the thermal conductivity of dry soil, with recommended values of *a*= 0.56 and *b*=0.51, respectively. The coefficient α_1, which takes values of 0.96 and 0.27 for coarse and fine-textured soils, respectively, indicates how soil type affects k_r.

i) Chen 2008

Based on eighty needle-probe experimental experiments on four distinct types of sandy soils with variable porosities and saturation levels, an empirical equation was developed. The empirical parameters in the formula, κ_1 and κ_2, were determined by fitting the data that was collected. The proposed values are κ_1 = 0.0022 and κ_2 = 0.78 [63].

$$k_s = k_w^n k_{sol}^{1-n}[(1 - \kappa_1)S_r + \kappa_1]^{\kappa_2 n} \quad \text{(II.20)}$$

j) Lu et al. 2014

Lu et al. [67] proposed an exponential function to express the nonlinear relationship between k_s and water content θ.

$$\begin{cases} k_s = k_{dry} + \exp(\beta - \theta^{-\omega}) \\ k_{dry} = -0.56n + 0.51 \end{cases} \quad \text{(II.21)}$$

Table II. 6. Empirical parameters *[66]*

soil	Bulk density (gcm^{-3})	Porosity (n)	ω	β	k_{dry} [$Wm^{-1}K^{-1}$]
sand	1.6	0.4	0.24	1.86	0.29
loam	1.2/1.3/1.4	0.51	0.35	1.58	0.23

k) Nowamooz et al. 2015

Nowamooz et al. [68] proposed a theoretical relationship between thermal conductivity k_s and S_r for multilayered soils.

$$k_s = (0.443x_s + 0.081\gamma_d)\frac{(4.4x_s + 0.4)S_r}{1 + (4.4x_s - 0.6)S_r} + 0.087x_s + 0.019\gamma_d \quad \text{(II.22)}$$

Where x_s and γ_d denote soil sand content, dry unit weight [kNm^{-3}] respectively.

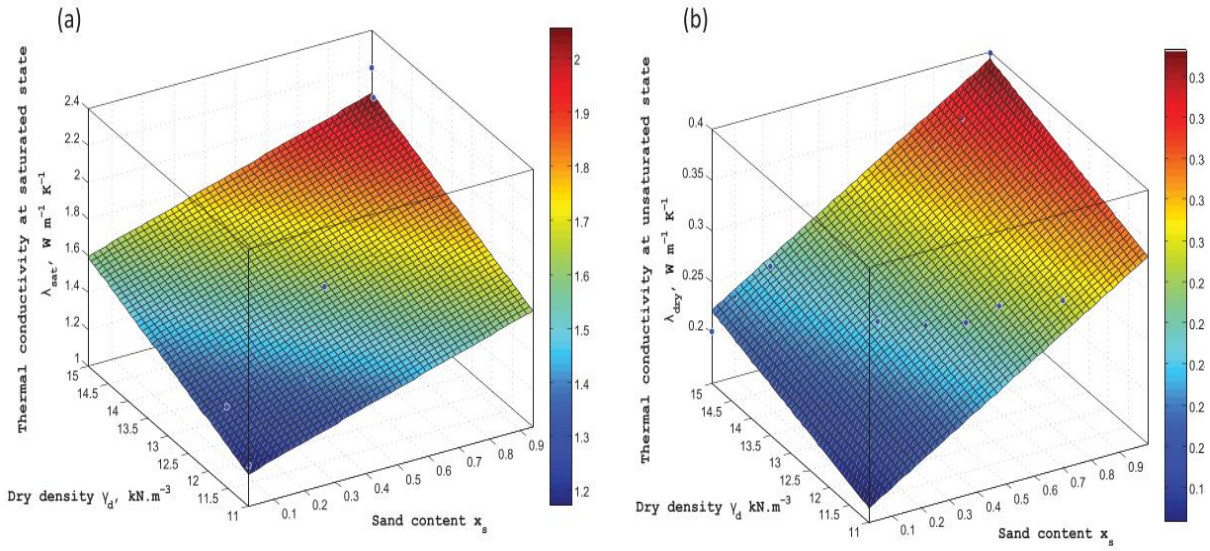

Figure II. 10. Thermal conductivity surface fitting values adapted from Lu et al. [66] for (a) saturated and (b) unsaturated condition as a function of sand content and dry density [68]

Figure II.10 presented by Nikoosokhan et al.[68] shows how sand content and dry density affect soil's thermal conductivity under both saturated and unsaturated situations. Sand content and dry density raise the saturated state's thermal conductivity, which indicates that water in the pores increases heat transmission. In the unsaturated conditions, the values are smaller than in the first condition; however, the curve's trend is similar. The reason for this discrepancy is that the air in the pores limits the heat conductivity and acts as an insolation. Though this effect is

reduced when the soil is unsaturated, heat conductivity generally rises with soil dry density and sand content. This indicates how composition and compaction affect the thermal characteristics of soils and support water's significant importance in thermal transmission.

a) Influence water content on the thermal conductivity

The heat transfer in soil depends a lot on moisture content and its texture. Research on various soil types indicates that the texture of the soil has little effect on how well it conducts heat when it is completely dry. However, as moisture levels increase, things change. Sandy soils typically have higher thermal conductivity than finer soils, with the highest values found in soils that contain a lot of quartz, which is excellent at transferring heat. However, not all soils experience the same increase in conductivity. The change occurs gradually in finer soils, rapidly in sandy soils, and much more slowly in clay. In particular, clay requires a lot more water before heat can pass through it effectively, probably due to its large surface area and small particles. All these results are illustrated in Figure II. 11, Which illustrates the k_s-θ relationship.

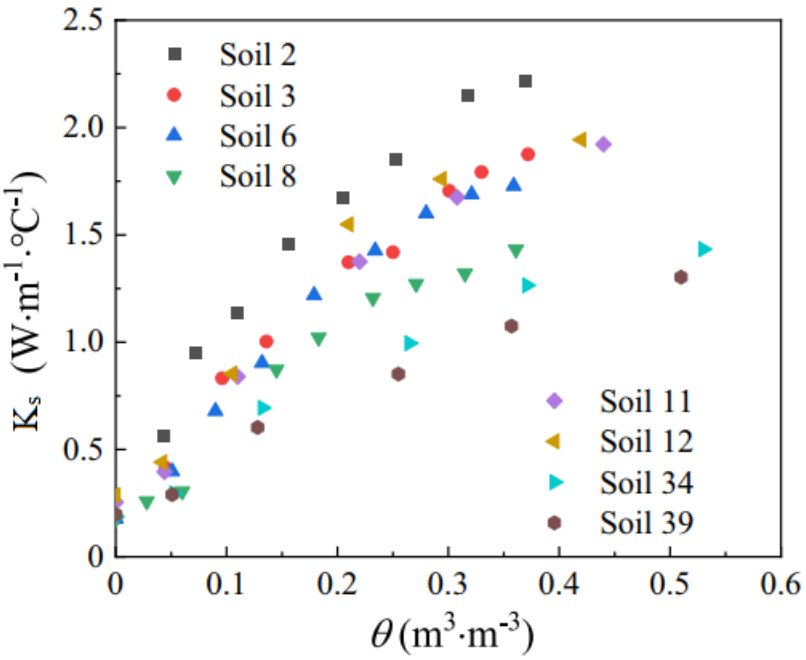

Figure II. 11. k_s-θ relationship [69]

Figure II.12 shows 3D graphs illustrating how thermal conductivity (k_s) varies with water content (θ) and bulk density (ρ_b) for three different soil types. The data range from dry to fully saturated conditions. All three soils follow a similar pattern as bulk density varies under dry conditions. However, as moisture and density increase, sand's thermal conductivity rises sharply at low moisture levels before stabilizing, while clay shows a much slower increase, becoming

noticeable only near saturation. All soils were modeled using the same scales giving a different value of maximum conductivity for each higher for sand and loam, and lower for clay. Actually, clay has more pores and its thermal conductivity at full saturation is probably closer to that of other soils than it appears in the same figure [67].

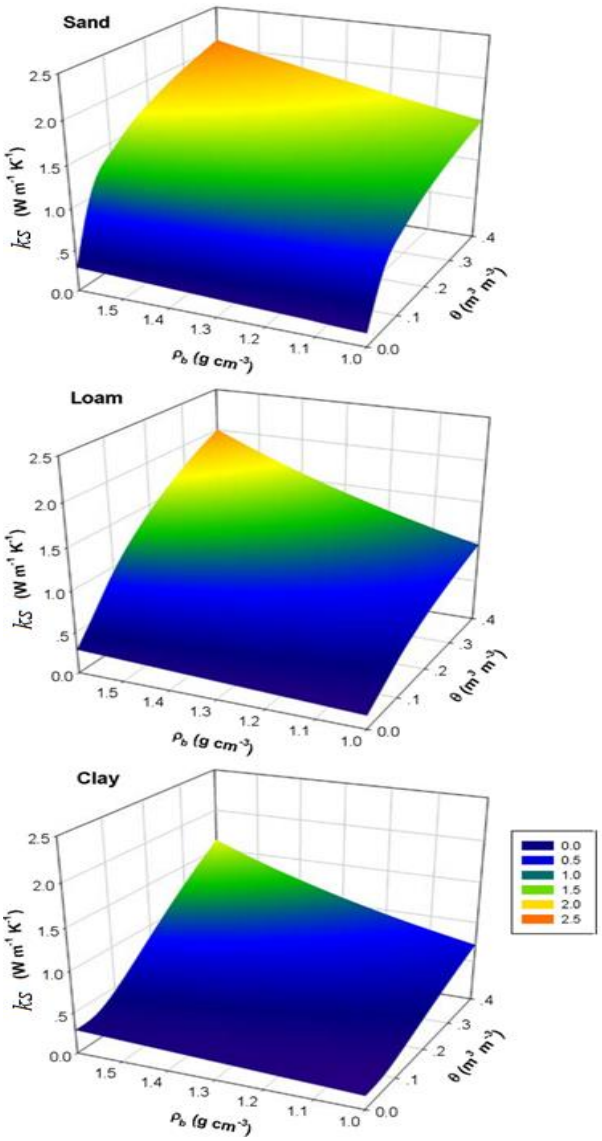

Figure II. 12. Thermal conductivity for three hypothetical soils as a function of bulk density and soil water content [67]

Researchers [66] investigated how soil texture and water content affect thermal conductivity, showing that water content plays the biggest role in how heat moves through soil in situ conditions. This finding supports previous studies that highlight the difficulty of measuring the thermal conductivity in the field, since water content constantly change, making direct measurement tricky

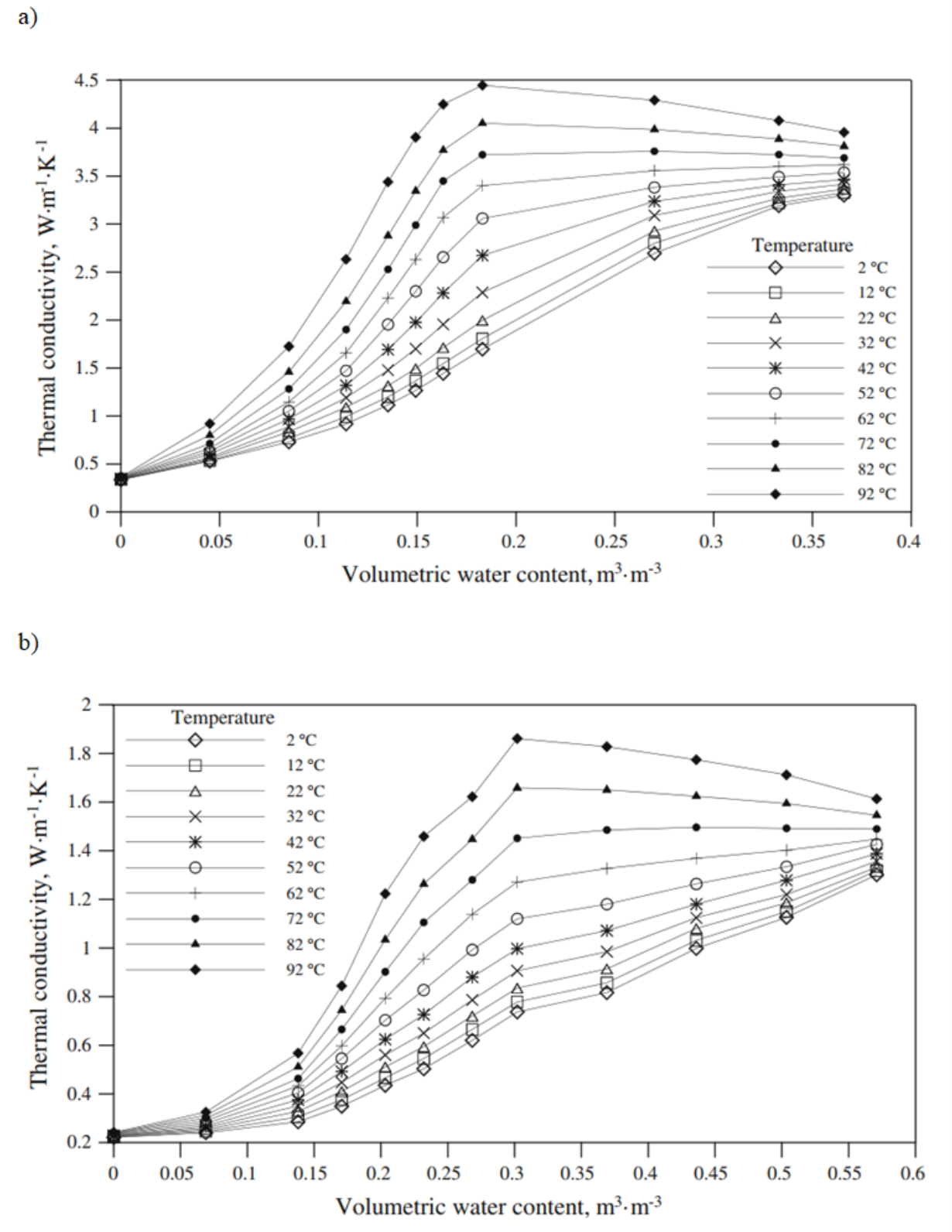

Figure II. 13. Variation in Thermal Conductivity with Volumetric Water Content and Temperature of (a) Ottawa Sand and (b) Richmond Hill Fine Sandy Loam [70]

. In order to cope with this problem, scientists have come up with models that can predict k_s using the basic properties of soils, which are easier to measure. These models help simplify the

process and make it more practical for applications such as geothermal energy, soil management, and climate studies. Since the texture and moisture of the soil interact in affecting the transfer of heat, the improvement of these models is the key to making more accurate predictions and a better understanding of how soil behaves under different conditions.

The thermal conductivity of Ottawa sand and Richmond Hill fine sandy loam varies with water content and temperature in three stages as illustrated in Figure II.13. First, conductivity gradually rises as water coats soil particles at low moisture levels. Because of vapor migration, conductivity increases dramatically as water fills the voids above the permanent wilting point, particularly at temperatures above 62°C. At very high temperatures (65–70°C), conductivity slightly drops because trapped air pockets limit heat transfer, and extra moisture has little effect beyond field capacity. The thermal conductivity of Ottawa sand is 1.5 to 2.6 times higher than that of Richmond Hill fine sandy loam. Conductivity varies very little at lower temperatures (2–30°C), where conduction predominates. However, above 40°C, vapor migration greatly improves heat transfer [70].

b) Influence of the porosity on the thermal conductivity

Compared to other soil properties, few studies examined the effect of porosity on soil thermal conductivity despite its crucial role in heat transfer. In 2001, research [71] was conducted to determine the impact of porosity on the thermal conductivity of soil.

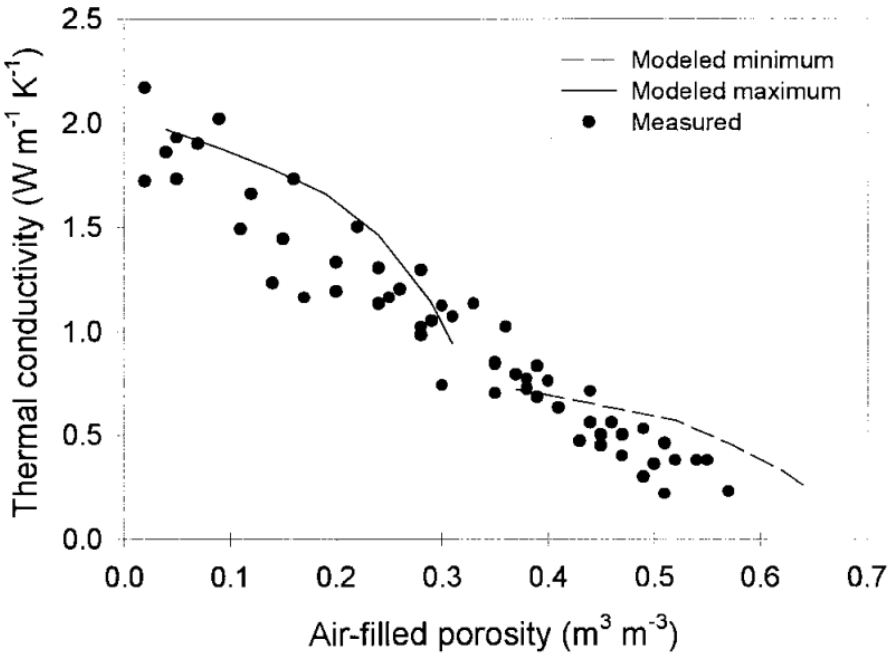

Figure II. 14. The relationship between air-filled porosity and thermal conductivity [71].

Figure II.14 illustrates this relationship, showing that thermal conductivity decreases as air-filled porosity (n) increases. This occurs because air is a poor conductor of heat compared to water, reducing overall heat transfer. Furthermore, the values predicted by the de Vries model closely align with experimental measurements, highlighting the critical role of porosity in soil thermal properties. Based on these findings, porosity must be carefully considered in geothermal applications.

Most of the earlier research believed that the primary determinants of soil thermal conductivity at room temperature were porosity and quartz content[61, 71]. The relationship between porosity (n) and dry conductivity (k_{dry}) is shown in Figure II.15. It is evident that k_{dry} decreases linearly with n, suggesting that porosity is an important factor in heat transfer. This leads to consider the impact of porosity on geothermal transfer and the use of energy Geostructures.

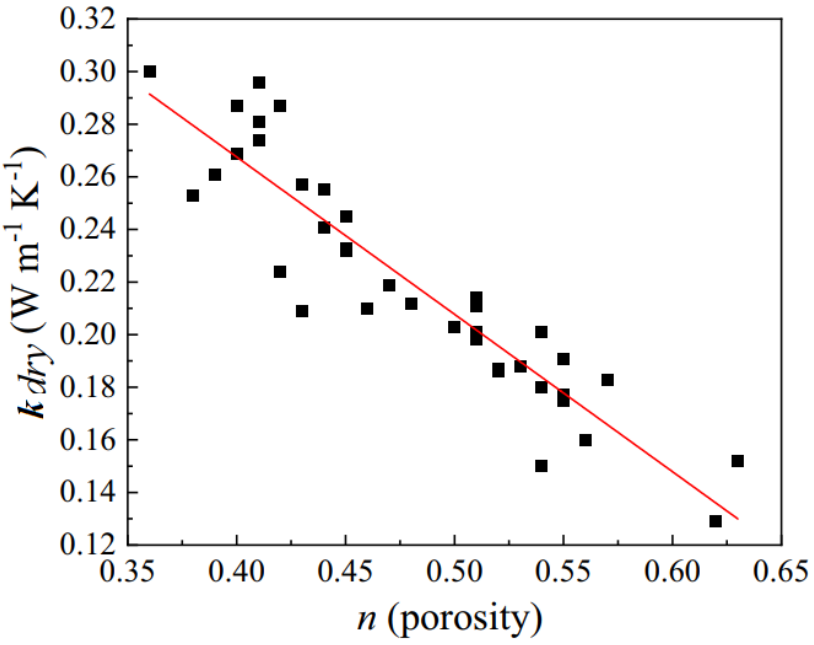

Figure II. 15. The correlation between porosity and dry soil thermal conductivity [69]

c) Influence of saturation level on thermal conductivity

The thermal conductivity of the soil is strongly influenced by its saturation stage, which goes through three distinct stages, as shown in Figure II.17: First Stage - In the initial saturation stage, the moisture starts forming a thin film around the soil particles, but the air-filled voids between the particles remain unfilled, and thus, only a minimal rise in thermal conductivity takes place.

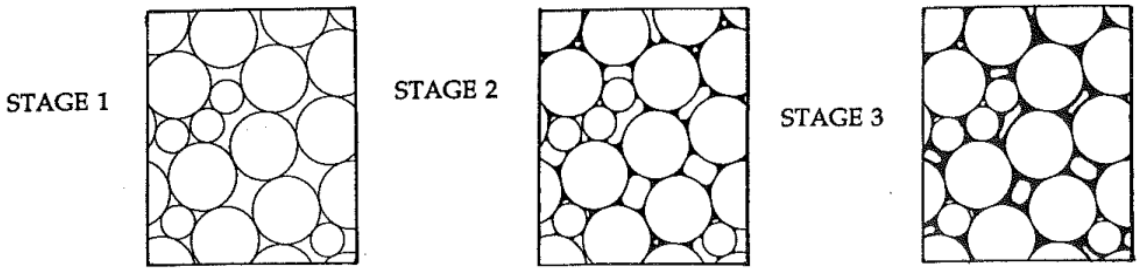

Figure II. 16. Saturation Stages in Granular Media: From Surface Coating to Void Filling [72]

In the second stage, as saturation increases, water will begin to fill these voids and create more efficient pathways for heat conduction, thus giving a steep rise in thermal conductivity. Finally, in the third stage, when the soil is fully saturated, and all the voids are filled with water, further moisture does not contribute to the heat transfer process, hence stabilizing thermal conductivity. This three-phase development shows how important saturation is in determining the thermal behavior of the soil [72].

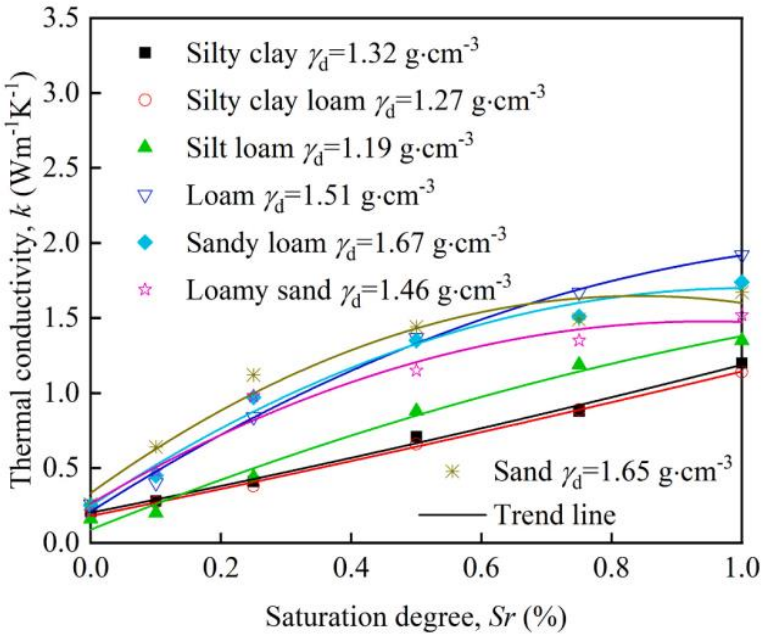

Figure II. 17. k_s-S_r relationship [73]

Another study [73] was conducted to analyze the impact of S_r on soil thermal conductivity, demonstrating its influence on heat transfer properties. Figure II.17 illustrates how the thermal conductivity value increases in tandem with saturation. The soil contains more water when the saturation values are higher. Additionally, water in the soil would create water bridges, or a water film, around soil particles, lowering the air content of the soil. These water films and bridges increase heat transfer because water has a much higher thermal conductivity than air.

The contact areas between particles grow as soil water saturation rises, which again makes it easier for heat transfer and, consequently, thermal conductivity to increase.

II.5.2. Volumetric heat capacity

The amount of heat energy required to raise a given volume of material's temperature by one degree is known as the volumetric heat capacity (c_v). In the case of soil, this property comes from a mix of its components, such as minerals, water, air, and vapor, all working together to determine how well it stores and transfers heat [74]. This makes it an essential factor in fields like engineering and agriculture, where understanding heat behavior in the soil is crucial [75]. In general, the volumetric heat capacity is calculated as represented in the equation bellow[53].

$$c_v = \rho\, c \tag{II.23}$$

As can be seen below, estimating volumetric heat capacity has been the subject of extensive research.

l) De Vries et al. (1963)

De Vries [76] developed an equation to calculate the volumetric heat capacity of frozen and unfrozen soils, formulated as follows:

$$\begin{cases} c_v = c_s(1-\theta_{sat}) + \theta\, c_w + \theta_{ice}\, c_{ice} \\ c_v = 0.46\rho_m + 0.60\rho_o + \rho_w \end{cases} \tag{II.24}$$

Where c and θ stand for volumetric heat capacity and water content, respectively, the indices s, sat, w and ice denote soil, saturated water, and ice, respectively [77]. The volume fractions of water, organic matter, and soil mineral matter are denoted by ρ_w, ρ_o and ρ_m, respectively.

m) Campbell (1985)

Based on the fundamental physical characteristics of soil, Campbell [78] proposed an equation to calculate the volumetric heat capacity, which is the sum of the specific heat of all soil constituents, as mentioned below

$$c_v = c_m\rho_m + c_w\theta + c_a\rho_a + c_o\rho_o \tag{II.25}$$

where ρ is the volume fraction of the component denoted by the indices a, o, w, and m, which represent the air, organic, water, and mineral constituents, respectively. since organic materials and minerals have very similar volumetric specific heats, the volumetric heat capacity was as follows[78]:

$$c_v = c_m(1-n) + c_w\theta \tag{II.26}$$

n) Ghuman et al. (1985)

Ghuman et al. [79] developed another equation to calculate the volumetric heat capacity formulated as follows:

$$c_v = \rho_b e^{-0.003X-1.071} \quad \text{(II.27)}$$

X is the total percentage of sand, silt, and organic matter; ρ_b is the bulk density of the soil [g cm^{-3}]

o) Sikora and Kossowski (1993)

As mentioned below, Sikora and Kossowski [80] proposed an empirical formula to calculate the volumetric heat capacity.

$$c_v = (c_s + 4.19 \times 10^{-3}\theta)\rho_b \quad \text{(II.28)}$$

ρ_b [Mgm^{-3}] is the bulk density, and c_s is the specific heat of the soil solid [Jkg^{-1} K^{-1}].

p) Abu-Hamdeh (2003)

A study conducted by Abu-Hamdeh [81] developed an equation to determine the volumetric heat capacity based on the density of both water and soil, as mentioned below

$$c_v = \rho_d c_s + \rho_w c_w \theta \quad \text{(II.29)}$$

Where ρ_d is the dry density of soil.

q) Tang and Nowamooz (2018)

Tang and Nowamooz [74] proposed a new approach to calculate the volumetric heat capacity in function of the saturation level of the soil

$$c_v = (4.18 - 0.95\rho_b - 0.3x_s)S_r + 0.9\rho_b - 0.2x_s \quad \text{(II.30)}$$

Estimating a material's volumetric heat capacity is typically easier than its thermal conductivity. In these situations, a representative estimate of the material's effective volumetric heat capacity can be obtained using a linear function of the capacities and volume ratios of the phases that characterize it, instead of estimating the effective thermal conductivity [39]. Table II. 7. lists typical volumetric heat capacity values for various materials used in energy Geostructures applications.

Table II. 7. Volumetric heat capacity of some materials *[39]*

Materials	Volumetric heat capacity [$MJm^{-3}K^{-1}$]	
	Dry	Saturated
Clay	1.5-1.6	1.6-3.4
Silt	1.5-1.6	1.6-3.4
sand	1.3-1.6	2.2-2.9
Gravel	1.4-1.6	2.4
Peat	0.5-3.8	
Claystone / Siltstone	2.1-2.4	
Sandstone	1.6-2.8	
Quartzite	2.1-2.2	
Marl	2.2-2.3	
Limestone	2.1-2.4	
Argillaceous schists	2.2-2.5	
Micaschists	2.2	
water	4.182	
Concrete	1.8-2.0	
Steel	3.12	

The change of the volumetric heat capacity as a function of water content for various dry densities of a material represented by Dysli 1991 [39, 82] is shown in Figure II.18. At low water contents, the volumetric heat capacity increases nearly linearly, but as saturation is reached, it slows down. The initial heat capacity of materials with higher densities is greater than that of materials with lower densities. All curves converge towards the upper limit of the heat capacity at saturation, which is represented by the dotted curve. In geotechnics and thermal engineering in particular, this relationship is essential for thermal modeling of soils, insulating materials, and heat storage applications [39].

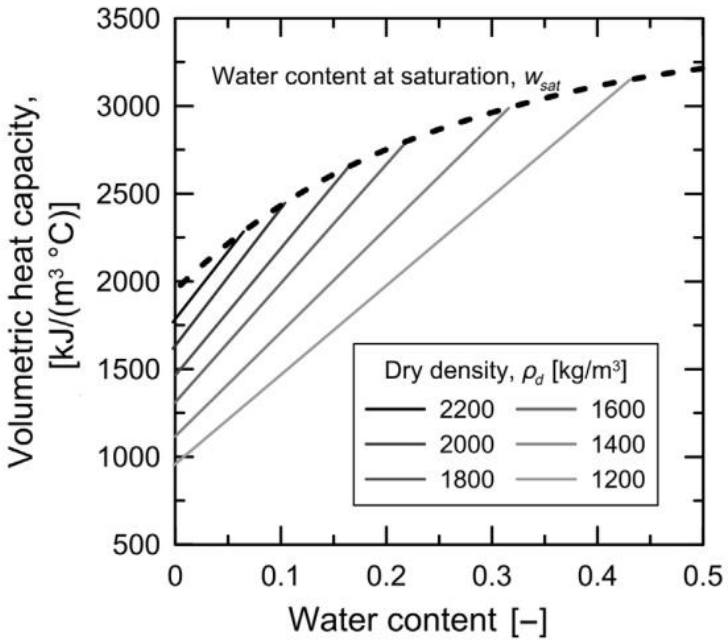

Figure II. 18. Volumetric heat capacity for unfrozen soils as a function of water content *[39, 82]*

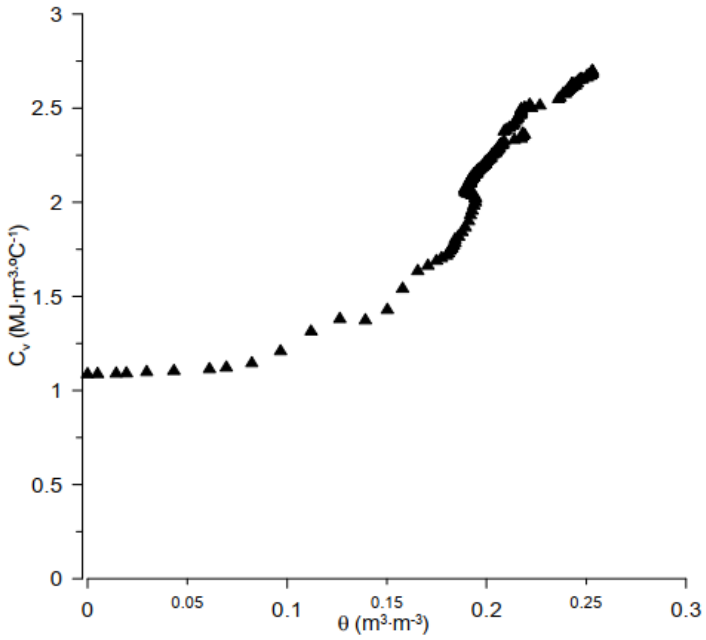

Figure II. 19. Influence of water content on the volumetric heat capacity [83]

Studies [83] were conducted to ascertain how water content affected the volumetric heat capacity of silt loam soil, as illustrated in Figure II.19. According to the results, the volumetric heat capacity increased as soil moisture increased. Water contents and volumetric water contents changed linearly.

II. 6. Conclusion

Regarding the practical storage and transfer of heat underground, soil is crucial to the operation of geothermal systems. This chapter examines some of the most critical soil characteristics that significantly impact the operation of geothermal installations, like density, water content, porosity, heat capacity, thermal conductivity, and saturation level. One of the most important conclusions drawn from this material is that heat transfer is most affected by soil density and moisture content. Although improved heat conduction results from more water in the soil, this effect peaks when the soil is completely saturated. Heat is generally transferred more effectively by denser soils than by large air-filled voids, which are essentially poor heat conductors.

Researchers and engineers developed numerous models and experimental techniques to forecast the thermal response of various soil types. The utilization of geothermal energy for space heating, cooling, and renewable energy generation will improve as the interactions will be better understood. Field testing and model building will be essential to improve soil characterization. Designing geothermal energy systems that are affordable and sustainable as a renewable energy source will be easier if the behavior of soil is well studied.

Chapter III

Heat Transfer in Soils: Fundamental Mechanisms and Governing Equations

III.1. Introduction

Heat is a type of energy that inherently transfers from an area of elevated temperature to an area of reduced temperature due to thermal gradients. This procedure persists until thermal equilibrium is attained. The kinetic energy of a substance's particles, which increases with temperature, drives heat transfer. As kinetic energy rises, increased particle vibration and interaction encourage heat transfer. This chapter offers an in-depth exploration of heat transfer phenomena, detailing the fundamental principles of thermal energy, heat, and temperature. It emphasizes the critical role of temperature gradients in driving heat flow. The governing equations, based on the principle of conservation, are presented to describe thermal and hydraulic transfer within the soil. Additionally, empirical models, including the Richards equation and the van Genuchten-Mualem model, are introduced to support the numerical analysis of moisture transport in unsaturated soils.

III.2. Thermal energy, heat and temperature

III.2.1. Thermal energy

According to thermodynamics, energy can be transferred as work and heat through interactions between a system and its surroundings. However, thermodynamics only considers the system's initial and final states at equilibrium; it does not reveal the type of interactions at play or how the system changes over time between the two equilibrium states.

In order for heat transfer to take place within a system, temperature gradients between its various components must exist. This indicates that the system is not in thermodynamic equilibrium, meaning that the temperature is not constant throughout. Temperature will change in both space and time as the system transitions to a final state of equilibrium. Finding the transfer modes involved in the transformation and quantitatively assessing the temperature variations at each system point over time are the goals of heat transfer analysis.

III.2.2. Heat

Heat is simply energy in motion, it moves from one place to another. When you put a warm object next to a cooler one, heat naturally flows from the warmer side to the cooler side until both reach the same temperature. In this process, the warmer object gives up some of its energy (ΔE), while the cooler one absorbs the same amount. In other words, heat isn’t something an object has; it’s the energy being transferred between them. That’s why we define heat as the

energy that moves between two systems (or between a system and its surroundings) due to a temperature difference [84].

III.2.3. Temperature

Temperature is essentially a measure of how much energy the molecules in a substance have as they move around randomly. The system has more energy overall and moves more quickly at higher temperatures. Since temperature indicates the amount of thermal energy actively involved, it can be thought of as the intensity of this movement. Although molecules are responsible for the majority of this energy, they can also rotate and vibrate in ways that do not affect temperature. The way that energy is distributed determines whether two objects with the same total energy have the same temperature.

III.3. Heat transfer mechanism

The exchange of thermal energy between physical systems, impacted by temperature variations and the medium's characteristics, is known as heat transfer. Heat transfer can occur in three main ways: conduction, convection, and radiation (Figure III.1). Direct contact causes conduction, also referred to as diffusion, whereas fluids move through convection spontaneously (free convection) or as a result of outside forces (forced convection). Radiation does not require a medium and occurs via electromagnetic waves. Heat transfer from high to low temperatures is regulated by the second law of thermodynamics, which raises the system's entropy until thermal equilibrium is achieved. A substance's volume changing due to temperature changes is called thermal expansion. Understanding energy flow and thermodynamic applications requires an understanding of these concepts [85].

Thermal modeling of the soil in this thesis relies on several simplifying hypotheses for the purpose of accurately representing its hydric and thermal behavior. The soil is represented at the representative elementary volume (VER) scale as a three-phase medium consisting of a rigid, homogeneous, and isotropic solid phase having thermophysical properties that are not dependent on temperature and that do not undergo chemical reaction with the fluids. The liquid phase is continuous in the pore space and comprises pure water only, and it is incompressible and non-dilatable. The gas phase is constituted by air and water vapor which are treated as perfect gases in thermodynamic equilibrium with a constant pressure which is equal to atmospheric pressure. Also, the mass heat of the various phases is assumed to remain constant in the temperature range under consideration, that is, between 0 and 100°C. The heat conduction

equation ensures an analytical solution to the thermal behavior of the soil under these conditions.

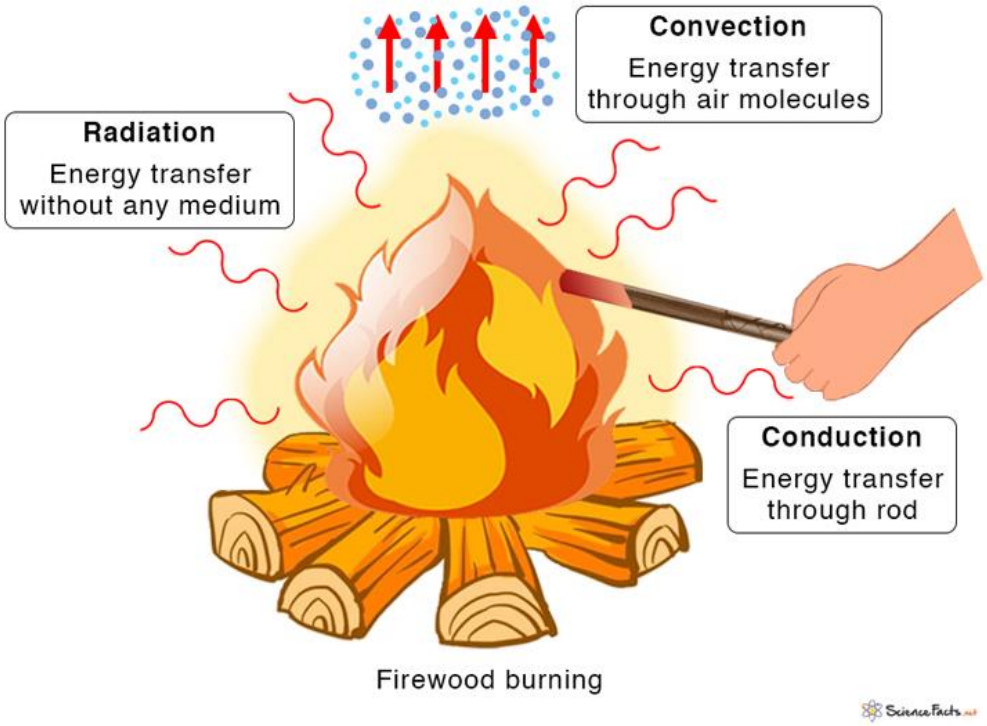

Figure III. 1. Heat transfer modes *[86]*

III.3.1. Conduction

Conduction is the way energy moves through a material without the material itself moving. Heat conduction is when fast (hot) molecules bump into slow (cold) ones, sharing their energy until everything reach the equilibrium temperature. The molecules don't move around physically, only vibrate in place. Energy is conveyed in electrical conduction by tiny, charged particles, such as electrons or ions, moving through a material. It works in solids, liquids, and gases, conducting heat or electricity through direct contact.

Fourier's law of heat conduction provides a mathematical description of how heat transfers through materials. It states that the rate of heat flow dQ/dt in a solid or porous material depends directly on the temperature gradient dT/dL in the direction of heat flow and the cross-sectional area A, as illustrated in Figure III.2 [87]. In other words, the greater the temperature difference, the higher the heat transfer rate per unit area [88].

The rate at which heat moves through a material follows a simple rule: it depends on how steep the temperature difference is across the material. This can be expressed as:

$$\frac{q}{A} \propto \frac{dT}{dx} \tag{III.1}$$

By introducing a proportionality constant, this can be refined to:

$$q = -kA\frac{dT}{dx} \tag{III.2}$$

Here's what each part means:

q is the heat transfer rate (how much heat flows per unit time).

A is the cross-sectional area the heat is passing through.

$\frac{dT}{dx}$ represents how quickly temperature changes over a certain distance (temperature gradient).

k is the thermal conductivity, which tells us how well a material conducts heat (measured in W/m/K)

The negative sign simply means that heat always moves from a hotter area to a cooler one, naturally flowing down the temperature gradient [87].

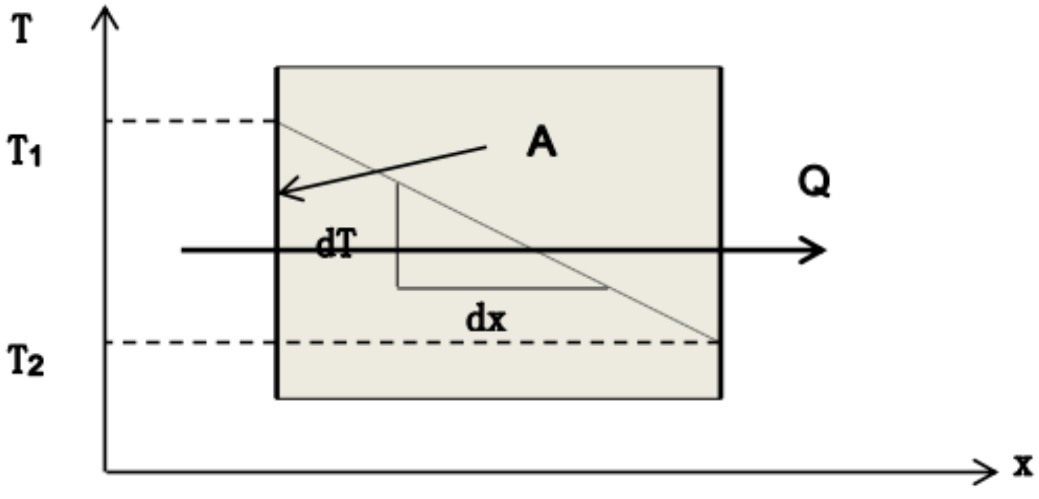

Figure III. 2 Conduction heat transfer in a single direction [87]

Conduction is the main heat transfer method in soils [53] though other processes may also be somewhat involved. Heat conduction in soil happens as thermal energy moves between individual particles and through pore fluids, meaning it takes place across all components of

the soil mass solids, liquids, and gases. The efficiency of heat transfer in soil depends on its thermal properties, the proportion of different soil constituents, and the temperature gradient driving the process.

III.3.2. Convection

Thermal convection is a heat transfer method in which a moving fluid carries thermal energy [84]. Although heat is initially transferred by conduction between an object and a fluid, the fluid's movement provides the majority of the transfer. Convection can occur in two ways: naturally (or freely) when temperature differences create density variations that cause the fluid to circulate and forced when external elements such as wind or a fan impose this movement. This phenomenon is also involved in phase changes, for example, when vapor bubbles rise during boiling or liquid droplets fall during condensation.

Heat transfer between a solid surface and a moving fluid follows a principle established by Sir Isaac Newton in 1701. He determined that this exchange is directly linked to the temperature difference between the two. The greater the difference, the greater the transfer. Newton's law of cooling is described as follows

$$q = hA(T - T_\infty) \tag{III.3}$$

where:

q is the flux of convective heat (W).

A is the area (m^2) where heat is transferred.

T represents the object's temperature (K).

T_∞ is the surrounding fluid's temperature (K).

h is the coefficient of convective heat transfer ($W/m^2/K$). This coefficient depends on numerous parameters (fluid, type of flow, surface condition, etc.) and is therefore very difficult to quantify precisely.

a) Reynolds number

The Reynolds number, which measures the significance of inertial forces in respect to viscous forces, is a dimensionless quantity that defines the forced convection flow regime. It is given by[89]:

$$R_e = \frac{inertia\ forces}{viscous\ forces} = \frac{VL_c}{v} = \frac{\rho V L_c}{\mu} \quad \text{(III.4)}$$

where:

V is the characteristic flow velocity (m.s^{-1}).

L_c is a characteristic length of the system studied (m).

v is the kinematic viscosity of the fluid (m^2/s)

μ is the dynamic viscosity of the fluid (kg.m^{-1}. s^{-1})

ρ is the fluid's density (kg.m^{-3})

b) Grashof number

The Grashof number, which measures the significance of Archimedean forces in respect to viscous forces, is a dimensionless quantity that defines the natural convection flow regime. It is given by [90]:

$$G_r = \frac{\text{Archimedean forces}}{viscous\ forces} = \frac{g\beta\Delta T L_c^3}{v^2} \quad \text{(III.5)}$$

where:

g is the acceleration of gravity (m.s^{-2})

β is the coefficient of thermal expansion (K^{-1})

ΔT is a characteristic temperature difference of the system studied (K).

L_c is a characteristic length of the system studied (m).

v is the kinematic viscosity of the fluid (m^2/s)

c) Prandlt number

As a measure of the relative importance of momentum diffusivity to thermal diffusivity, the Prandtl number characterizes fluid behavior with respect to convective heat exchange. It is given by[91]:

$$P_r = \frac{\text{momentum diffusivity}}{thermal\ diffusivity} = \frac{v}{\alpha} \quad \text{(III.6)}$$

v is the kinematic viscosity of the fluid, which measures the fluid's resistance to flow.

α is the thermal diffusivity of the fluid, which measures the rate at which heat diffuses through the fluid.

d) Nusselt number

The relative importance of heat flux by convection and conduction is measured by the Nusselt number. It is given by [92]

$$N_u = \frac{convective\ flux}{conductive\ flux} = \frac{hL_c}{k} \quad \text{(III.7)}$$

L_c is a characteristic length, k is the fluid thermal conductivity, and h is the effective heat transfer coefficient.

The Nusselt number can be defined locally, as a function of the heat flux exchanged at a specific point, or globally, over an entire surface. The type of flow and fluid involved determine how convection is calculated. In forced convection, it is correlated with Reynolds and Prandtl numbers, while in natural convection, it depends on Grashof and Prandtl numbers.

Groundwater flow is an excellent illustration of forced convection, which has a significant impact on heat transfer in rock and soil. Convection has the potential to raise the soil's apparent thermal conductivity by 20% in certain situations [53].

Convection is crucial in soils, particularly in saturated and partially saturated media. It intensifies with increasing pore size, especially in granular soils with easy water circulation [53]. Convection in soil can be divided into two categories:

r) Natural convection is caused by temperature and density variations, mainly in surface-dry soils.
s) Forced convection which occurs when water or air is forced through the pores of the soil or rock by external pressure (pump, fan…).
t) When two forms of convection coexist in a system, it is called mixed convection.

Convection is a natural phenomenon all around us, frequently without our awareness. It makes the smoke in a fireplace rise, moves the water in a saucepan on the stove, or makes it possible for a room to be warmed by underfloor heating. Conduction in the atmosphere is what causes clouds, thunderstorms, and even tornadoes to form. It is also utilized in technology, such as solar towers that use heated air to generate energy, nuclear power plant cooling, and hot-air balloons. In the oceans, it powers ocean currents that redistribute heat around the planet. Beneath our feet, convection in the Earth's mantle moves tectonic plates and fuels volcanoes.

In the Earth's core, it plays a key role in forming its magnetic field. Convection is a driving force behind our world, impacting our natural balance and everyday lives [93].

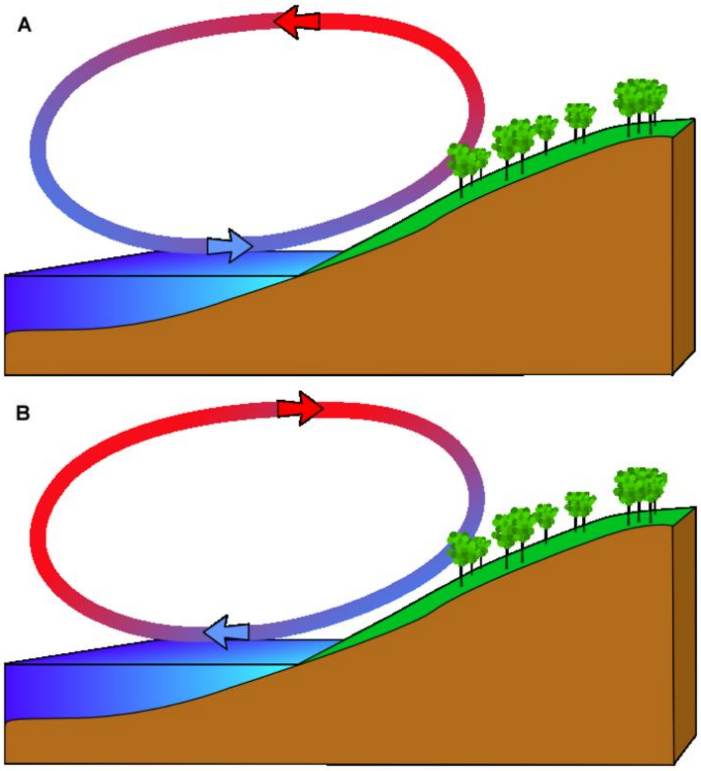

Figure III. 3.Sea Breeze and Land Breeze: Air Circulation in Coastal Areas *[93]*

Figure III.3 illustrates the sea and land breezes caused by thermal convection. During the day (A), warm air over land rises, drawing in cooler air from the sea. The air flow is reversed towards the sea at night (B) as the land cools more quickly than the water. This phenomenon regulates the coastal climate.

III.3.3. Radiation

Thermal radiation is a method of heat transfer that occurs without direct contact between objects as illustrated in Figure III.4. Unlike conduction and convection, which require a material medium to transport heat, radiation relies on the emission and absorption of electromagnetic waves. This allows the Sun to heat the Earth, even though icy space [84, 94].

In this process, a hot body emits energy in the form of electromagnetic waves that travel until another object takes them in. The intensity of this radiation depends on the object's temperature and its ability to emit or absorb heat. The amount of energy emitted has a simple rule stipulated by Stefan Boltzmann's law [84]:

$$q_e = \sigma A T^4 \quad \text{(III.8)}$$

where:

q_e is the amount of heat (W) released.,

σ represents the Stefan-Boltzmann constant ($5.699\times10^{-8}\, W/m^2/K^4$).

A is the surface area of the object (m^2),

T is the absolute temperature (K).

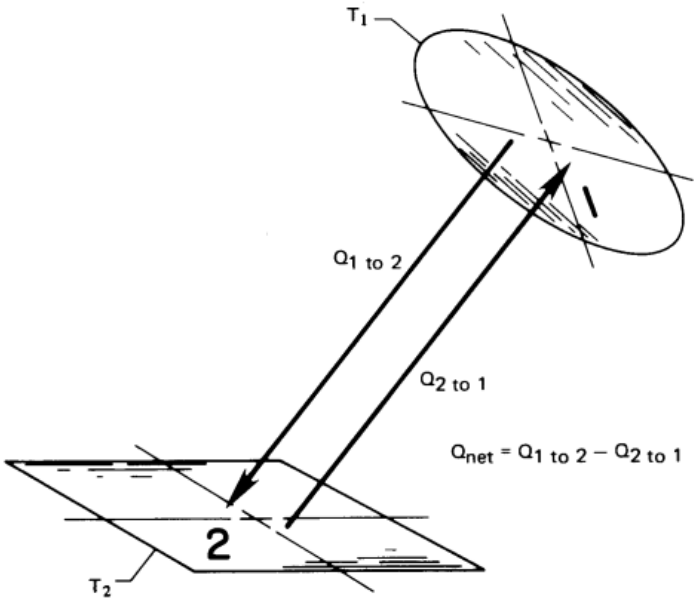

Figure III. 4. Two arbitrary surfaces' radiation *[95]*

When there is an exchange of heat by radiation between two objects at different temperatures, the heat transmitted is given by:

$$Q = -\varepsilon\sigma(T_a^4 - T_b^4) \quad \text{(III.9)}$$

The material's emissivity, denoted by ε, is near 1 for a black body, and T_a and T_b denote the absolute temperatures of the objects (K).

Radiation is a significant factor in the overall energy balance on Earth, affecting the ratio of radiation reflected back into space to that received from the Sun. However, under normal temperatures, radiation typically makes up less than 1% of the total heat transfer in soils, making it a negligible contributor to heat transfer [96]. Nevertheless, in soils with large particles (greater than 20 mm), like dry crushed stone, its effect can become more pronounced, up to 10% [53]. The ability of radiation to transfer heat over long distances is utilized in applications

like solar thermal energy. Mirrors can effectively concentrate the sun's rays, producing energy or heating surfaces [84].

Radiation comes in two primary forms. Short-wave radiation is direct solar radiation, the intensity of which depends on the absorption capacity of the material and the strength of the solar radiation received. Long-wave radiation is emitted by surfaces as a function of their temperature. It follows Stefan-Boltzmann's law, where the amount of heat radiated depends on the material's emissivity, the geometry of the interacting surfaces and the temperature difference between the source and the receiving surface. These phenomena play a key role in areas such as heating buildings, absorbing solar energy and dissipating heat from exposed surfaces [85]. The intensity of those two forms is illustrated in Figure III.5.

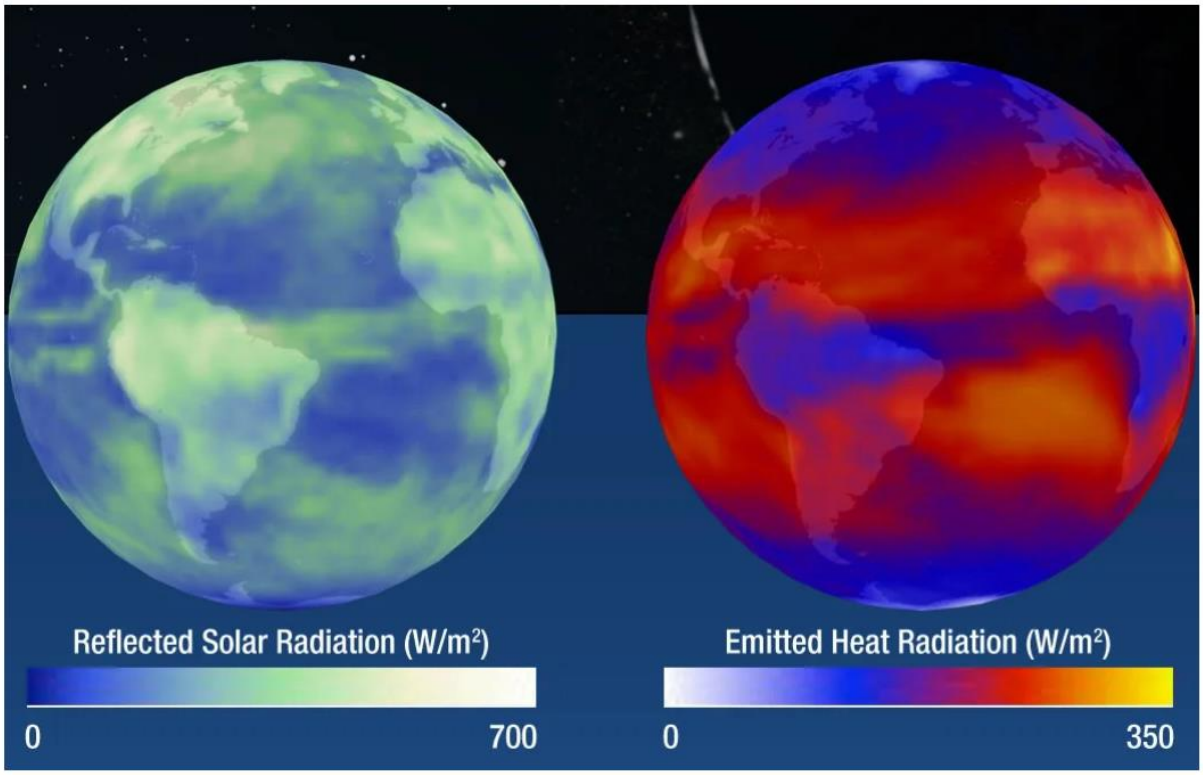

Figure III. 5. Reflected Solar Radiation vs. Emitted Heat Radiation *[97]*

III.4. Heat transfer and fluid flow governing equations

The fluid flow equations are developed from fundamental conservation principles, including mass conservation, Newton's second law, and the first law of thermodynamics. Fluid dynamics describe fluids as continuous media, ignoring molecular structure and describing behavior using macroscopic properties like velocity, pressure, density, and temperature. An analysis of fluid motion includes studying a small fluid element with size δx, δy, δz (Figure III.6) and

investigating changes in mass, momentum, and energy due to fluid flow. For notational simplicity, coordinates and time are typically suppressed. Exact properties at multiple points are represented approximately by a Taylor series expansion [98].

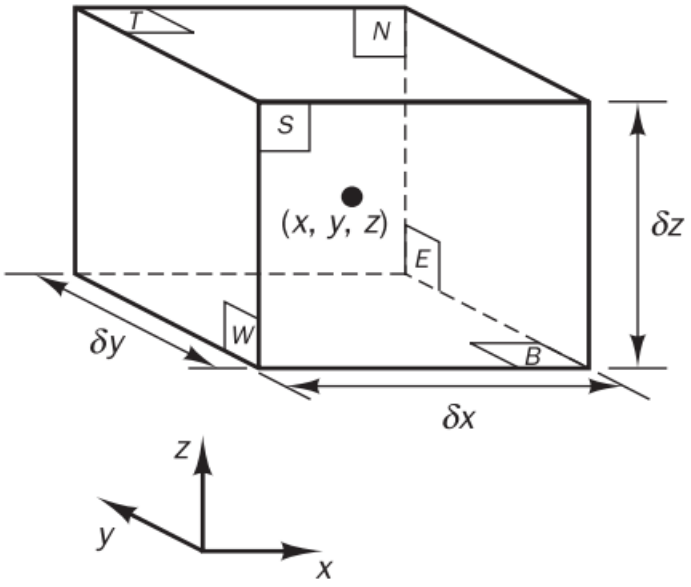

Figure III. 6. A fluid component of conservation laws *[98]*

III.4.1. Mass conservation equation

The first step in getting the mass conservation equation is to have a mass balance for a very small fluid element. This balance states that [98]:

Rate of mass increase within the fluid element = Net mass inflow into the fluid element

The element's internal mass fluctuates over time and can be represented as follows:

$$\frac{\partial}{\partial t}(\rho \delta x \delta y \delta z) = \frac{\partial \rho}{\partial t}\, \delta x \delta y \delta z \qquad \text{(III.10)}$$

Where:

ρ is the fluid density (mass per unit volume),

$\delta x, \delta y, \delta z$ are the dimensions of the small fluid element.

This equation states that the rate at which mass changes in the element is related to how density varies over time.

The mass flow rate across each of the fluid element's faces must then be taken into account. This rate is calculated by multiplying the density by the cross-sectional area and the velocity

component perpendicular to the face. The net mass inflow through the element's boundaries can be written as follows, as shown in Figure III.7.

$$\left(\rho u - \frac{\partial(\rho u)}{\partial x}\frac{1}{2}\delta x\right)\delta y\delta z - \left(\rho u - \frac{\partial(\rho u)}{\partial x}\frac{1}{2}\delta x\right)\delta y\delta z + \left(\rho v - \frac{\partial(\rho v)}{\partial y}\frac{1}{2}\delta y\right)\delta x\delta z - \left(\rho v - \frac{\partial(\rho v)}{\partial y}\frac{1}{2}\delta y\right)\delta x\delta z + \left(\rho w - \frac{\partial(\rho w)}{\partial z}\frac{1}{2}\delta z\right)\delta x\delta y - \left(\rho w - \frac{\partial(\rho w)}{\partial z}\frac{1}{2}\delta z\right)\delta x\delta y = 0 \quad \text{(III.11)}$$

A positive sign is assigned to flows that are directed into the element, which increase its mass, and a negative sign is assigned to flows that are exiting the element.

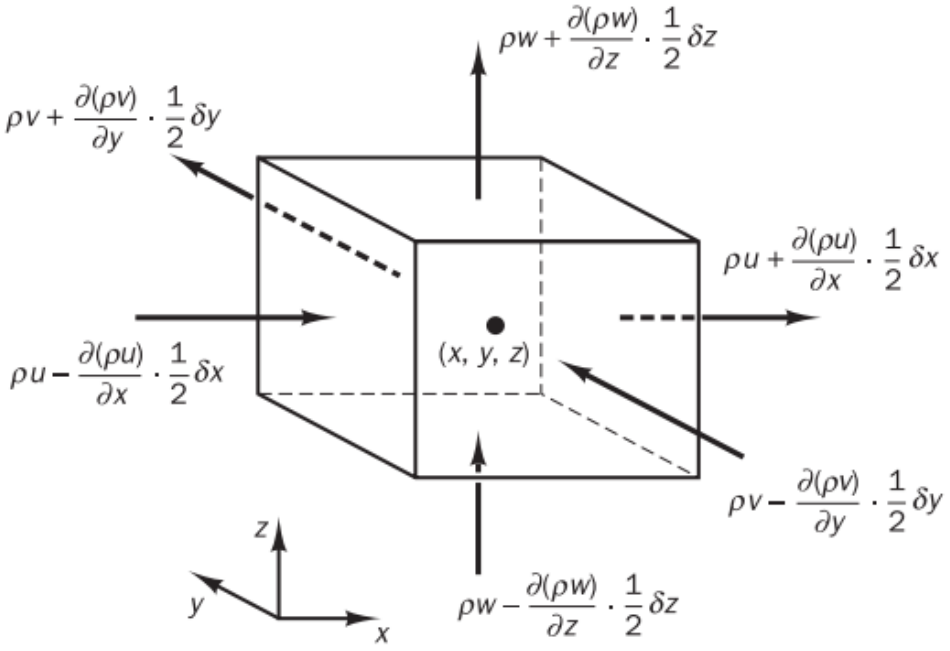

Figure III. 7. Mass flows in and out of fluid element *[98]*

The net rate of mass flow into the element across its faces (III.6) is now equal to the rate of mass increase inside the element (III.5). The expression is divided by the element volume δxδyδz, and all terms of the resulting mass balance are arranged on the left side of the equals

sign. This results from the unsteady, three-dimensional continuity or mass conservation equation at a point in a compressible fluid.

$$\frac{\partial \rho}{\partial t} + \text{div}\,(\rho \boldsymbol{u}) = 0 \tag{III.12}$$

The first term on the left is the rate at which the density (mass per unit volume) changes over time. The second term, known as the convective term, characterizes the net mass flow out of the element across its boundaries. For incompressible fluids div $\boldsymbol{u} = 0$

III.4.2. Energy conservation equation for a solid

The energy transfer equation for a differential control volume in a Cartesian coordinate system is represented in Figure III.8. It represents the heat flux components (q_x, q_y, and q_z) entering and leaving a small fluid element through its faces. The heat flux at each face varies according to its gradient ($\frac{\partial q_x}{\partial x}$, $\frac{\partial q_y}{\partial y}$, and $\frac{\partial q_z}{\partial x}$), showing how heat is transferred through conduction.

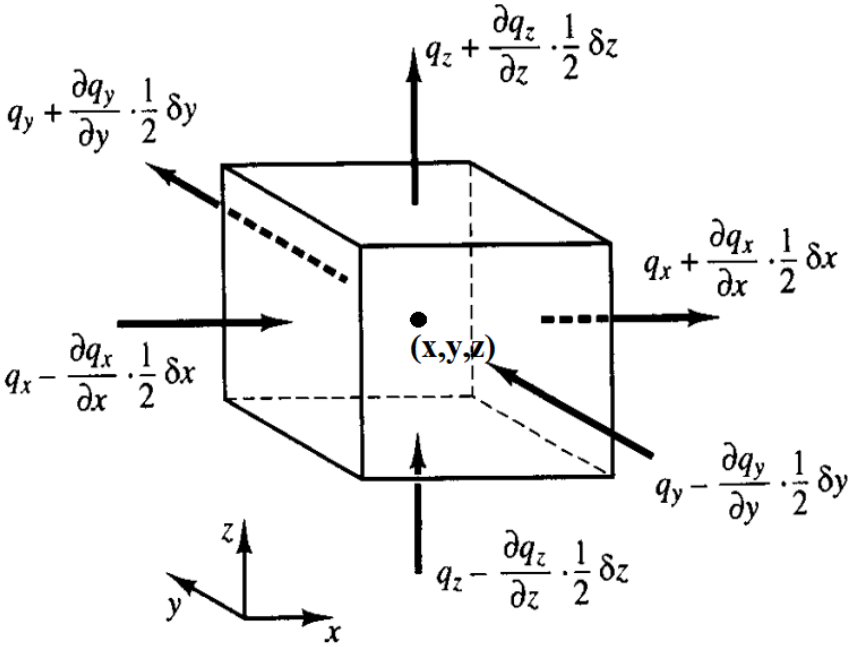

Figure III. 8. Representation of heat flow in three directions on a volume element [99]

In the (x) direction, the difference between the fluxes is the net rate of heat flux.

$$\left[\left(q_x - \frac{\partial q_x}{\partial x}\frac{1}{2}\delta x\right) - \left(q_x + \frac{\partial q_x}{\partial x}\frac{1}{2}\delta x\right)\right] \delta y \delta z = -\frac{\partial q_x}{\partial x}\delta x \delta y \delta z \tag{III.13}$$

In a similar way in the other two directions (y and z):

$$\left[\left(q_y - \frac{\partial q_y}{\partial y}\frac{1}{2}\delta y\right) - \left(q_y + \frac{\partial q_y}{\partial y}\frac{1}{2}\delta y\right)\right]\delta x\delta z = -\frac{\partial q_y}{\partial y}\delta x\delta y\delta z \quad \text{(III.14)}$$

$$\left[\left(q_z - \frac{\partial q_z}{\partial z}\frac{1}{2}\delta z\right) - \left(q_z + \frac{\partial q_z}{\partial z}\frac{1}{2}\delta z\right)\right]\delta x\delta y = -\frac{\partial q_z}{\partial z}\delta x\delta y\delta z$$

The sum divided by the elementary volume ($\delta x\delta y\delta z$) yields the total net rate of heat flux per unit volume in the three directions, which is equal to:

$$-\frac{\partial q_x}{\partial x} - \frac{\partial q_y}{\partial y} - \frac{\partial q_z}{\partial z} \quad \text{(III.15)}$$

Using the integral or global form of the conservation law and noting the elementary volume dV

$$\frac{\partial}{\partial t}\iiint \rho T dV + \iiint -(\frac{\partial q_x}{\partial x} + \frac{\partial q_y}{\partial y} + \frac{\partial q_z}{\partial z})dV = \iiint S dV \quad \text{(III.16)}$$

The law that J.B. Fourier established in 1822 connected the temperature gradient to the conductive heat flux vector q [99]. It asserts that the thermal gradient and the conduction heat flux are proportional. The heat flux for an isotropic material in a Cartesian direction, such as the x axis, is expressed as follows:

$$q_x = -k\frac{\partial T}{\partial x} \quad \text{(III.17)}$$

where k is the material's thermal conductivity. The heat conduction equation is based on this idea, which also holds true for the other y and z directions.

The local form of the heat conservation equation is expressed as follows.

$$\frac{\partial}{\partial t}(\rho c T) - \left(\frac{\partial q_x}{\partial x} + \frac{\partial q_y}{\partial y} + \frac{\partial q_z}{\partial z}\right) = S \quad \text{(III.18)}$$

By applying Fourier's law and replacing the heat flux, we obtain a suitable formulation.

$$\frac{\partial}{\partial t}(\rho c T) - \left(\frac{\partial}{\partial x}(-k\frac{\partial T}{\partial x}) + \frac{\partial}{\partial y}(-k\frac{\partial T}{\partial y}) + \frac{\partial}{\partial z}(-k\frac{\partial T}{\partial z})\right) = S \quad \text{(III.19)}$$

When the thermophysical properties of the material are constant and no heat source S is present, the heat equation simplifies to the following form:

$$\rho c\frac{\partial T}{\partial t} = k\left(\frac{\partial^2 T}{\partial x^2} + \frac{\partial^2 T}{\partial y^2} + \frac{\partial^2 T}{\partial z^2}\right) \quad \text{(III.20)}$$

Where:

ρ : Density [kg/m^3]

c : Specific heat capacity [J/(kgK)]

T: Temperature [K]

x, y, and *z*: Spatial dimensions [m]

III.4.3. Equation of moisture transfer

The transfer equation of moisture in an unsaturated medium were established for the first time in the case of unsaturated, non-deformable soils under gaseous phase continuity. This means that the air pressure can be assumed to always be equal to atmospheric pressure. These assumptions are valid in sands, where the air inlet pressure corresponds to low suctions. The first calculations were made by Richards.

III.4.3.1. Hydraulic head in unsaturated soils

In a non-deformable unsaturated soil, the approach is similar to that for saturated soils. The hydraulic head expression is derived from the water potential and is expressed as follows:

$$H = \frac{p}{\rho g} + z \tag{III.21}$$

where:

H is the hydraulic head (m)

z is the elevation of measurement point (m)

p is the water pressure at measurement point (force (weight) per unit area)

ρ is the density of water (Kg/m^3)

g is the gravitational constant (m/s^2)

III.4.3.2. Darcy's Law

Henry Darcy was a pioneering hydraulic engineer whose research on water flow through porous media evolved into Darcy's Law, a fundamental hydrogeology and fluid mechanic's concept. In 1856, under controlled sand filtration experiments, he demonstrated that the flow rate (Q) of water is proportional to the cross-sectional area (A) and piezometric head difference (h_1-h_2) and inversely proportional to the length of the medium (L). It is expressed mathematically as:

$$Q = KA\frac{(h_1 - h_2)}{L} \tag{III.22}$$

where K is hydraulic conductivity. Darcy also defined the term hydraulic gradient ($i = \frac{(h_1 - h_2)}{L}$) and specific discharge $(q = KA)$, representing water flow per unit area through porous materials. His finding revolutionized groundwater hydraulics, which became a model for present research on aquifers, well development, and soil permeability. Besides hydrogeology, Darcy's Law is widely applied in civil and environmental engineering, petroleum reservoir simulation, and computational fluid dynamics. His rigorous experimental approach shown in Figure III.9, and mathematical formulation are still the cornerstone of worldwide water resource planning and engineering applications [100].

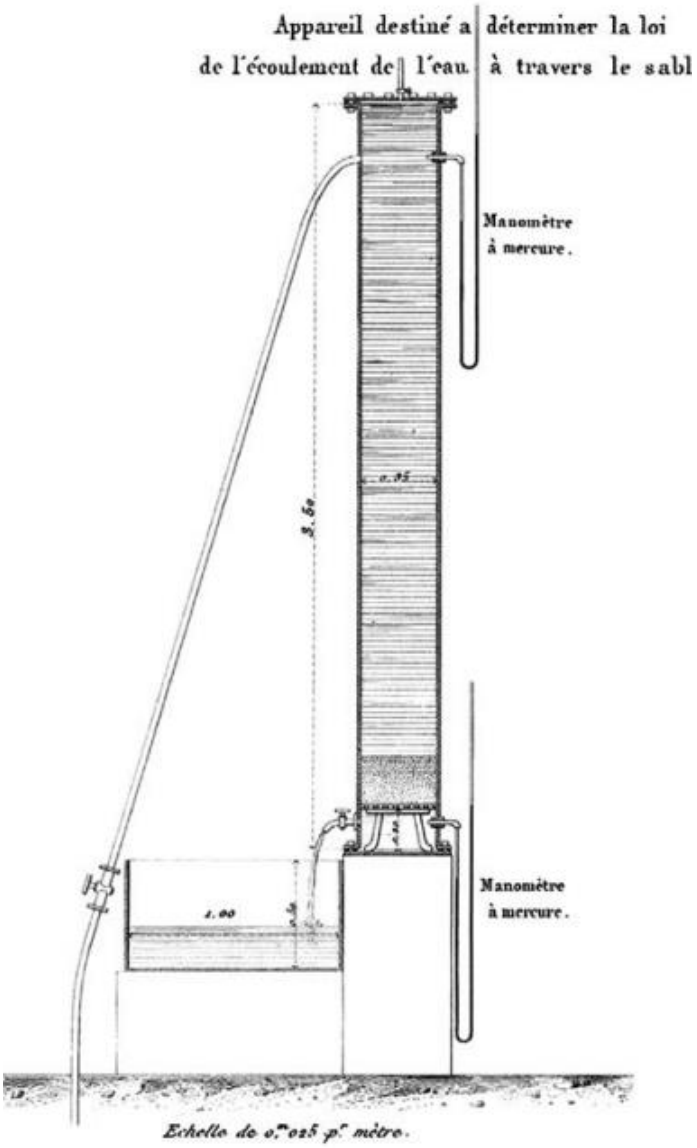

Figure III. 9. Darcy's original sand column apparatus [101]

III.4.3.3. Richard equation

Many researchers have studied different aspects of modelling unsaturated water flow using Richards' equation. This equation combines Darcy's law with mass balance principles to describe how water moves through the soil. To solve it numerically, the soil is divided into small elements or voxels, which can be one-, two-, or three-dimensional. Various algorithms are then used to track changes in the hydraulic head (h), water potential (y), or water flux (q) over time for each element [102]. Most advanced models use a finite-element method and a Picard time-iterative approach [103] to find solutions. The equation becomes much easier to work with in simpler cases, such as when water flows vertically through isotropic soil in one dimension. For a homogeneous and non-deformable soil, Richards' equation for the case of unidirectional flow is as follows [102]

$$\frac{\partial \theta}{\partial t} = \frac{\partial}{\partial z}\left[K(\theta)\frac{\partial h}{\partial z}(h+z)\right] \tag{III.23}$$

where θ is the soil's volumetric water content [m^3/m^3], t is time [s], K is hydraulic conductivity [m/s], h is pressure potential [m], and z is depth [m].

Table III. 1. Empirical retention curve models

Model	Equation
Brooks and Corey (1964)	$\Theta = \frac{\theta - \theta_r}{\theta_s - \theta_r}$ $\Theta\,(h) = \frac{h_{ea}}{h}^{N}$
van Genuchten (1980)	$\Theta = \frac{\theta - \theta_r}{\theta_s - \theta_r}$ $\Theta\,(h) = \frac{1}{[1 + (a.h)^n]^m}$
van Genuchten Burdin (1980)	$\Theta = \frac{\theta - \theta_r}{\theta_s - \theta_r}$ $\Theta\,(h) = \frac{1}{[1 + (a.h)^n]^{(1-\frac{2}{n})}}$
Feng and Fredlund (1999)	$\Theta = \frac{\theta_s b - \theta_r}{\theta_s - \mathrm{h}^d}^{d}$

Table III.1. lists the various empirical models that are used to numerically solve the Richards equation. Among these are the models developed by Brooks and Corey (1964), van Genuchten-

Mualem (1980), and other widely used techniques. These models are crucial because they make it possible to estimate the hydraulic conductivity *K(θ)* from the retention curve *θ(h),* which is easier to measure in a lab. The necessary parameters are obtained by fitting the experimental data of *θ(h),* and then *K(θ)* is deduced. Table III.2. presents the van Genuchten–Mualem model parameters for some type of soils.

Table III. 2. The parameters of the van Genuchten–Mualem model [104]

	θ_s ($cm^3.cm^{-3}$)	θ_r ($cm^3.cm^{-3}$)	a (cm^{-1})	n (-)	Ks ($cm.min^{-1}$)
Silty clay	0.070	0.360	0.005	1.09	0.0003
Silty clay loam	0.089	0.430	0.010	1.23	0.0012
Sandy clay	0.100	0.380	0.027	1.23	0.0020
Clay	0.068	0.380	0.008	1.09	0.0033
Clay loam	0.095	0.410	0.019	1.31	0.0043
Silt	0.034	0.460	0.016	1.37	0.0042
Silt loam	0.067	0.450	0.020	1.41	0.0075
Loam	0.078	0.430	0.036	1.56	0.0173
Sandy clay loam	0.100	0.390	0.059	1.48	0.0213
Sandy loam	0.065	0.410	0.075	1.89	0.0737
Loamy sand	0.057	0.410	0.124	2.28	0.2432
Sand	0.045	0.430	0.145	2.68	0.4950

III.5. conclusion

This chapter has provided a comprehensive analysis of heat transfer mechanisms and their relevance to soil thermal behavior. The discussion highlighted the fundamental concepts of thermal energy, heat, and temperature, emphasizing the role of temperature gradients in driving heat movement. The three primary heat transfer mechanisms, conduction, convection, and radiation were examined, with a particular focus on conduction as the dominant mode of heat transfer in soils. The governing equations for heat and fluid flow, derived from conservation laws, were presented to describe thermal and hydraulic interactions within the soil. Additionally, empirical models, such as the Richards equation and van Genuchten–Mualem model, were introduced to facilitate the numerical analysis of moisture movement in unsaturated soils. These theoretical foundations serve as a basis for the thermal modeling

approach adopted in this research, enabling a more accurate representation of soil thermal and hydric behavior under various environmental conditions.

Chapter IV

Soil-Atmosphere Interaction and Influencing Factors

IV.1. Introduction

The interaction between soil and atmosphere is a key factor influencing the thermal and moisture dynamics of the ground. This chapter looks at the mechanisms that control these exchanges and analyzes their impacts using meteorological data, including air temperature, humidity, wind speed, solar radiation, and precipitation. These elements act as boundary conditions that have an immediate effect on the soil's ability to transfer heat and moisture.

The most important mathematical formulas for modeling soil-atmosphere interactions are shown, and various methods are contrasted before the best model for this investigation is chosen. The assumptions, computational procedures, and parameterization strategies used to guarantee accurate simulations are described in detail in the section devoted to the numerical model.

This study also analyzes the physical, thermal, and chemical characteristics of the soil. Physical characteristics, such as porosity, density, and texture, are considered in relation to their influence on moisture retention and heat transfer. To ascertain how the soil reacts to temperature changes, thermal characteristics such as diffusivity, heat capacity, and thermal conductivity are investigated. In order to comprehend their role in soil behavior under various environmental conditions, chemical aspects are also assessed, including mineral composition and interactions with water.

This chapter provides a framework for precisely simulating soil-atmosphere interactions and evaluating their effects on heat and moisture transfer within the soil by combining meteorological data, mathematical modeling, and soil properties.

IV.2. Soil atmospheric interactions

To estimate the ground temperature of soil at a certain depth, different methods can be used, the methods applied in our study is the sol-atmospheric interaction which refers to the dynamic, two-way interaction between the soil and the surrounding atmosphere with the exchange of energy, water, gases, and nutrients. It regulates important processes such as evaporation, infiltration, heat transfer, and gas exchange (e.g., carbon dioxide and oxygen). It is important in the regulation of environmental conditions, climatic patterns, water cycles, ecosystem health, and Geostructures applications. Understanding this interaction is central to addressing problems like drought, soil degradation, and climate change because it allows prediction of how

atmospheric conditions (e.g., temperature, humidity, wind) affect soil conditions (e.g., moisture content, soil's temperature, structure) and vice versa.

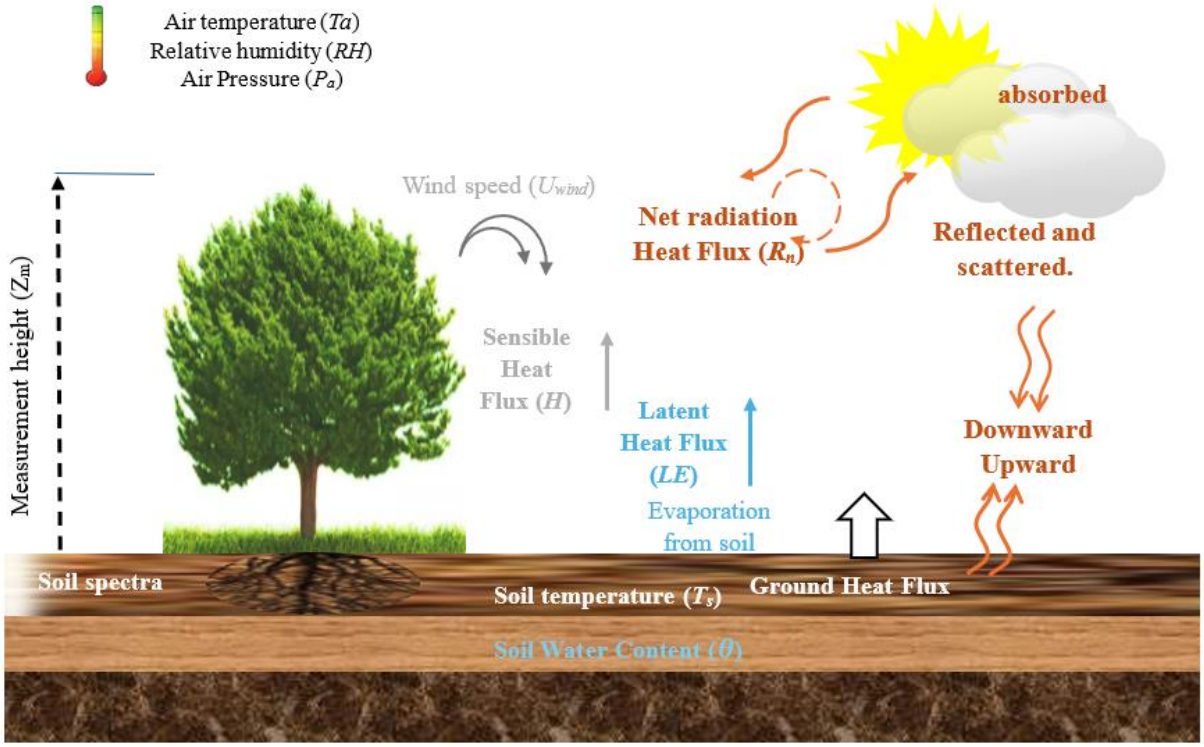

Figure IV. 1. Heat and Energy Exchange in Soil-Atmosphere Interactions [105]

The soil-atmosphere interface is governed by complex energy exchange processes that regulate temperature and moisture activities close to the surface as illustrated in Figure IV.1. Net Radiation (R_n) is one of the significant inputs of this exchange, encompassing the difference between incoming and outgoing radiation at the soil's surface. Net radiation consists of shortwave radiation (R_s), mainly from solar radiation reaching the ground, and longwave radiation (R_a), including terrestrial radiation from the Earth's surface and atmospheric radiation returned [106, 107]. The atmospheric to ground heat flux caused by temperature and latent heat (LE) gradients used for water phase changes like evaporation and condensation is referred to as sensible heat flux (H), which is controlled by this energy balance [108]. Some energy is transmitted to the ground as ground heat flux (G) which regulates subsurface temperature gradients and is a critical element of soil thermal dynamics [109]. Interconnected energy fluxes are behind these features and are functions of atmospheric state, soil type and moisture content, and thus need to be quantified in order for soil-atmosphere interactions on climate and environment to be described. This interaction is determined by [110]

$$R_n + H - LE = G \tag{IV.1}$$

It is important to note that while latent heat flux only accepts positive values, sensible heat flux and net radiation can have both positive and negative values. Heat circulation within the ground is indicated by a positive value, whereas heat dissipation from the ground is indicated by a negative value. The net radiant heat flux, sensible heat flux, and latent heat flux must all be calculated in order to get the exact ground heat flux.

IV.2.1. Net Radiation heat Flux

The equilibrium between incoming and outgoing radiation at a surface is known as net radiation heat flux, and it is essential to comprehend environmental processes. It involves the difference between shortwave radiation absorbed by the Earth's surface and longwave radiation emitted back into the atmosphere. This equilibrium affects how energy is distributed into different forms, such as ground heat flux, sensible heat flux, and latent heat flux. The Stefan-Boltzmann law for thermal radiation describes the net radiation heat transfer between two bodies, which influences the energy exchange between the constituents of Earth. When evaluating climate dynamics and environmental changes over time, net radiation heat flux, which is commonly expressed in W/m², is essential and it can be calculated as follows [111]

$$R_n = (1 - a_l)R_s + (R_a - \varepsilon\sigma T_s^4) \quad \text{(IV.2)}$$

R_s and R_a (W/m^2) represent the incoming shortwave and longwave radiation, respectively. The ground surface emissivity is represented by ε, and the Stephan-Boltzmann constant (Wm^{-2}K^{-4}) by σ. The ground temperature is denoted by T_s. On the other hand, the surface albedo is represented by a_l, which is a function of several variables such as the zenith angle, surface vegetation, soil water content, and soil color [112], it has a value ranging from 0 to 1, Table IV.1 provides a range of surface albedo values corresponding to different types of surfaces.

Table IV. 1. Albedo values for various surface types [113]

Surface type	Abedo
Sand grey	0.18-0.23
Grey clay (humid)	0.16
Sand yellow	0.35
Blue clay (dry)	0.23
Snow (fresh-fallen)	0.90
Grass (fresh, dry)	0.26

Shortwave and longwave radiation are two major sources of energy that influence our climate and weather. The sun emits shortwave radiation, which carries energy in the form of UV and visible light (Figure IV.2). Climate change affects the Earth's surface, weather patterns, and photosynthesis [114]. Some of this energy is scattered or reflected by clouds and aerosols, cooling the atmosphere [115]. Longwave radiation, on the other hand, is the heat released by the earth as a result of solar absorption. Longwave radiation is frequently studied using models because of its intricate interactions with the atmosphere, in contrast to shortwave radiation, which is simple to measure [116].

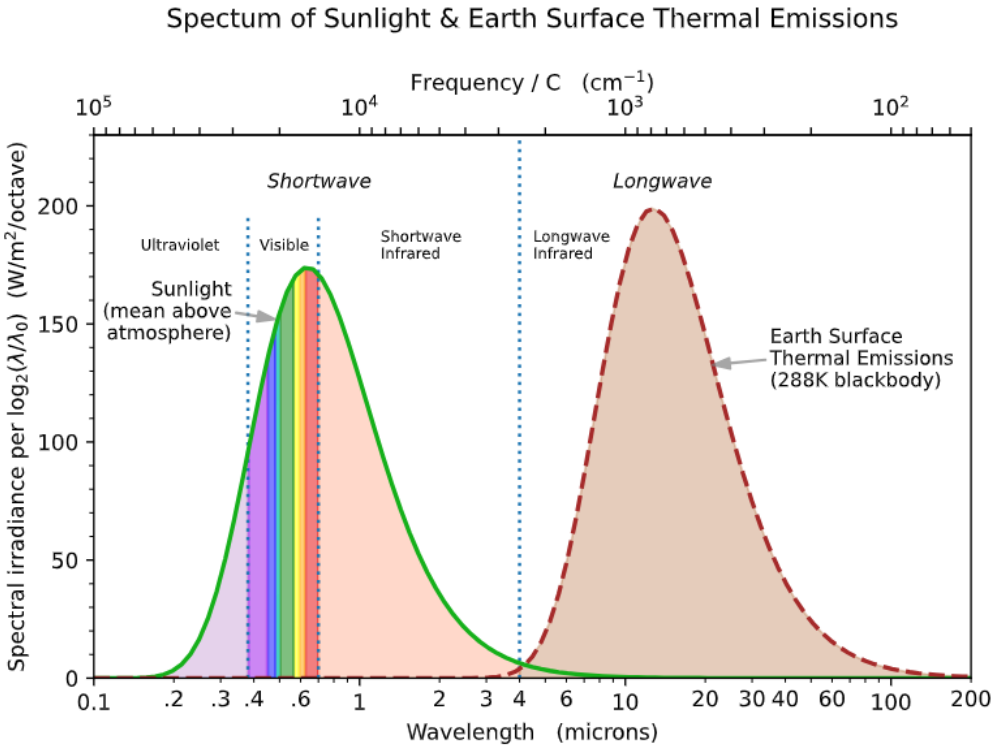

Figure IV. 2. Difference between shortwave and longwave radiation *[117]*

The calculation of R_a follows the equation below [118]

$$R_a = G_{SC}\, d_r[\omega_s \sin\varphi \sin\delta_s + \cos\varphi \cos\delta_s \sin\omega_s] \qquad \text{(IV.3)}$$

G_{SC} correspond to the solar constant which is equal to 1367 W/m^2. d_r is the relative distance between the Earth and the Sun. ω_s is the angle that corresponds to sunset time, while φ stand for latitude and δ_s for solar declination which is an important parameter for understanding the Sun's location relative to the Earth's equator and its effect on solar radiation distribution. It is defined as the angular distance of the Sun from the celestial equator, measured along the right ascension line.

$$\begin{cases} d_r = 1 + 0.033\cos\left(\frac{2\pi}{365}J\right) \\ \omega_s = \arccos[-\tan(\varphi)\tan(\delta_s)] \\ \delta_s = 0.409\sin\left(\frac{2\pi}{365}J - 1.39\right) \end{cases} \quad \text{(IV.4)}$$

R_s is calculated using the longwave radiation as follow [119]

$$R_s = (0.75 + 2 \times 10^{-5}e)R_a \quad \text{(IV.5)}$$

Where e is the station elevation above sea level [m]

IV.2.2. Sensible heat flux

The movement of heat driven by temperature differentials from the Earth's surface to the atmosphere is known as sensible heat flux. It represents the convective heat transfer between the ground surface and the surrounding air. It plays a crucial role in the surface energy balance, which affects the climate and weather [120, 121].

Numerous techniques, such as large-aperture scintillometers, eddy covariance systems, and reanalysis datasets, are used in studies to measure Sensible heat flux. These techniques offer high-resolution data that is necessary to comprehend temporal and spatial variations [122, 123]. Despite the effectiveness of experimental methods, this study focuses on the numerical method for determining sensible heat flux as follow [124]

$$H = \frac{\rho_a C_{p-a}(T_a - T_s)}{r_a} \quad \text{(IV.6)}$$

In this case, ρ_a stands for air density, C_{p-a} for air heat capacity, T_a for air temperature, and ra for aerodynamic resistance to heat transfer. This resistance can be expressed using the following formula [125]

$$r_a = \frac{\ln\left(\frac{Z_m - d}{Z_{om}}\right) \times \ln\left(\frac{Z_m - d}{Z_{oh}}\right)}{K_v^2 U_{Wind}} \quad \text{(IV.7)}$$

Z_m is the altitude at which wind speed, air temperature, and humidity are measured. The von Karman constant is represented by K_v, while the wind speed at elevation Z_m is shown by U_{Wind}. The Fictive ground surface where the wind speed is zero is denoted by d, and it can be calculated as

$$d = \frac{2h_c}{3} \quad \text{(IV.8)}$$

h_c is the vegetation height, Z_{om} is the roughness length for momentum transfer, calculated by

$$Z_{om} = 0.123 h_c \quad \text{(IV.9)}$$

Z_{oh} is the roughness length for vapor transfer:

$$Z_{oh} = 0.1 Z_{om} \quad \text{(IV.10)}$$

IV.2.3. Latent heat flux

The energy transferred when water undergoes a phase change at the Earth's surface, such as evaporation or condensation, is referred to as latent heat flux. It plays a vital role in the hydrological cycle and climate dynamics, making it an essential part of the Earth's energy balance. The flux is influenced by surface temperature, relative humidity, wind speed, and the vertical gradient of water vapor [126, 127]. Besides the Remote Sensing and Satellite-Based Methods to estimate the latent heat flux, there are other ones as mentioned in Table IV.2.

Table IV. 2. Methods for estimating Latent heat flux

Method	Description
Bulk Aerodynamic	Uses wind speed, humidity, and transfer coefficients to estimate flux.
Penman-Monteith	Combine energy balance and mass transfer for accurate flux estimation.
Remote Sensing (SEBAL)	Utilizes satellite data and temperature decomposition for large-scale fluxes.

In this study, the latent heat flux *LE*, formed by the combination of L and E, is calculated by evaluating the evaporation potential E_P at the soil surface when the soil water supply is not limited, using the Penman-Monteith equation [118]

$$E = P \times \left[1 + \left(\frac{E_P}{P}\right)^{-2}\right]^{-\frac{1}{2}} \quad \text{(IV.11)}$$

P is the precipitation rate (mm/s) and E_P is the evaporation potential (mm/s)

$$E_P = \frac{1}{L}\left[\frac{\Delta \times R_n + \frac{\rho_a C_{p-a}(e_s - e_a)}{r_a}}{\Delta + \delta\left(1 + \frac{r_c}{r_a}\right)}\right] \quad \text{(IV.12)}$$

The rate of change of the saturation vapor pressure curve, denoted as Δ (kPa/K). The saturation vapor pressure is represented as e_s (kPa), and the actual vapor pressure is expressed as e_a (kPa).

The psychrometric constant is symbolized by δ (kPa/K), and the canopy resistance (s/m), is denoted by r_c.

$$\begin{cases} \Delta = \dfrac{4098 e_s}{(T_a - 35.85)^2} \\ e_s = \dfrac{0.6108 \times \exp(17.27(T_a - 273.15))}{(T_a - 35.85)} \\ e_a = \dfrac{RH \times e_s}{100} \end{cases} \quad \text{(IV.13)}$$

Here RH is the relative humidity (%). The psychrometric constant is determined through the application of the following formula.

$$\gamma = \frac{C_{p-a} \times P_{at}}{(L \times r_{mw})} \quad \text{(IV.14)}$$

Where P_{at} is atmospheric pressure (Pa), r_{mw} is the molecular weight of water vapor relative to dry air.

$$r_c = \frac{r_1}{(0.5 \times LAI)} \quad \text{(IV.15)}$$

Where r_1 is the stomatal resistance of a single leaf (s/m), LAI is the Leaf Area Index which measures the amount of leaf surface area per unit of ground area, is a crucial biophysical parameter. It is defined as the total area of leaves divided by the ground area beneath the vegetation canopy [128]. LAI is a key variable in understanding various ecological processes, including photosynthesis, respiration, and energy balance in ecosystems. It is also essential for modeling plant growth, crop yield estimation, and climate change studies [129]. For precise estimations on a large scale, the LAI estimates derived from remote sensing data exhibit the greatest potential. The two primary categories of current methods are active light detection and ranging (LiDAR) remote sensing and passive optical remote sensing [130]. Figure IV.3 displays a conceptual diagram of various LiDAR systems.

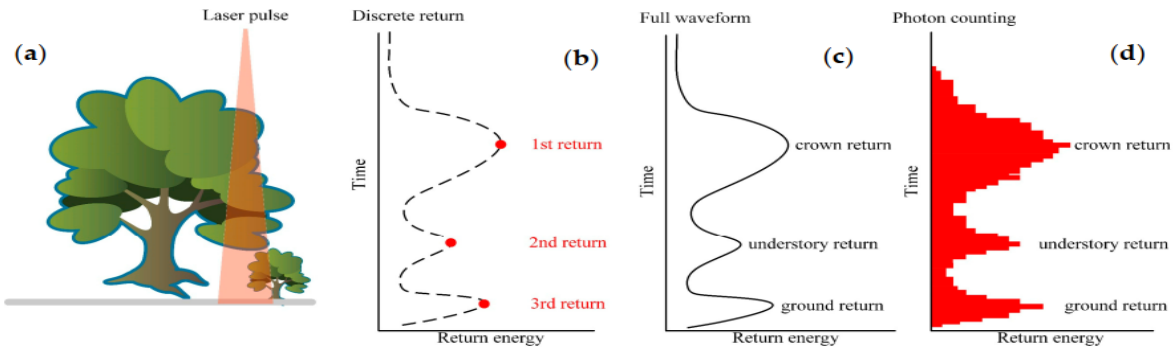

Figure IV. 3. Diagrammatic representation of various light detection and ranging (LiDAR) systems *[130]*

In this study *LAI* is calculated as follow [131].

u) For clipped grass (h_c= 0.05~0.15 m)

$$LAI = 24 \times h_c \tag{IV.16}$$

v) For different types of crops

$$LAI = 5.5 + 1.5 \ln(h_c) \tag{IV.17}$$

IV.3. Governing equation

Our study is structured into four main parts.

- The first part examines the influence of a multilayer soil on geothermal transfer. The four fluxes mentioned above were calculated, and the overall effect of soil stratification was analyzed.
- The second part assesses the impact of soil type on geothermal transfer. Three types of soil were modelled, and one of them was identified as the best performing in terms of heat transfer.
- The third part studies the effect of salinity on geothermal transfer by integrating both solute transfer and hydrothermal transfer.
- Finally, the last part analyses the influence of certain physical properties, such as porosity and density, on geothermal transfer.

IV.3.1. Moisture transfer in unsaturated soils

The moisture transfer in an unsaturated soil is calculated using the Richards equation as follows [132].

$$C(h)\frac{\partial h}{\partial t} - \nabla\, K(h)\nabla h - \frac{\partial K}{\partial z} = 0 \tag{IV.18}$$

The function $C(h) = \frac{\partial \theta}{\partial h}$ represent the specific moisture capacity as a function of water content, h represents the suction head (m), and $K(h)$ denotes the unsaturated hydraulic conductivity. For the calculation of this parameters, the Mualem-van Genuchten formulations were applied [133, 134].

$$\begin{cases} \theta(h) = \theta_r + (\theta_s - \theta_r)[1 + (\alpha h)^{n_1}]^{-m} \\ K(h) = K_s S_e^l \left[1 - (1 - S_e^{l/m})^m\right]^2 \\ S_e = \dfrac{\theta - \theta_r}{\theta_s - \theta_r} \end{cases} \quad \text{(IV.19)}$$

Where K_s is the saturation hydraulic conductivity (m/s), S_e is the effective degree of saturation, θ represents the volumetric soil water content (m³/m³), θ_r and θ_s denotes the residual and saturated water contents (m³/m³), respectively [135].

IV.3.2. Heat transfer in unsaturated soils

The energy conservation equation in the soil used in this study is represented by [111]

$$\rho_s c_{p-s} \frac{\partial T_s}{\partial t} = \nabla(k_s \nabla T_s) + \nabla\left(\rho_w c_{p-w} u_w T_s\right) + Q_s \quad \text{(IV.20)}$$

Where ρ and cp are the density (kg/m³) and the heat capacity (J/kg/K), the s and w indexes represent the soil and water, u_w is the soil water velocity (m/s) obtained from the resolution of Richard equation, Q_s denotes the heat source (W/m³) which was neglected in our study. The thermal conductivity is represented by k_s. The value of $\rho_s c_{p-s}$ is known as the volumetric heat capacity.

1) Thermal conductivity

The soil thermal conductivity can be calculated using different models and equations as discussed in chapter II. This parameter plays a crucial role in determining the soil temperature and for the application of Geostructures. Table V1.3 illustrates the equation used in this study to determine the soil thermal conductivity.

Table IV. 3. Thermal conductivity equations

Study	Thermal conductivity equation	Ref.
1st	$k_s = (0.443x_s + 0.081\gamma_d)\dfrac{(4.4x_s + 0.4)S_r}{1 + (4.4x_s - 0.6)S_r} + 0.087x_s + 0.019\gamma_d$	[68]
2nd and 4th	$k_s = b_1 + b_2\theta + b_3\theta^{0.5}$	[64]
3rd	$k_s = (A_1\theta^2 + B_1\theta)C^2 + (A_2\theta^2 + B_2\theta)C + (A_3\theta^2 + B_3\theta)$	[57]

2) Volumetric heat capacity

The soil volumetric heat capacities were obtained using the formulation represented in Table IV.4.

Table IV. 4. Volumetric heat capacity equations

Study	Volumetric heat capacity equation	Ref.
1st	$C_v = (4.18 - 0.095\gamma_d - 0.3x_s)S_r + 0.09\gamma_d - 0.2x_s$	[74]
2nd, 3rd and 4th	$C_v = \rho_d c_{p-s} + \rho_w c_{p-w}\theta$	[81]

IV.3.3. Solute transfer in unsaturated soils

Solute transfer in unsaturated soils is a complex phenomenon governed by various parameters such as water content, soil structure, and flow conditions. Fick's law of the diffusion phenomenon holds a prominent position while analyzing and simulating the solute transfer in soils. This chemical transfer was conducted using the following formula which is knowns as the convection-dispersion equation [136]

$$R\frac{\partial \mathrm{C}}{\partial t} = \mathrm{D}\frac{\partial^2 \mathrm{C}}{\partial z^2} - v\frac{\partial \mathrm{C}}{\partial z} \quad \text{(IV.21)}$$

Where D is the diffusion coefficient, z is the spatial coordinate, C is the solute concentration, v refers to the pore water capacity ($v = Q/\theta$), both Q and θ denote the darcy flux and the volumetric water content, respectively. R is the coefficient of retardation.

IV.4. Meteorological data

As mentioned previously, our study was divided into four parts: the meteorological data of two regions were considered. The choice of region was based on climate data. The first region, located near the sea, has a semi-arid climate and non-saline soils. In contrast, the second region was selected due to its arid conditions and the salinity present in its soils.

IV.4.1. Oran region

The first region is Oran, which is situated on the Mediterranean coast in northwest Algeria at roughly 35.7° N latitude and 0.6° W longitude, as shown in Figure IV.4. Occupying an area of

about 2,201 square kilometers, Oran is a well-known city that is important to the economics and culture of the area. Its strategic location along the coast and size makes it an important port and urban center in Algeria.

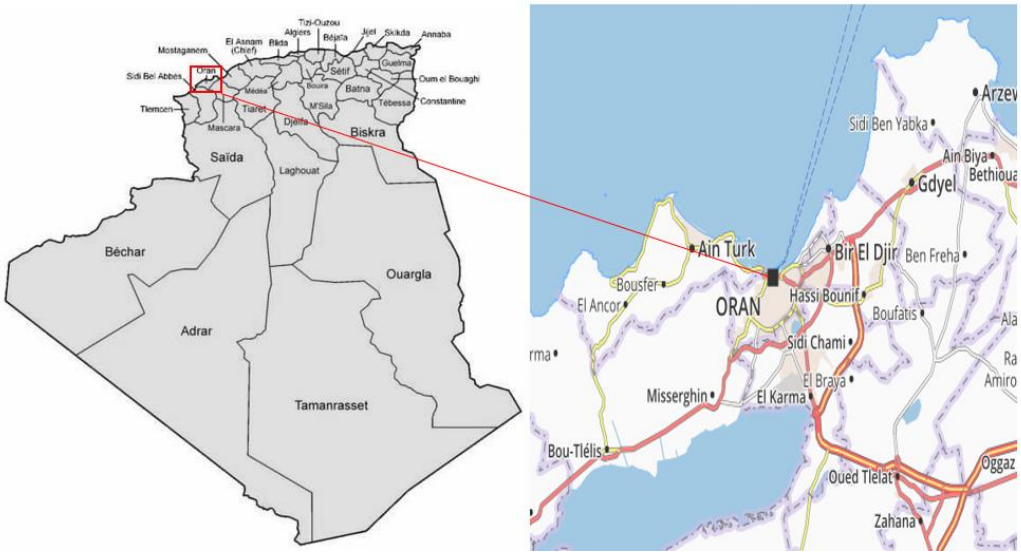

Figure IV. 4. The Oran region [105]

Oran experiences a semi-arid climate with distinct seasonal variations. Summers are hot and dry, with temperatures peaking at 35°C, while typical highs and lows range between 30°C and 21°C. Rainfall is scarce during this period, and the skies remain mostly clear. Winters, though mild, are noticeably cooler, with average highs of 15°C and lows of 6°C, rarely exceeding 20°C.

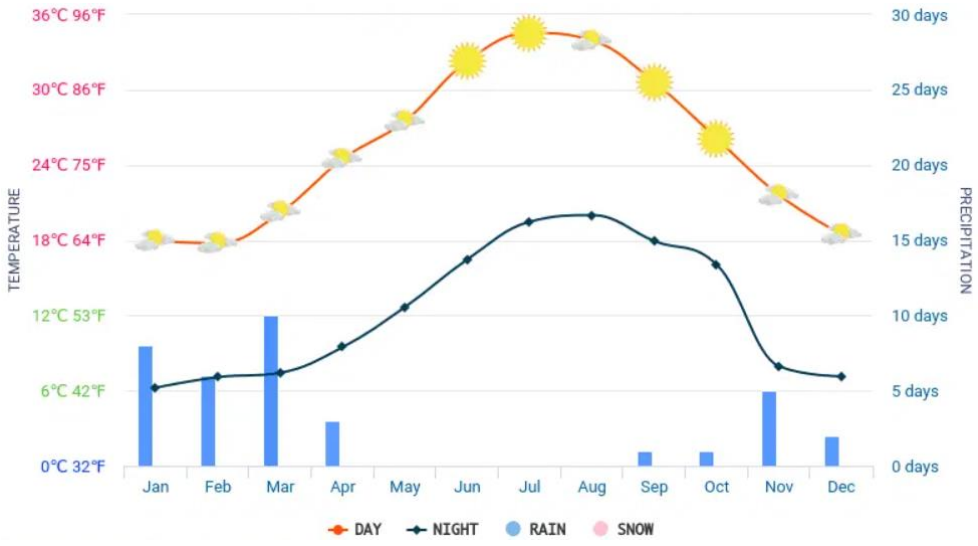

Figure IV. 5. Oran weather, Average monthly temperature and precipitation [137]

Precipitation is more frequent between November and March, contributing to an annual rainfall of approximately 380 mm. Wind speeds in Oran are generally moderate, with summer breezes

ranging from 11 to 16 km/h, providing some relief from the heat. January sees the highest relative humidity at 74.13%, whereas July records the lowest at 63.81%. In terms of sunshine, June is the sunniest month, averaging 11.77 hours of sunshine per day (364.88 hours in total), while January has the least, with an average of 7.22 hours daily (223.73 hours in total). Over the year, Oran enjoys a total of 3,472.57 hours of sunshine, averaging 114.08 hours per month. Despite its semi-arid classification, the Mediterranean coastal influence moderates the climate, making Oran's weather generally pleasant with abundant sunny days [138]. Figure IV.5 shows how temperatures changed in Oran over the course of 2022. The fitted curve aligns almost perfectly with the data, with an R^2 value of 0.99, indicating a very strong correlation.

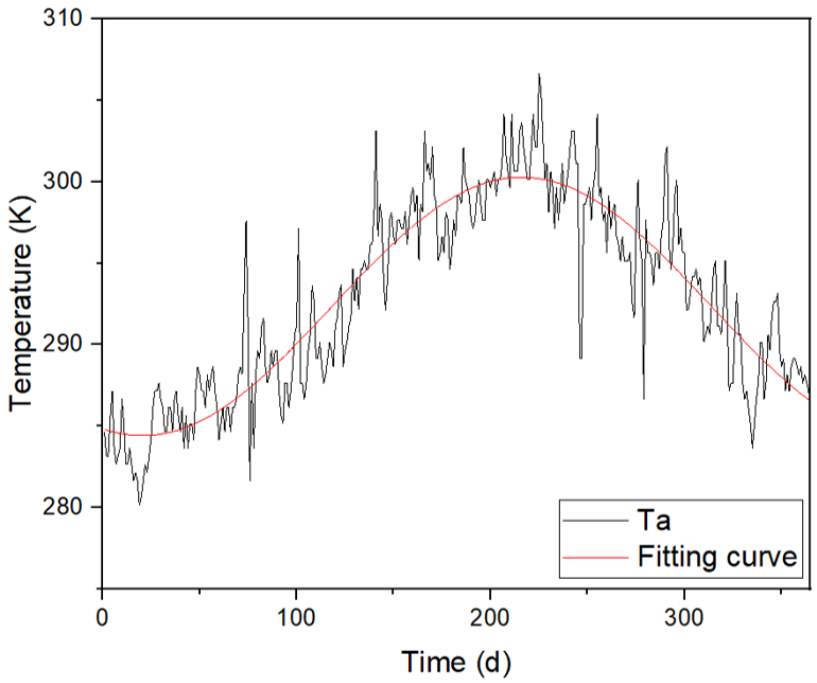

Figure IV. 6. Average temperature of Oran

The fitting equation effectively captures the trend of average ambient temperature throughout the year, with t representing the time of year.

$$T_a = 292.35339 + 7.93851 * \sin\left(\frac{\pi(t-118.31754)}{195.54746}\right) \quad \text{(IV.22)}$$

IV.4.2. Adrar region

Adrar, situated in southern Algeria within the vast Sahara Desert, lies at approximately 27.87° N latitude and 0.29° W longitude, as shown in Figure IV.7. Spanning around 427,368 km², the region is dominated by desert landscapes, featuring towering sand dunes, rocky plateaus, and arid plains. With an average elevation of 258 meters above sea level, its sand—composed mainly of fine quartz grains—forms massive dunes that can reach several hundred meters in

height, continuously reshaped by strong desert winds. Adrar experiences an extreme desert climate, with summer temperatures often exceeding 45°C and minimal rainfall. Despite its harsh conditions, the region's geology presents promising opportunities for geothermal energy exploration. The presence of high thermal gradients beneath the surface could enable sustainable heat extraction, making Adrar a potential hub for renewable energy development in Algeria.

Figure IV. 7. Adrar region

Adrar has a harsh desert environment, with very high temperatures, low humidity, and little rainfall. In summer, temperatures in Adrar can reach 48°C, with normal highs ranging from 40°C to 45°C. During the winter, temperatures are gentler, with average lows ranging from 10°C to 15°C, while overnight temperatures can occasionally drop below freezing, despite these seasonal changes, the region has an average yearly temperature of around 27°C. Figure IV.8 illustrates the maximum, average and minimum temperatures of the year.

Adrar's humidity is often low, frequently dipping below 20%, which, paired with high temperatures, adds to the dry conditions. Wind plays a crucial role in Adrar, with typical wind speeds ranging from 20 to 30 km/h. These winds, especially in the spring, may cause frequent and powerful sandstorms, which affect the region's landscape.

Adrar receives less than 5 mm of precipitation per year on average, making it one of Algeria's driest regions. Rainfall is typically in the form of brief, powerful storms that can cause flash

floods in normally dry riverbeds (wadis). Extreme heat, low humidity, high winds, and little rainfall characterize Adrar's severe desert environment.

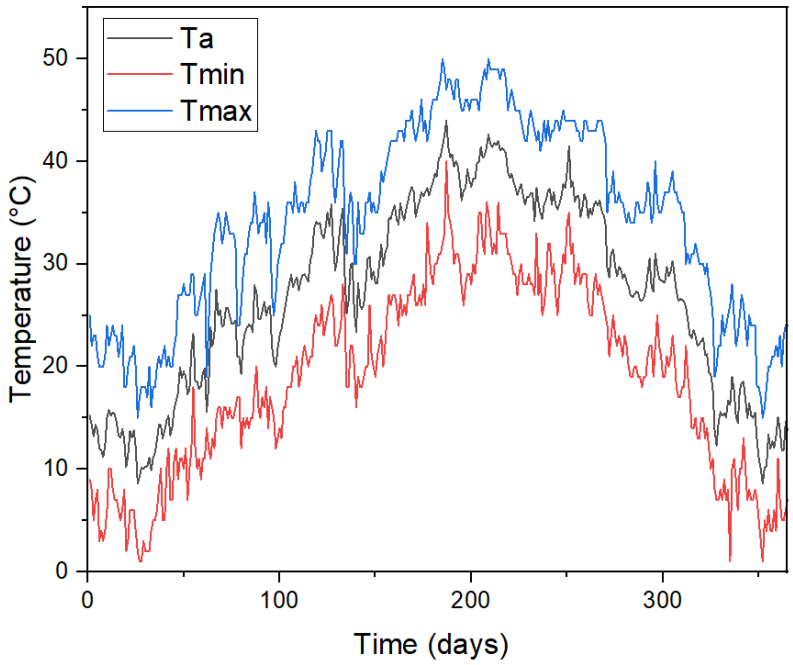

Figure IV. 8. Variations in Adrar's Maximum, Average, and Minimum Temperatures *[139]*

The combination of low rainfall and high evaporation rates in the Adrar region has led to an increase in soil salinity.

IV.5. Numerical Model

Our study's numerical model was created using COMSOL Multiphysics software; each section will be covered in detail below. The study took into account various parameters and variables.

IV.5.1. Numerical simulation

w) First part

A 2D numerical simulation (20m × 10m) was designed (Figure IV.9) to study how heat moves through multilayer soil by analyzing ground temperature and different types of heat flux, sensible, latent, net radiation, and overall ground heat flux. The model considers parameters like soil composition, moisture content, and atmospheric conditions, ensuring a realistic representation of how heat transfers through the ground. By setting appropriate boundary conditions, the simulation closely mimics natural environmental constraints. It also tracks temperature and heat flux changes over time, offering valuable insights for improving thermal management, optimizing building foundations, and enhancing agricultural practices.

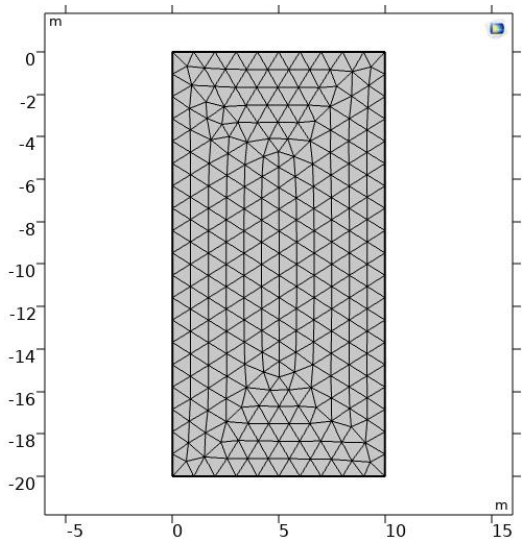

Figure IV. 9. 2D Numerical Model

The study was conducted on a multilayers soil, as illustrated in Figure IV.10. The study examined the effect of multilayers soil in the geothermal transfer. The studied region was Oran. The heat and moisture transfer equations were taken into consideration. The soil-atmospheric interaction was chosen to determine the soil temperature. For the equation of the thermal conductivity and volumetric heat capacity, Nowamooz and Tang equations were chosen, the physical parameters of each soil are Mentioned in Table IV.5. x_s represents the soil sand content and γ_d denotes the dry unit weight (kNm^{-3}). Table IV.6 lists the hydrothermal properties of the multilayer soils under study.

Table IV. 5. Physical properties of multilayers soil

Soil Type	x_s(-)	γ_d (kN/m^3)
Clay loam	0.35	13.5
Sandy loam 1	0.80	16.0
Loam	0.50	14.2
Sandy loam 2	0.60	16.0

Table IV. 6. Hydrothermal properties of multilayers soil

Soil type	K_s (m/s)	l	α(1/m)	n_1	θ_s	θ_r
Clay loam	1.53×10^{-6}	0.5	1.99	1.22	0.5	0.03
Sandy loam 1	1.78×10^{-5}	0.5	2.60	1.52	0.39	0.02
Loam	2.19×10^{-6}	0.5	2.35	1.38	0.47	0.02
Sandy loam 2	1.45×10^{-5}	0.5	2.48	1.50	0.40	0.02

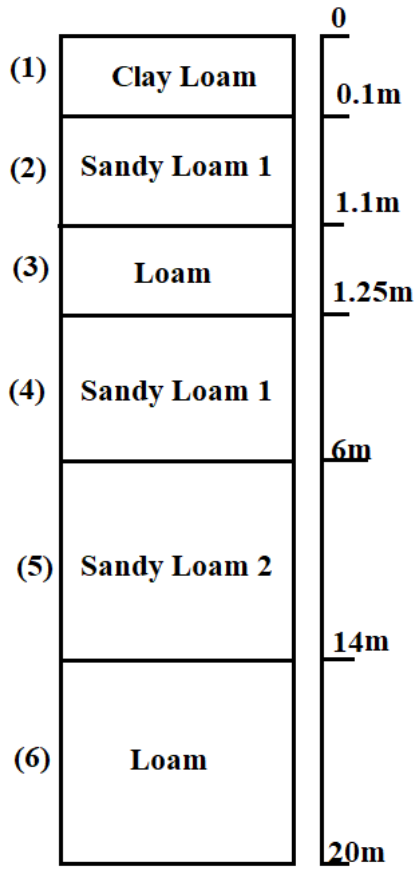

Figure IV. 10. Multilayers soil of the first study

x) Second Part

A 3D numerical simulation (20m×10m×10m) was developed to analyze geothermal heat transfer by evaluating temperature distribution and fluxes behavior. The computational domain was discretized into 105,033 tetrahedral elements and 6,528 triangular elements, with a coarser surface mesh to improve computational efficiency as illustrated in Figure IV.11. The model incorporates meteorological conditions and soil properties, ensuring a realistic representation of subsurface thermal dynamics. Appropriate boundary conditions were applied to capture heat exchange processes within the soil over time accurately.

This study examines three soil types: clay, loam, and sand, to determine which soil offers the best geothermal performance. Their physical properties were assessed in relation to heat retention and transfer efficiency. The findings contribute to optimizing geothermal system design, enhancing heat storage solutions, and improving overall energy efficiency. Table IV.7 and Table IV.8 lists the hydrothermal properties of the studies soils, and the parameters used for the energy balance at the soil atmospheric interface, respectively.

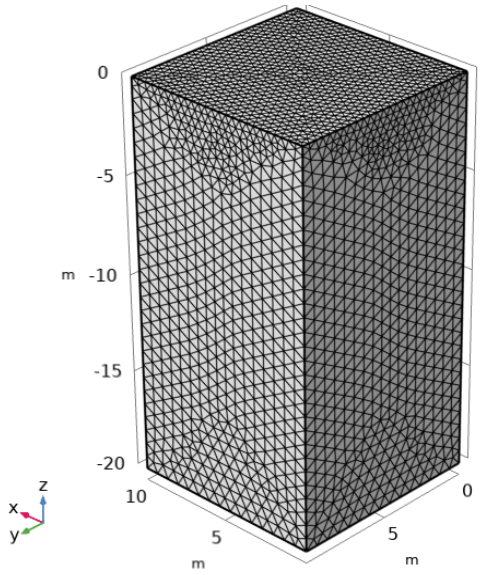

Figure IV. 11. Meshing of the studied domain

Table IV. 7. Hydrothermal properties of the three soil's type

Soil type	l	α(1/m)	n_1	θ_s	θ_r	K_s (m/s)	$C_{p\text{-}s}$ (J/kg/K)	ρ_d (kg/m^3)
Clay	0.5	0.43	1.36	0.52	0.03	0.2×10^{-5}	1350[81]	1200[140]
Loam	0,5	1.55	1,50	0.48	0,01	0.7×10^{-5}	1450[141]	1360[111]
Sand	0.5	3.28	1.54	0.44	0.0	2.5×10^{-5}	910[81]	1520[140]

Table IV. 8. Energy balance parameters of the ground surface

Parameter	value
h_c	0.05 m
Z_m	2 m
U_{Wind}	2.5 m/s
K_v	0.41
P	100620 Pa
L	2.257×10^{6} Jkg^{-1}
σ	5.67×10^{-8} Wm^{-2}K^{-4}
a_l	0.25
$c_{p\text{-}a}$	1004.7 Jkg^{-1}K^{-1}
$c_{p\text{-}w}$	4181 Jkg^{-1}K^{-1}

y) Third part

This study explores how salinity affects geothermal heat transfer in arid region soils using a 3D numerical model. The simulation replicates year-round ground temperature changes in the Sahara region, factoring in atmosphere-soil interactions and actual meteorological conditions for a realistic analysis. The computational domain (20m×10m×10m) is divided into 8097 tetrahedral elements and 1100 triangular elements, ensuring precise thermal calculations, as illustrated in Figure IV.12.

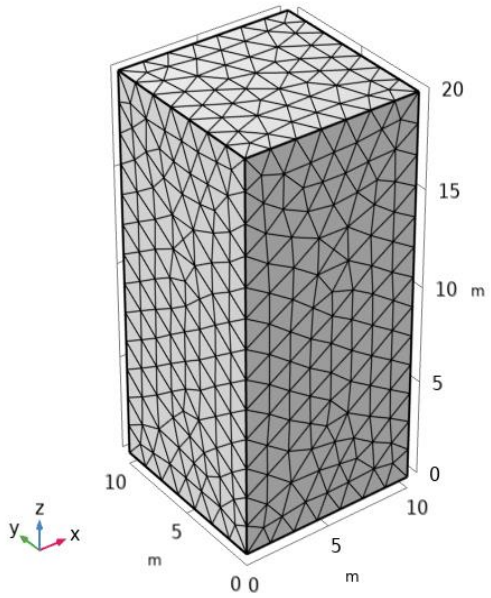

Figure IV. 12. Numerical model

To understand the impact of salinity, the study examines two soil types, sand and sandy loam, under three salinity levels (C = 0 M, C = 0.1 M, and C = 0.2 M), which was applied only on the upper 40 cm layer. The hydrothermal characteristics of the investigated soils are listed in Table IV.9, while the parameters utilized for the energy balance at the soil-atmosphere interface are listed in Table IV.10.

Table IV. 9. Hydrothermal properties of sandy soils

Soil type	l	α(1/m)	n_1	θ_r	K_s (m/s)	$C_{p\text{-}s}$ (J/kg/K)	ρ_d (kg/m^3)
Sand	0.5	3.28	1.54	0.01	2.5×10^{-5}	910	1520
Sandy loam	0,5	2.60	1,52	0,02	1.78×10^{-5}	1040[142]	1600

Table IV. 10.Energy balance parameters of the ground surface

Parameter	Value
h_c	0.05 m
Z_m	2 m
U_{Wind}	5.25 m/s
K	0.41
P	9808844.7 Pa
$c_{p\text{-}a}$	1004.7 $Jkg^{-1}K^{-1}$
$c_{p\text{-}w}$	4181 $Jkg^{-1}K^{-1}$
L	2.257 $\times 10^3$ Jkg^{-1}
a_l	0.18

z) Forth part

This study develops a hydrothermal numerical model to examine how soil interacts with the atmosphere in the Oran region of Algeria. It considers three levels of porosity (n = 0.4, 0.6, 0.8) and two different soil types, clay and sand, with varying dry densities. The aim of the study is to understand how these factors influence heat and moisture transfer. The computational domain extends 20m deep and 10m wide, as shown in Figure IV.9, which provides a schematic of the modeled soil structure. The simulation divides the domain into 3,148 triangular elements, ensuring a precise and realistic representation of thermal and moisture dynamics within the soil. The hydrothermal parameters and soil-atmospheric parameters are identical to those listed in Table IV.7 and IV.8, respectively.

Table IV.11 lists the boundary conditions for the fourth type of our study.

Table IV. 11. Boundary conditions

Surface	Hydraulic condition	Thermal condition
Top	Neumann	Neumann, Eq. (IV.1)
Lateral	Adiabatic	Adiabatic
Bottom	Dirichlet, Pressure head (m)	Dirichlet, Temperature (K)

To better understand the methodology of our study, Figure IV.13 illustrates the flowchart of the process for predicting soil temperature profiles. It begins with input parameters and state variable initialization and creates a numerical model. Energy and ground heat flux are computed at each time step, and soil temperature and water content are updated. This iterative process continues until the specified end time, providing the final soil temperature profile as output.

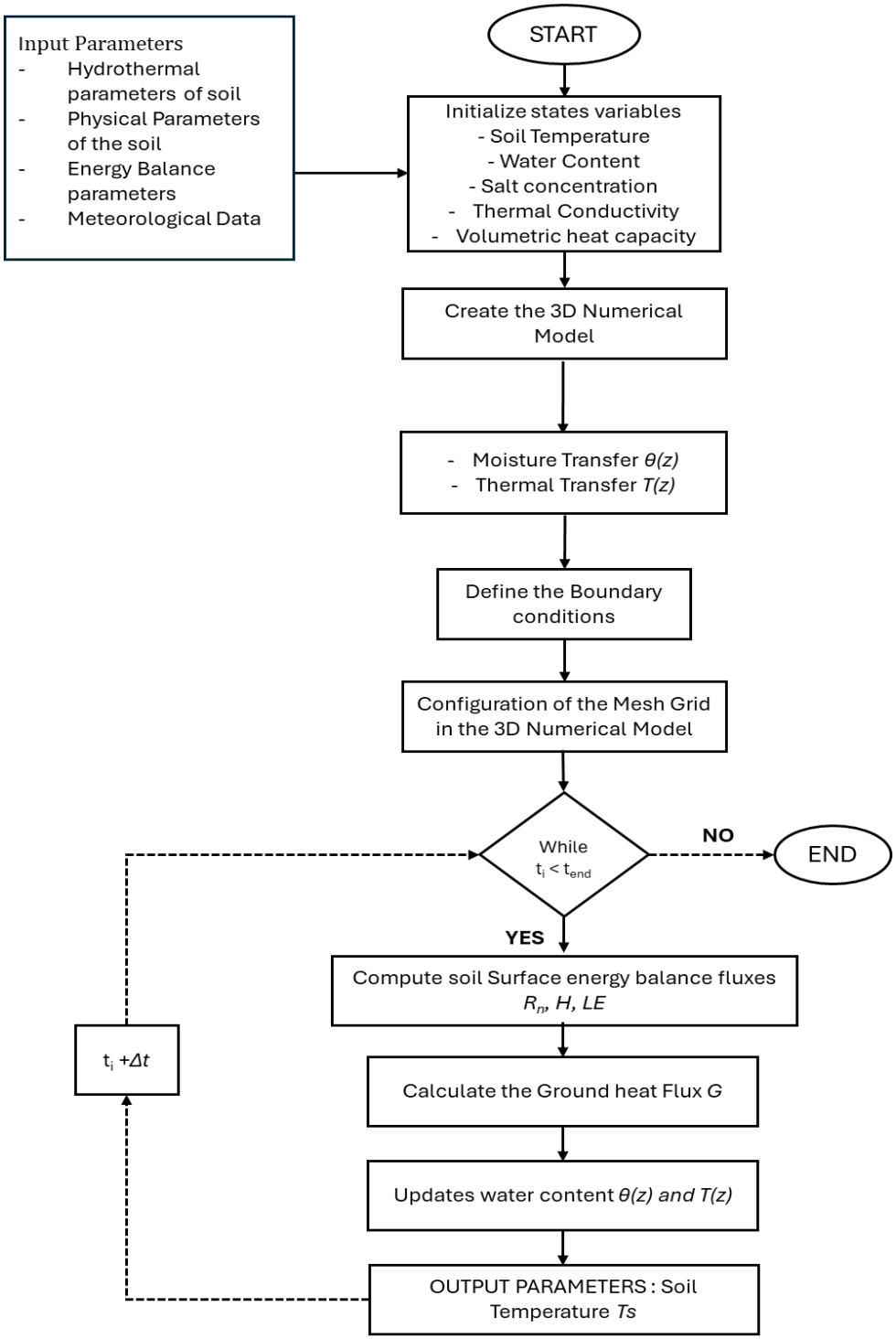

Figure IV. 13.Process Flowchart for Soil Temperature Profile Prediction

IV.5.2. Validation of the numerical model

Experimental data [143, 144], which represent clay soil in Viamão, southern Brazil, with a density of 1400 kg/m³ and a specific heat capacity of 1010 J/kg/K, were used to validate the model. The following equation [143] was used to adjust the boundary condition at the soil's upper surface in order to fit the experimental data:

$$T_a = 291.70 + 6.28 \times \sin\left(200 * 10^{-9} t + 26.24\right) \quad \text{(IV.21)}$$

The comparison between experimental and numerical results in Figure 6 shows a strong match, confirming the model's accuracy in simulating soil temperature profiles for both summer (July 28) and winter (January 26). The fact that the model was originally validated with data from Brazil but performs well under Algerian conditions highlights its adaptability to different geographical regions. It's important to note that the model uses averaged values for key variables like relative humidity, precipitation rate, and wind speed, even though these factors naturally fluctuate over time. This variability explains the small differences observed in Figure IV.14.(a). However, despite these minor uncertainties, the close agreement between experimental and numerical results reinforces the model's reliability.

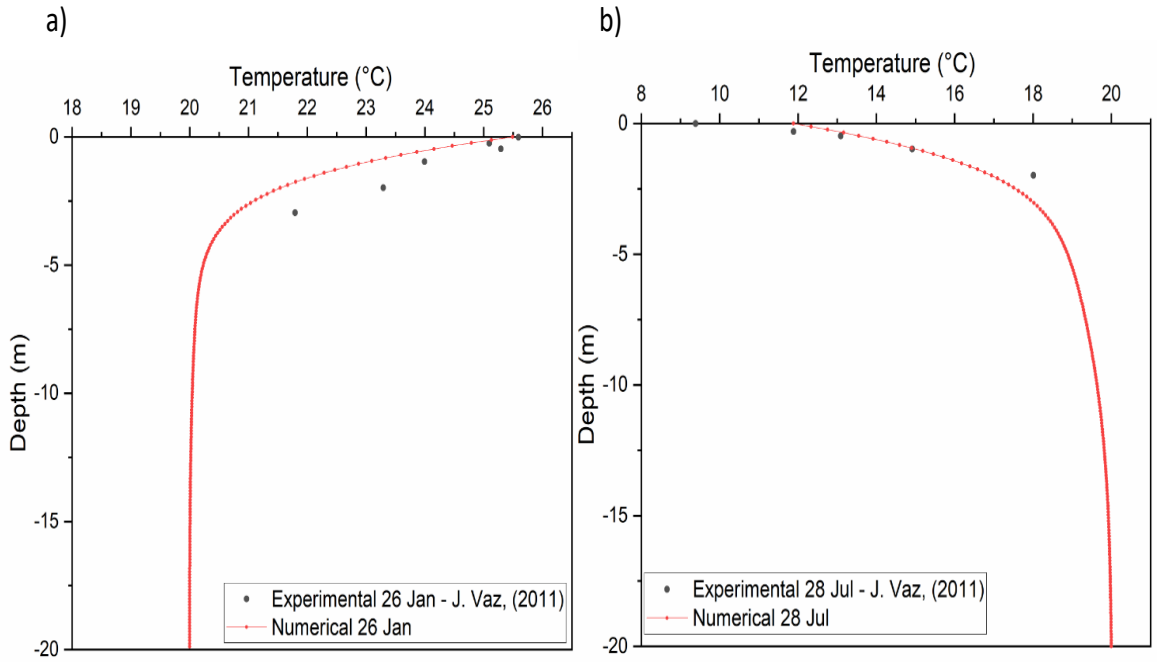

Figure IV. 14. Distribution of Soil Temperature by Depth for (a) January 26 and (b) July 28

IV.6. Conclusion

This chapter explained the soil-atmosphere interaction and its influence on heat and moisture transfer in the ground. Based on the analysis of meteorological data, mathematical models, and

numerical simulations, the study explored the most significant environmental and physical parameters affecting thermal behavior. The research focused on net radiation, sensible heat flux, and latent heat flux and highlighted their role in ground heat exchange. A computational model using COMSOL Multiphysics was developed to study geothermal heat transfer under different conditions, including variations in soil type, salinity, porosity, and density. The study was divided into four main sections, one of which dealt with one factor influencing heat transfer. For consistency, the model was validated using experimental data and proved to show a high level of correlation with measurements in actual settings. Although there were slight fluctuations depending on different meteorological conditions, the results confirmed the precision and adaptability of the model under different geographical environments.

Chapter V

Results and discussion

V.1. Introduction

This chapter presents the main results of our study, structured into four main sections. Firstly, we examined the flux and the temperature variation in a multilayer soil, taking into account hydrothermal transfer and analyzing the impact of soil stratification. Next, we studied the influence of different soil types on heat transfer, modeling three variants (clay, loam, and sand) and identifying the one that offered the best performance. The different fluxes resulting from soil-atmosphere interaction were analyzed and compared, along with the optimum temperature and distance for Geostructures placement. We then explored the role of salinity, taking into account both solute transfer and hydrothermal transfer, in order to understand their interactions. Finally, we studied the impact of certain physical properties, such as porosity and density, on geothermal and moisture transfer, enabling us to refine our understanding of the factors involved.

V.2. Results and discussion

Once the numerical framework has been validated, this section presents the simulation results, considering soil-atmosphere interactions.

V.2.1. Influence of multilayer soil

The net radiation heat flux was calculated using the equation IV.2. The numerical model was simulated over a 10-year period to improve the accuracy of the results. The region studied is Oran, and the meteorological data used are from the same region. The properties of the multilayer soil have already been detailed in Chapter IV. Figure V.1 represents the net radiation for the Oran region in 2023, with the fitting curve showing a strong correlation to the data, as confirmed by a 98% coefficient of determination, indicating a good fit. The flux starts at approximately -80 W/m² in the early days of the year, gradually increases, and reaches a peak of around 180 W/m² near day 180 (mid-year, likely summer). It then decreases, returning to -80 W/m² by the end of the year. The short-term variations in net radiation suggest daily weather influences, such as cloud cover and temperature fluctuations. Understanding surface energy balance in geothermal and climate studies requires an understanding of this seasonal pattern, which reflects the natural cycle of solar radiation, where energy absorption is highest in summer and lowest in winter.

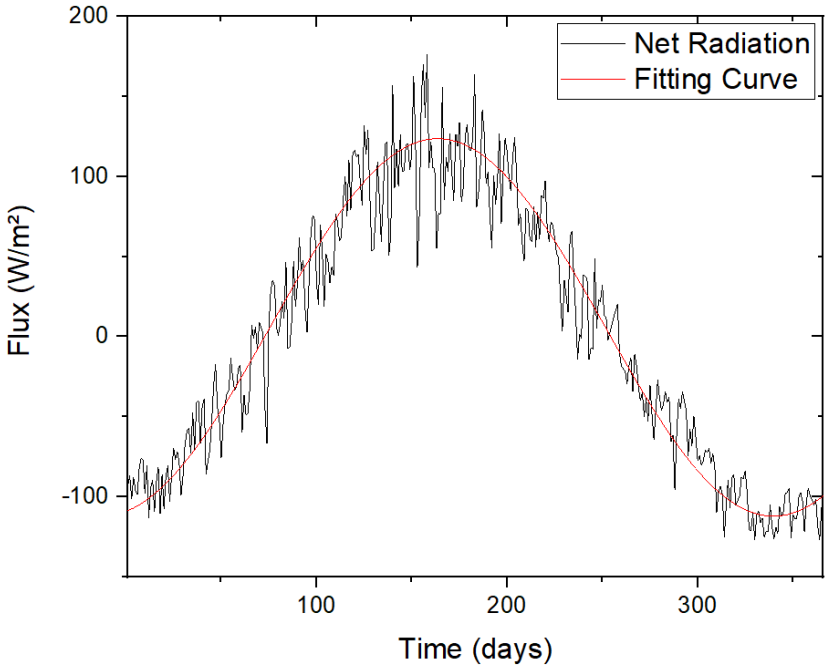

Figure V. 1. Annual Variation of Net Radiation in the Oran Region for 2023

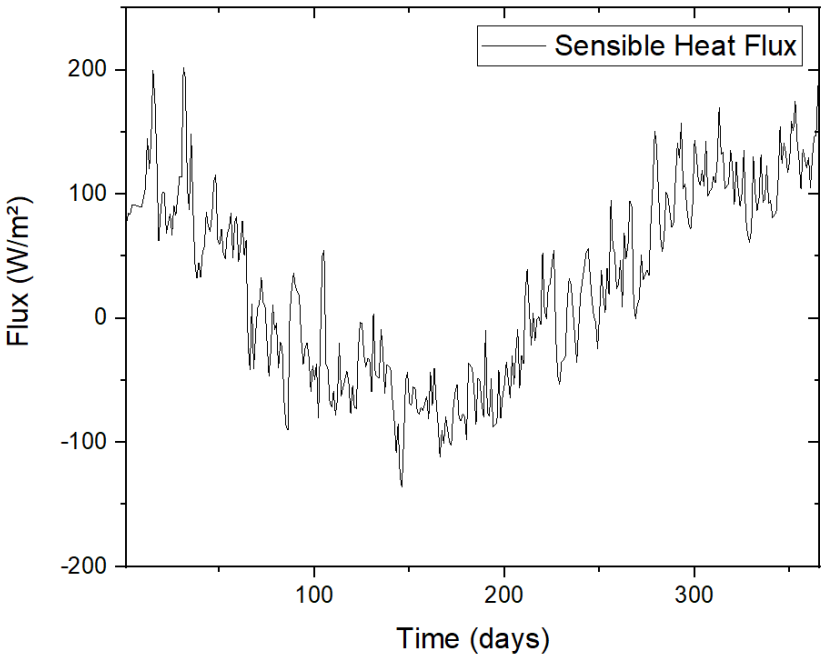

Figure V. 2. Annual Variation of Sensible heat flux in the Oran Region for 2023

Figure V.2 illustrates the variation of sensible heat flux over time in the Oran region for 2023, representing the convective heat exchange between the soil and atmosphere. The flux variation is reaching a maximum of 200 W/m² and a minimum of -140 W/m², reflecting seasonal shifts in energy transfer. Positive flux at the start and end of the year indicates that the soil is losing heat to the atmosphere, which is typical during cooler months when the ground retains more

heat than the air. Conversely, negative flux occurs around mid-year (~days 150-200), suggesting that heat is transferred from the atmosphere to the soil, likely due to increased air temperatures and solar radiation. These variations are further influenced by daily weather conditions, including wind speed, temperature fluctuations, and cloud cover, which impact convective heat exchange.

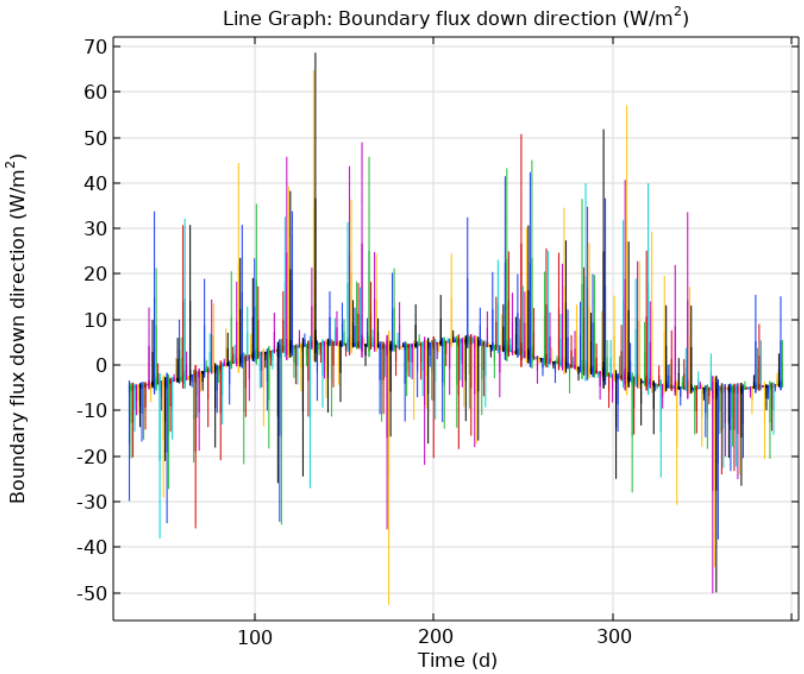

Figure V. 3. Ground heat flux in the Oran Region for 2023

Figure V.3 shows the evolution of ground heat flux (W/m²) over time (days), demonstrating the variations in heat transfer between the ground surface and the atmosphere. Strong positive and negative oscillations can be observed throughout the year, reflecting the influence of daily and seasonal solar radiation cycles. The flux reaches maximum values of around +70 W/m², indicating peaks in heat gain, probably during periods of intense sunshine, while the greatest heat losses are down to -50 W/m², suggesting cooling of the ground, particularly at night or under unfavorable weather conditions. A slight increase in heat flux is visible between 100 and 200 days, followed by a gradual decrease after 250 days, illustrating the effect of the seasons on the storage and dissipation of thermal energy. These variations demonstrate the importance of heat exchange between soil and atmosphere, influenced by climatic factors such as air temperature, humidity and weather conditions. To optimize the use of soil thermal energy by seasonal demands, these data are essential for applications in geothermal energy, climate modeling, and agricultural management.

After deriving the initial section head profile, the volumetric water content and thermal conductivity are obtained.

a) b)

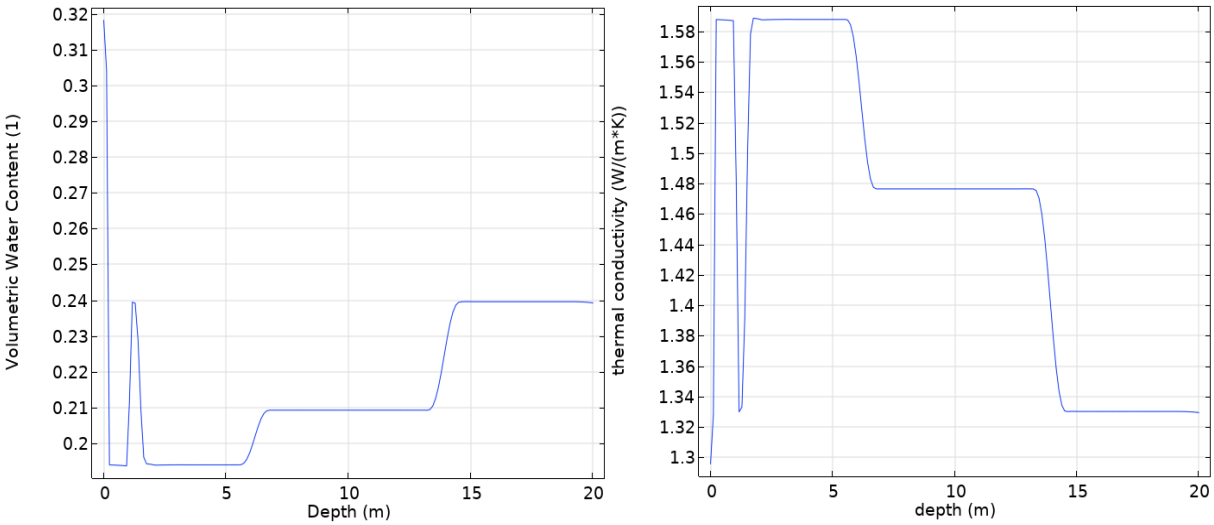

Figure V. 4. Initial Profiles as function of depth of of a) Volumetric Water Content and b) Thermal Conductivity

Figure V.4 presents the initial profiles of volumetric water content and thermal conductivity as a function of depth. In Figure V.4.a, the volumetric water content fluctuates, with a peak near the surface, likely due to surface moisture from precipitation or evaporation. In Figure V.4.b, thermal conductivity starts high (~1.58 W/m·K) near the surface, suggesting compacted or dry soil, but drops significantly at ~5 meters, indicating a transition to a different soil layer with lower heat transfer properties. A second decline occurs at ~15 meters, where conductivity stabilizes around 1.33 W/m·K. The differences in thermal conductivity and water content point to a stratified subsurface with discrete soil layers that affect heat transfer and moisture retention. Since these profiles shed light on the dynamics of moisture and heat beneath the surface, they are essential for geothermal energy research, soil heat transfer modeling, and environmental evaluations.

Figure V.5 shows the evolution of ambient temperature (green curve) and surface temperature (blue curve) over time (days). Both curves follow a seasonal trend, with a gradual rise in temperature to a maximum of around 200 days when the surface temperature reaches around 32 °C before gradually falling again. Surface temperatures follow a smoother, more regular pattern, while ambient temperatures show marked fluctuations influenced by meteorological factors such as wind, cloud cover, and humidity. As temperatures rise and fall, the surface temperature remains more stable, this can be explained by the thermal inertia of the ground,

which absorbs and releases heat slowly, thus absorbing sudden variations in ambient temperature. Key components for climate modeling, geothermal energy, and infrastructure energy management are highlighted in this analysis, including the function of soil in thermal regulation and the relationship between the surface and the atmosphere.

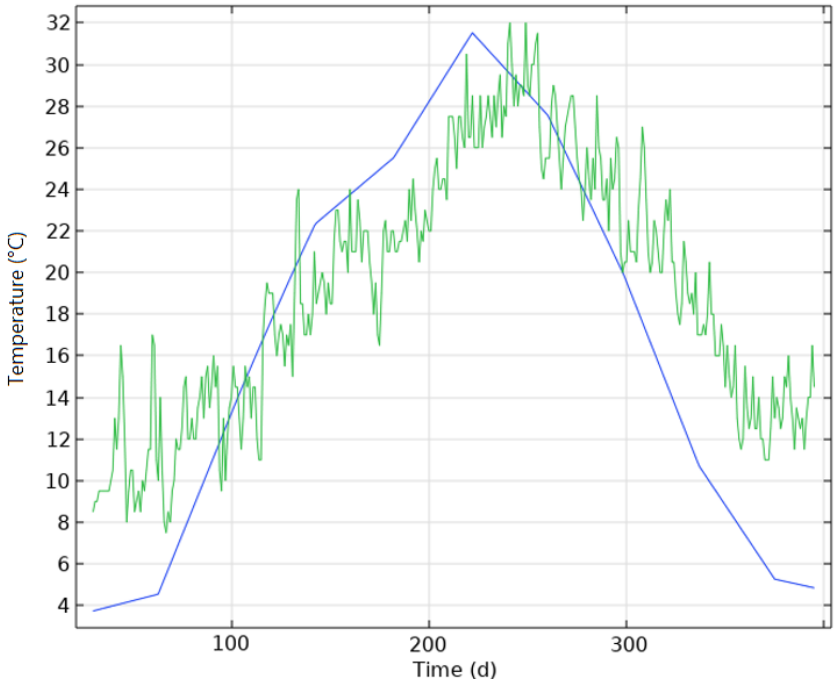

Figure V. 5. Variations in Ground Surface Temperature and Ambient Temperature

The temperature profile of multilayered soils in the Oran region is illustrated in FigureV.6. this temperature undergoes evident seasonal variations, particularly at upper levels. The temperature at the surface (from 0 to 4m) varies vastly through the year, with the highest values during summer season (June to August) and the lowest ones during winter season (December to February) as illustrated in Figure V.7, hence, these variations reflect direct solar radiation effects. The variations are attenuated (from 4m to 8m), as the temperature changes linked to the surface act slowly, due to the thermal inertia of the soil. Below 8m, the temperature is almost constant, at around 16°C, evidencing the fact that deep layers are insulated against seasonal temperature fluctuations. This pattern is explained by the thermal lag effect, which refers to the delay in temperature changes as heat penetrates deeper into the soil. This occurs because the ground has thermal inertia, which means that it takes time to absorb, store, and transfer heat. As a result, while surface temperatures change rapidly with the seasons, deeper layers experience a delayed response. For example, during summer, the surface quickly heats up through direct solar radiation, while increased penetration from the sun may take weeks or

months to get to the lower layers. Likewise, winter will show a rapid cooling of the surface compared to the inner layers, which slowly lose heat.

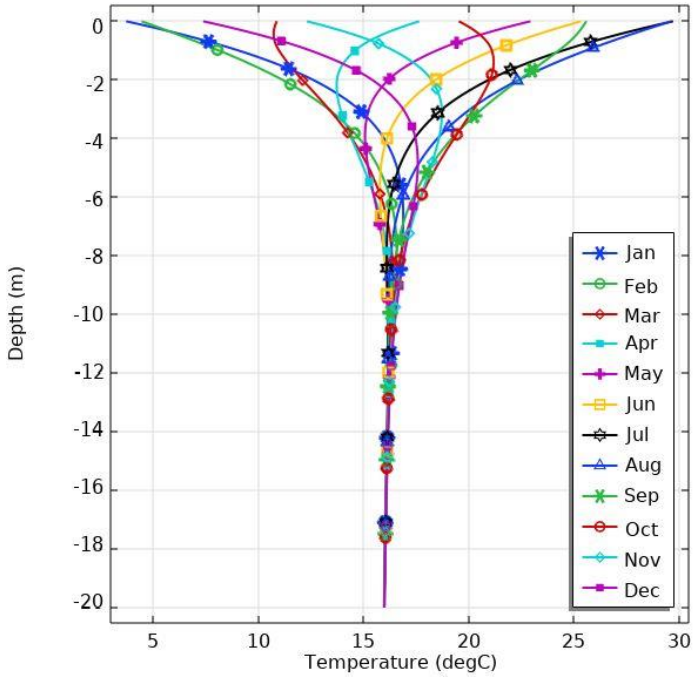

Figure V. 6. Profile Temperature of the Oran region of 2023

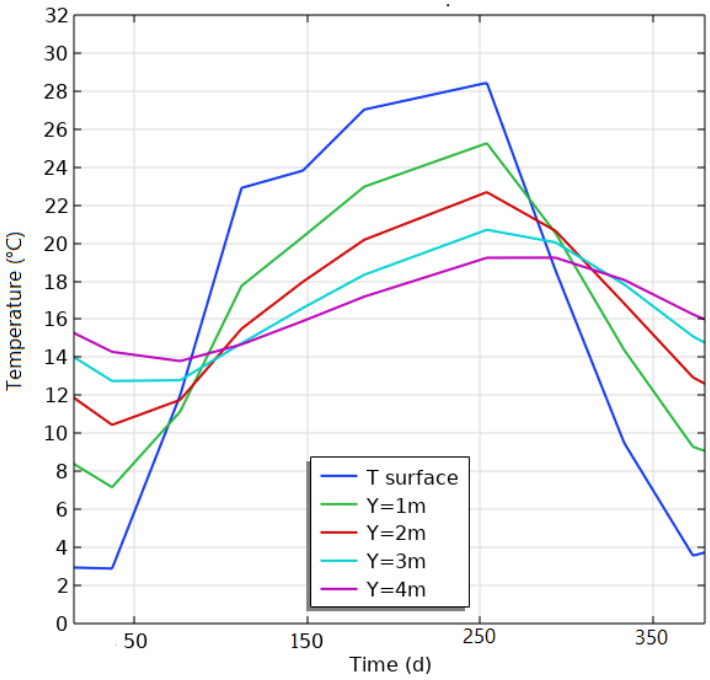

Figure V. 7. Soil's Temperature at different depth

The phenomenon, therefore, becomes important in areas where seasonal temperature variations are very pronounced, such as Oran. These thermal characteristics are practically important for certain applications. In agriculture, for example, soil temperature variation can offer useful

information for the optimization of the timing of sowing and irrigation. For specific applications in geothermal energy systems, comparatively stable deep-soil temperature around 16°C is a good opportunity for the application of shallow geothermal heat exchange systems. Additionally, in construction, knowledge of soil temperature profiles is crucial for designing well-insulated foundations and infrastructure that can withstand seasonal temperature fluctuations.

1. **First Conclusion**

The study emphasizes the seasonal variation of heat flux and thermal behavior of the multilayered soil of the Oran region under soil atmospheric interactions, which greatly influenced the thermal surface-and-subsurface distribution due to the solar radiation and meteorological data. The temperature of the soil fluctuated significantly at the upper surface (0–4 m) due to direct sun exposure, but after 8 m, temperatures were kept almost constant at about 16°C. The deeper layers would eventually reach thermal stabilization. Such stabilization would occur in a multilayered soil at a certain depth depending on the composition and the physical properties of the upper surface, and if there isn't any external heat source to generate heat such as thermal sources. These findings tend to benefit geothermal energy applications, agricultural planning, and the designing of infrastructure by ensuring the knowledge of the thermal properties of soils used to optimize heat-extracting systems. Future perspectives would be extracting this heat using shallow ground heat exchangers.

V.2.2. Influence of soil's type

In this part of our study the influence of three type of soil is studies to analyze the performance of each one, and to determine which one is suitable of the geothermal application at shallow depth. The soil atmospheric interaction fluxes were determined as presented below.

a) **Soil atmospheric interactions**

Figures V.8, V.9, and V.10 present the variation of shortwave radiation throughout the year 2022 for the three soil types under study: sand, loam, and clay, respectively. The unique absorption and reflection properties of each soil type are highlighted in these figures, which show how they interact with shortwave radiation over various seasons.

Because of its higher albedo and lower moisture content, which allow more radiation to be reflected rather than absorbed, sand exhibits significant fluctuations in shortwave radiation, as

seen in Figure V.8. During the summer, the peaks are higher. The fitting curve provides a more apparent trend of radiation over the year, which adjusts the daily variations.

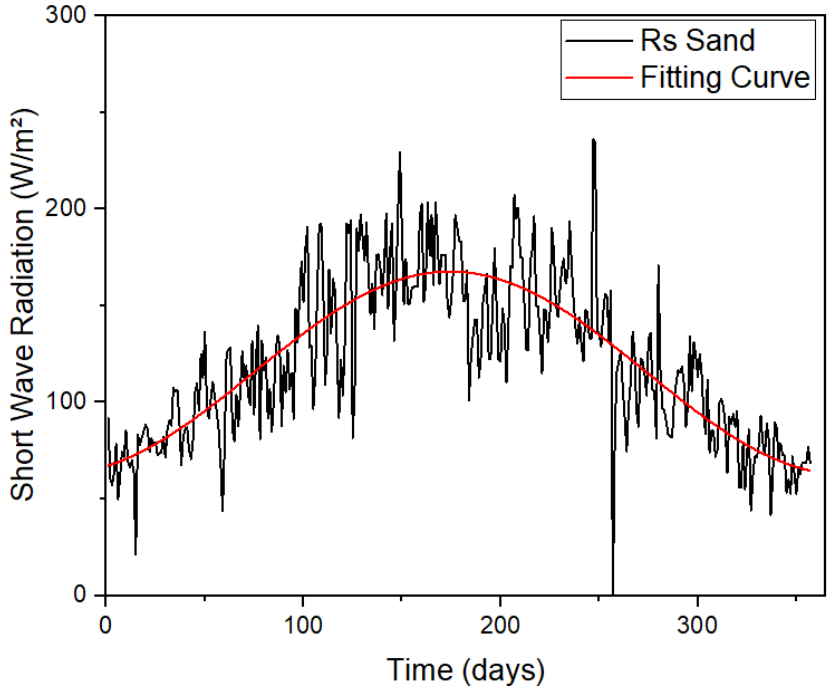

Figure V. 8. Shortwave radiation in Oran for sand (2022)

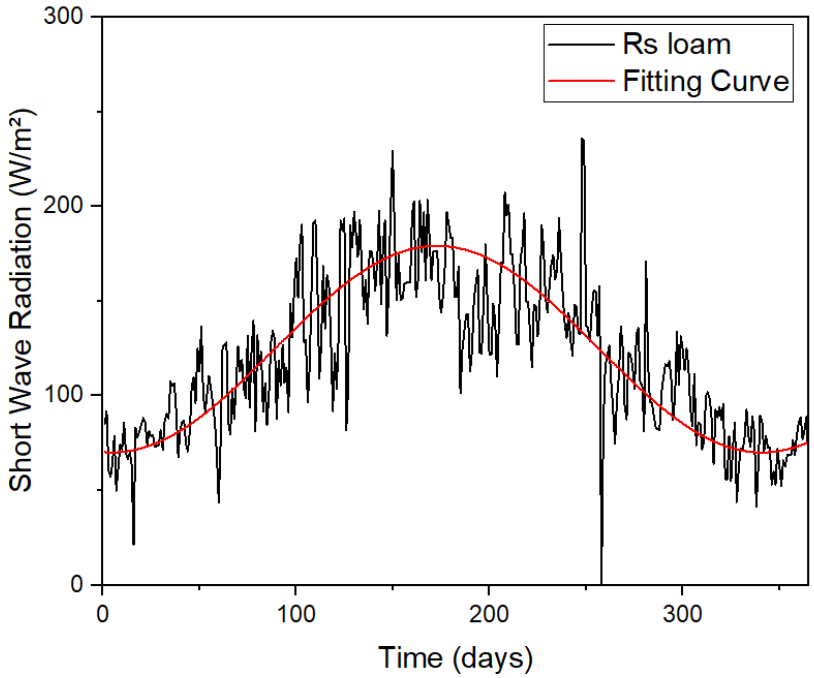

Figure V. 9.Shortwave radiation in Oran for Loam (2022)

Figure V.9 illustrates the shortwave radiation pattern for loam soil, which responds more moderately compared to sand. Due to its balanced composition of sand, silt, and clay, loam

interacts with radiation in a more stable manner. The fitted curve in this figure highlights the soil's ability to absorb and retain heat, showing fewer extreme peaks and dips than sand.

In Figure V.10, the shortwave radiation data for clay soil are presented. With its fine particles and higher moisture content, clay absorbs more radiation and reacts more slowly to sunlight changes compared to sand and loam. The fitted curve reflects clay's ability to retain heat for extended periods, resulting in a more gradual and steady radiation trend throughout the year. The fitting equations of the three soil's type are listed in Table V.1.

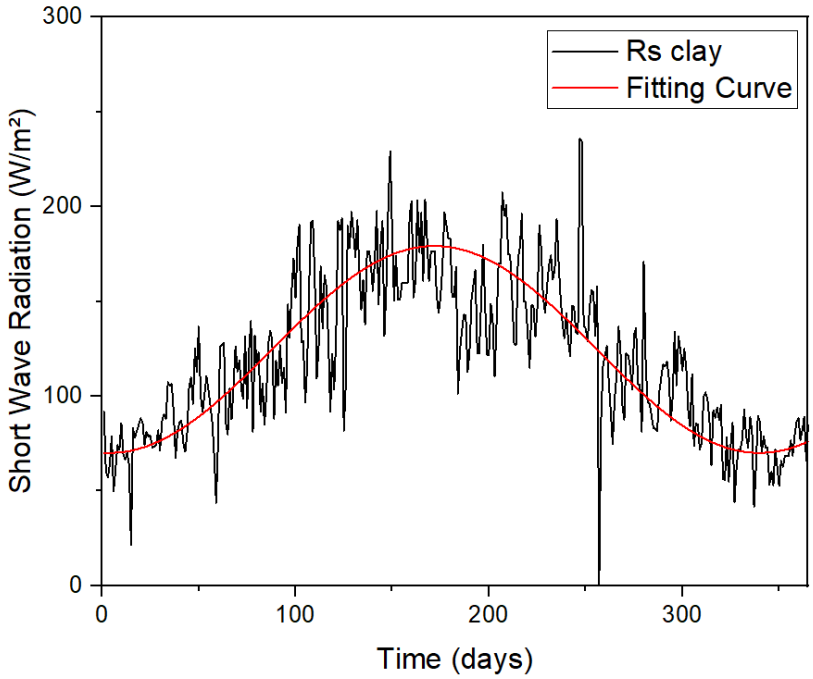

Figure V. 10. Shortwave radiation in Oran for Clay (2022)

Table V. 1. Fitting equations of Shortwaves radiation

soil	R_s
sand	$R_s = 115.25 + 52.39\sin\left(\frac{\pi(t-74.54)}{199.92}\right)$
loam	$R_s = 124.65 + 54.51\sin\left(\frac{\pi(t-88.85)}{168.09}\right)$
clay	$R_s = 124.65 + 54.57\sin\left(\frac{\pi(t-87.84)}{168}\right)$

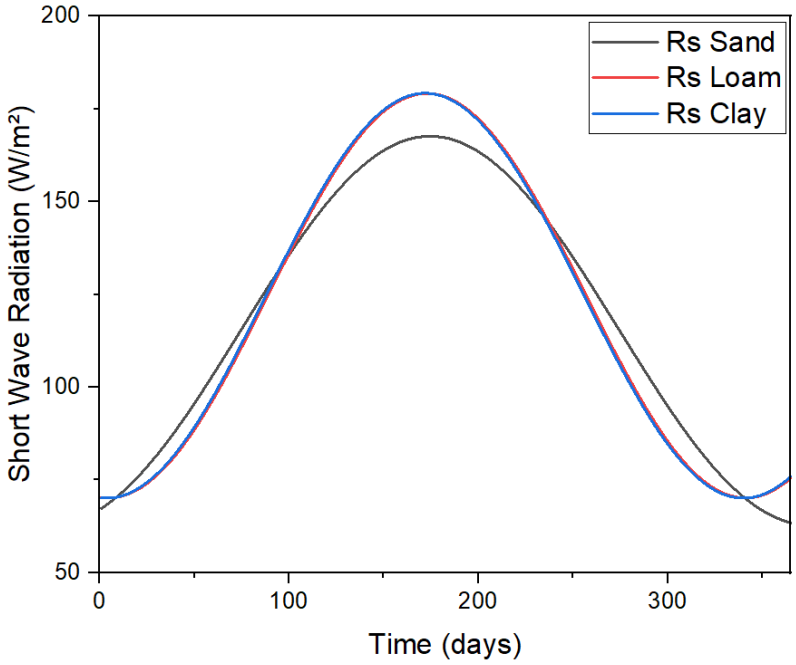

Figure V. 11. Shortwave radiation for three types of soil in Oran (2022)

The three fitting curves are illustrated in Figure V.11. Shortwave radiation absorption varies seasonally across sand, loam, and clay soils throughout the year. All three soil types follow a similar trend, with radiation levels reaching their highest around mid-year and decreasing at the start and end of the year. During peak periods, clay and loam absorb the most shortwave radiation, reaching approximately 180 W/m², while sand has a slightly lower peak at around 168 W/m². The differences in the curves indicate that although the overall pattern is the same, clay and loam retain more radiation at their peak compared to sand.

Figure V.12 shows a yearly mean of net radiation heat flux (R_n) for three types of soils: clay, loam, and sand. Their respective curves have a typical pattern characterized by an increase in heat flux, followed by a peak in the middle of the year, and a decline when the year comes to an end. For clay soil, the peak net radiation heat flux is around 68 W/m², which is the highest among the three soils. This means that clay absorbs the most radiation during the peak period as a result of its fine texture and high moisture retention.

Loam soil has a peak net radiation heat flux of approximately 61 W/m², and it follows a pattern similar to that of clay. Loam might therefore not be such a strong heat-absorbing soil, but its composition ought to contribute towards an equally notable peak. Sand has the least peak, slightly below loam with a peak of 60 W/m². With such coarse texture and low moisture retention, its heat-absorbing power would be even lower, leading to faster heat loss. This would certainly cause it to have a much lower peak than both clay and loam as well as a rather lesser

overall net radiation heat flux. On the other hand, for the majority of soils, net radiation heat flux is negatively driven at both ends of the year. This means that during the winter months, net heat loss was higher from the soil surface than absorption from it. Conversely, it becomes positive in the middle of the year, indicating net heat gain as the soil absorbs more radiation as a result of the intensity of the sun's radiations

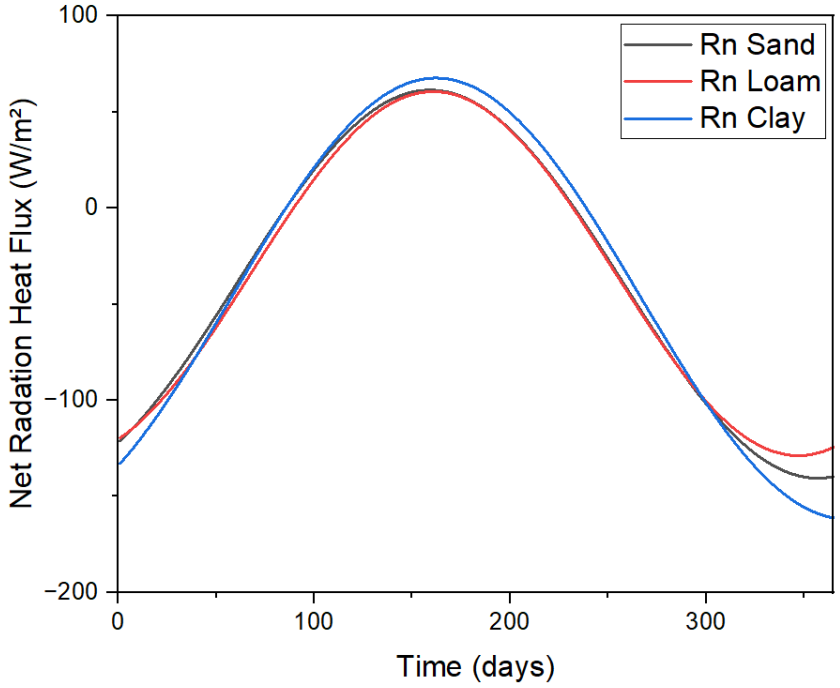

Figure V. 12. Net radiation Heat flux for three types of soil in Oran (2022)

For convective heat fluxes such as sensible heat flux (*H*), which considers precipitation, wind, and humidity, Figure V.13 shows the annual variation in sensible heat flux for sand, loam, and clay soils, which is basically the heat transferred between the surface of Earth and the atmosphere. During warmer periods, the maximum value for loam is the highest at approximately 140 W/m², followed by sand at about 105 W/m² and clay at around 100 W/m²; all peak around day 300. Sand and clay decrease to nearly -50 W/m² while loam's would go down to about -45 W/m² on about day 150, suggesting a temperature decrease. The way different kinds of soils retain and lose heat does influence the energy balance between the surface and the atmosphere as suggested by such patterns.

Latent heat flux (*LE*) of three soils: clay, loam, and sand is presented in Figure V.14 with respect to time. The flux begins at about 0.043 W/m² with lower values at 0.01 W/m² for sand and loam, and 0.015 W/m² for clay, around day 150. Then, the flux begins to increase. By the end of 365 days, the maximum flux reaches to 0.075 W/m² for clay, followed by loam at around 0.067 W/m² and sand at about 0.063 W/m². This pattern shows how soils differently retain and

evaporate water. Sand shows a lower latent heat flux through time, clay shows relatively larger latent heat flux due to water retention ability.

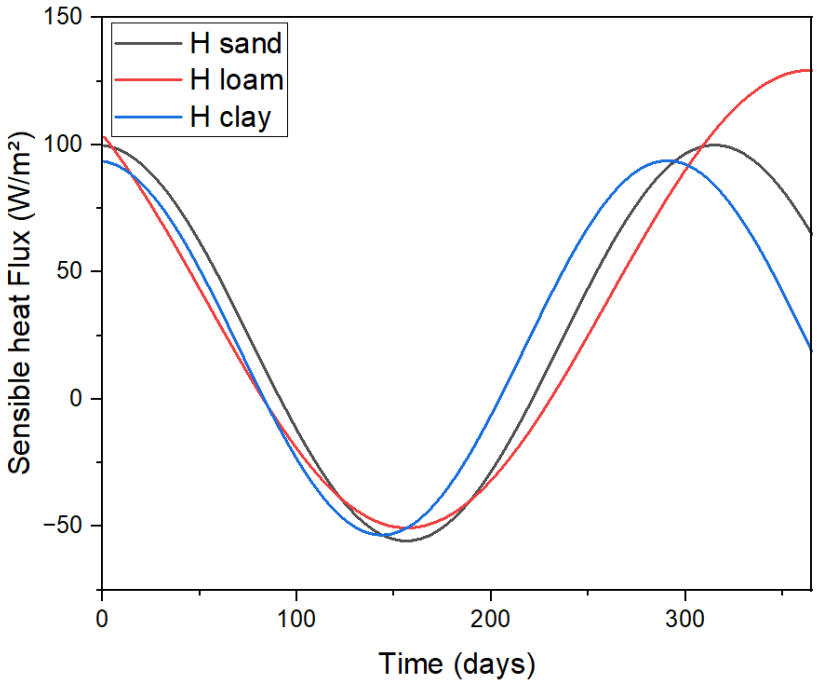

Figure V. 13. Sensible heat flux for three types of soil in Oran (2022)

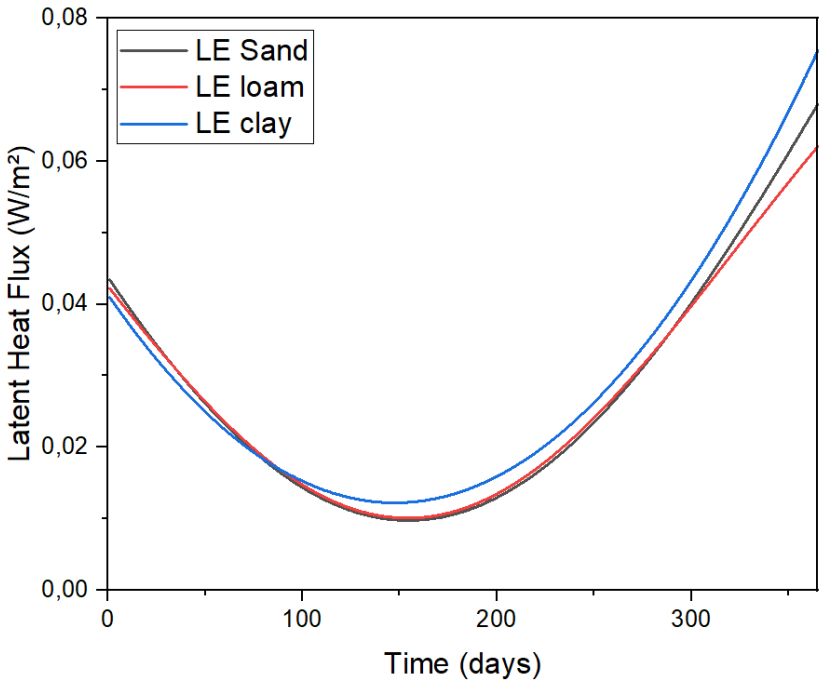

Figure V. 14. Latent Heat flux for three types of soil in Oran (2022)

The variation in soil heat flux over time for three different soil types: clay, loam and sand is shown in figure V.15. The thermal inertia of clay is the highest of the three soil types, reaching a maximum of around 110 W/m² and falling to around -50 W/m². While loam reaches a

maximum of around 40 W/m² and falls to around -40 W/m², sand reaches around 60 W/m² and falls to around -50 W/m². Each soil profile follows a similar pattern, with a peak occurring around 150-160 days after minimums between 0 and 300 days. Compared to loam and sand, clay exhibits the largest oscillation amplitude, indicating superior heat retention.

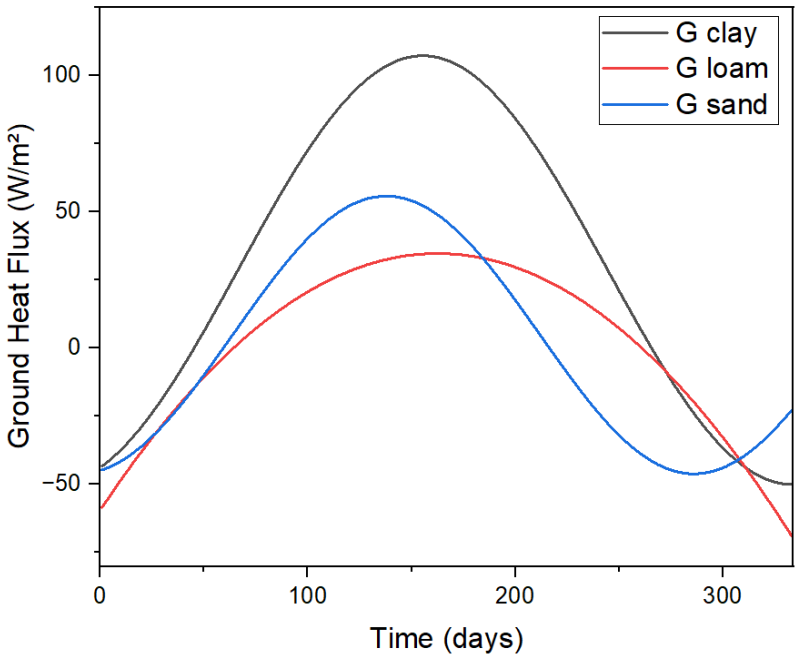

Figure V. 15.Ground Heat flux for three types of soil in Oran (2022)

b) Hydrothermal Transfer

The simultaneous movement of heat and moisture in soil is known as hydrothermal transfer, and it varies greatly depending on the type of soil, clay, loam, or sand. Sandier soils are more susceptible to abrupt temperature changes because of their larger particle size and reduced moisture retention, which speed up heat transfer but restrict moisture movement. Loam's balanced composition of sand, silt, and clay allows for moderate heat and moisture transfer, which makes it perfect for agriculture because it retains moisture while allowing for adequate airflow and temperature control. In contrast, clay soils have fine particles and retain a lot of moisture, which slows down heat transfer and decreases moisture movement. Clay is more sensitive to temperature changes when wet, even though it efficiently retains heat over long periods of time. The efficiency of geothermal energy systems, soil respiration, and plant growth are all impacted by these unique hydrothermal characteristics.

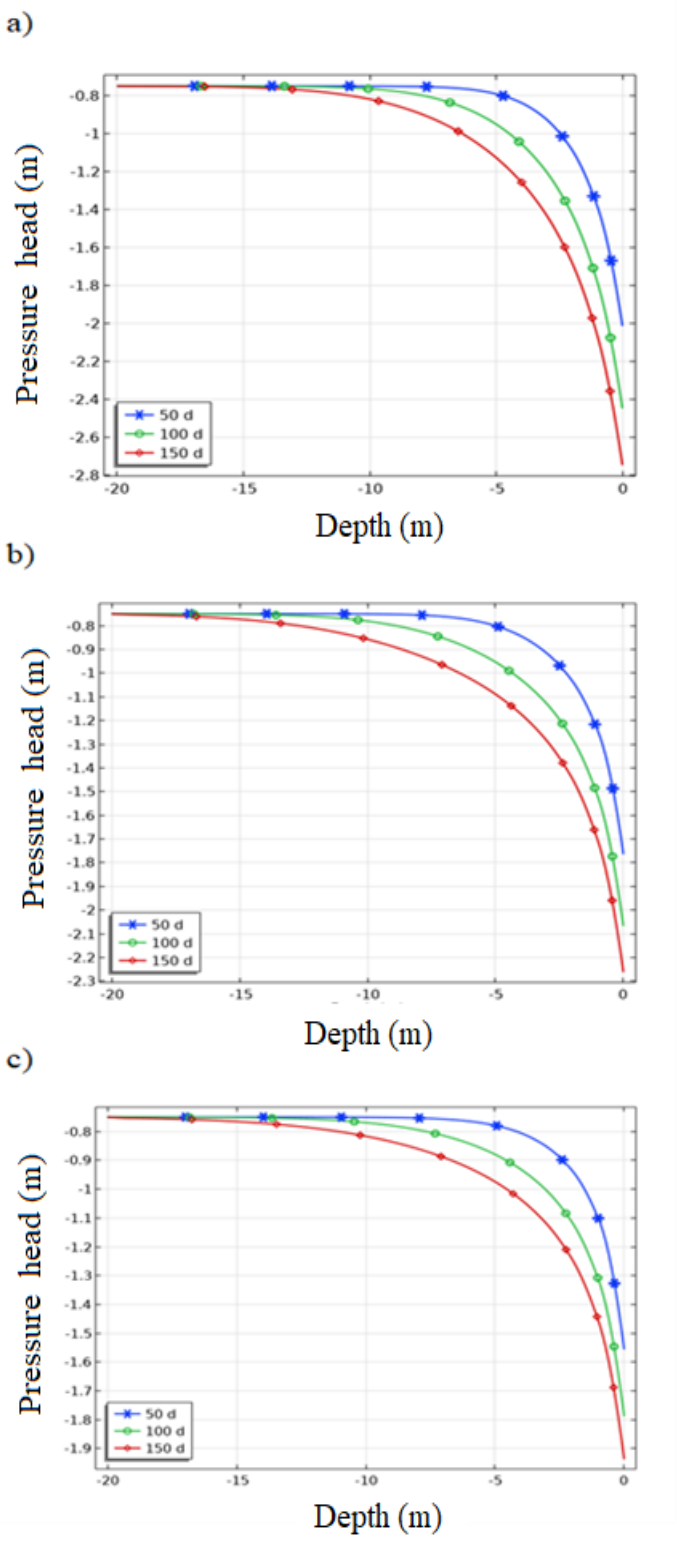

Figure V. 16. Pressure Head as a Function of Depth for Different Soil Types Over Time: a) Clay, b) Loam, and c) Sand

The pressure head for clay, loam, and sandy soils over 50, 100, and 150 days is shown in figure V.16 as a function of depth. The pressure head of clay in Figure V.16.a is negative at shallow

depths but significantly less negative as depth increases, suggesting significant drying over time, particularly by 150 days. A balanced mixture of sand, silt, and clay in loam (Figure V.16.b) maintains higher (less negative) pressure heads at all depths, indicating improved moisture retention and a slower drying process. Sand, on the other hand (Figure V.16.c), shows the least amount of negative pressure heads, which indicates the least amount of water retention and the quickest drying with the least amount of change over time. These figures show that loam provides stable moisture, sand dries the fastest with little water retention, and clay initially retains water but dries out quickly.

The effects of water content on two important soil characteristics: thermal conductivity and volumetric heat capacity for clay, loam, and sand, respectively, are depicted in Figures V.17, V.18, and V.19. Both characteristics show a linear increase with increasing water content. This is because wetter soil is better at conducting and storing heat because water has a higher thermal conductivity and heat capacity than air.

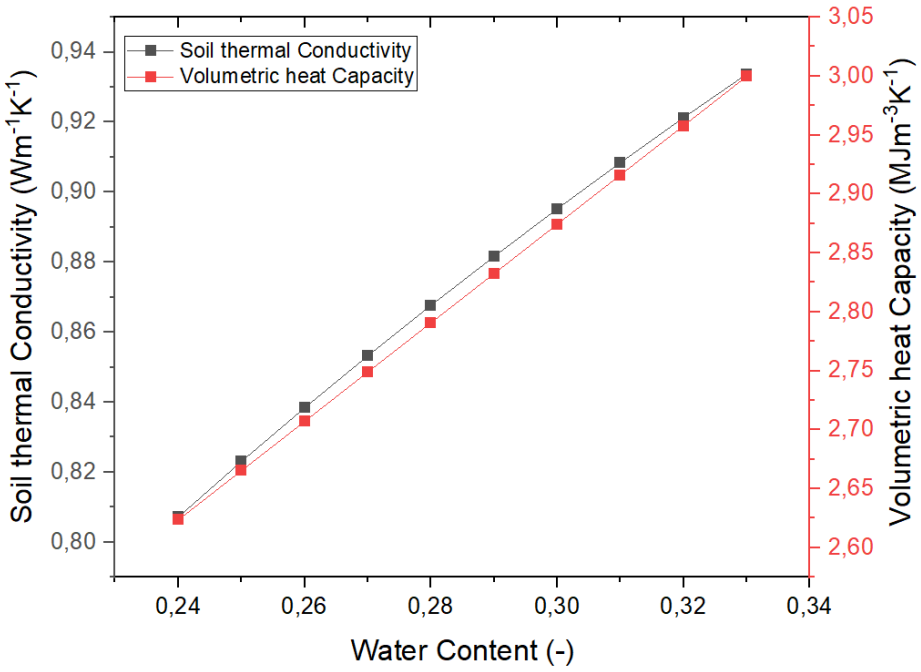

Figure V. 17. Thermal Conductivity and Volumetric Heat Capacity of Clay

A strong and consistent relationship is indicated by the close alignment of data points for both properties, highlighting the significant influence of moisture levels on soil thermal behavior. Although the rate of change varies slightly depending on the composition of the soil, this trend is visible in all three types of soil: clay, loam, and sand. All three follow a similar pattern of increasing thermal conductivity and heat capacity with higher water content.

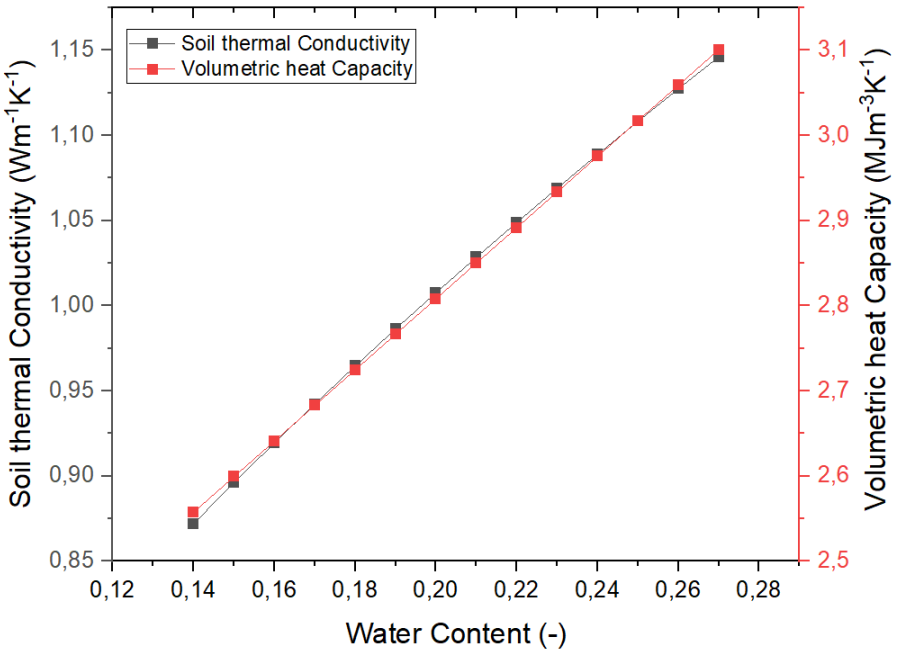

Figure V. 18. Thermal Conductivity and Volumetric Heat Capacity of Loam

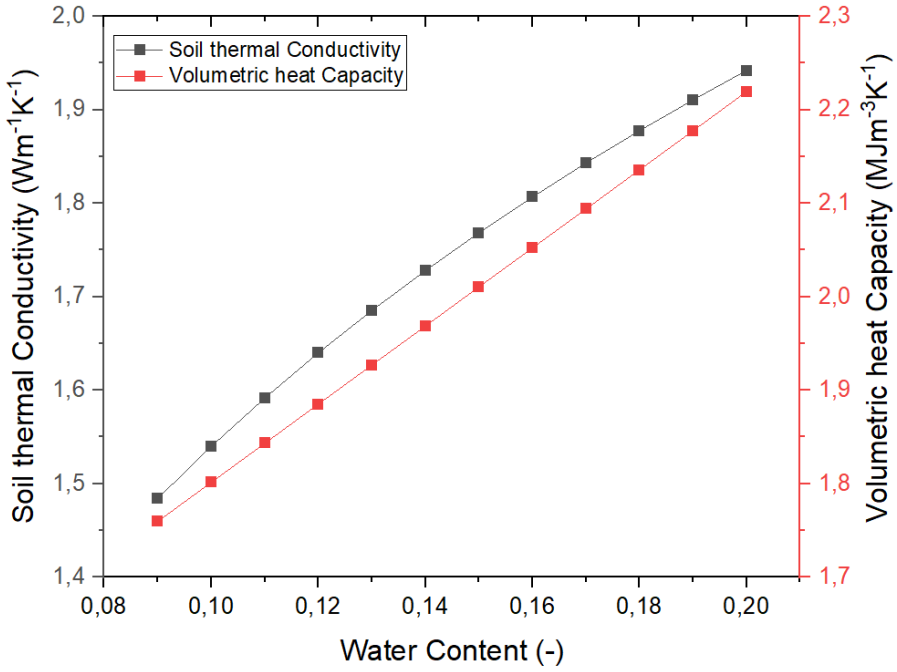

Figure V. 19. Thermal Conductivity and Volumetric Heat Capacity of Sand

c) Soil Temperature

After obtaining the soil temperature of the studied soils, the surface temperature was compared to the Equation V.1, proposed by Badache et al. [145], which calculates the surface temperature as a function of ambient temperature as illustrated in Figure V.20. The analyses of temperature data from both datasets show seasonal fluctuations, with temperature peaks around day 200, or midsummer, followed by declines toward the year's start and end. The correlation between simulated soil temperature and soil temperature proposed by Badache et al. signifies a very good fit. In fact, considering that temperature readings can accurately reflect changes in the real world, it serves as a great point of reference for model validation. The similarity seen in temperatures simulated against the Badache et al. equation indicates that the techniques promoted in this study are indeed well implemented, giving a high degree of conformity with the temperature pattern simulation. Such a result confirms the robustness of the measured data not only in evaluating the model performance but also in validating the effectiveness of the methodology.

$$T_s = 17.898 + 0.951\ T_a \quad \text{(V.1)}$$

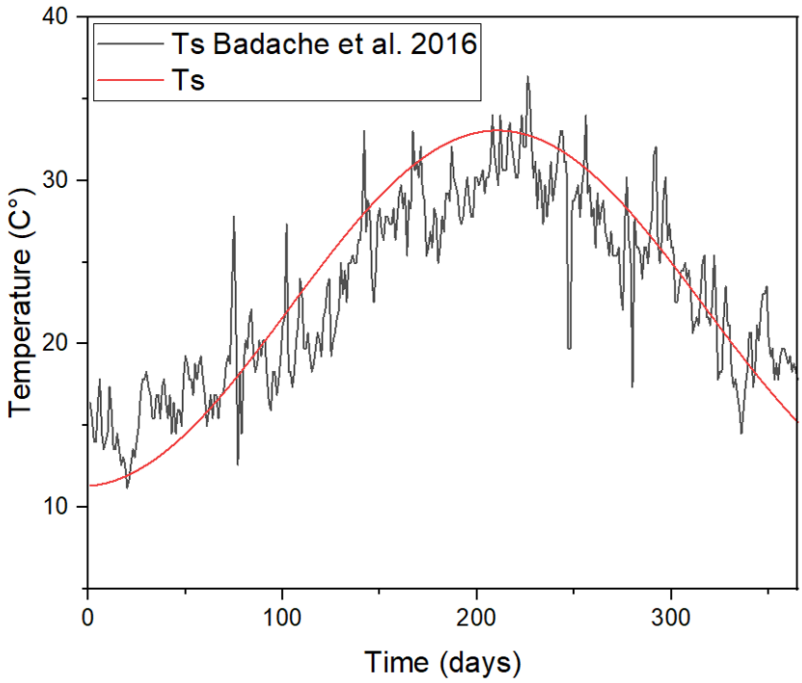

Figure V. 20. Comparison of Surface Temperature Variations Over Time

Figure V.21 shows the variation in temperature in function of time for three types of soils: clay, sand, and loam. two depths were taken into consideration, at the surface and 2 m below ground. Surface temperatures of all soils show seasonal variations, with temperature peaks during the warm season and seasonal lows during the cold season. Sand has shown the greatest variations at the surface compared to clay and loam. In contrast, clay exhibits the most stable temperature

profile, with smaller fluctuations. The 2 m subsurface temperatures show less variation than at the surface, with a marked time lag, which implies slower transfer of heat through the ground. Because of its slower rate of heat absorption and release, clay stays cooler and more stable among the deeper layers, whereas sand undergoes more noticeable temperature changes. Loam behaves in an intermediate manner, fluctuating in temperature moderately. All these pieces of evidence serve to mark the differences in heat transfer influenced by the type of soil and depth; for instance, clay shows a better performance for the geothermal application.

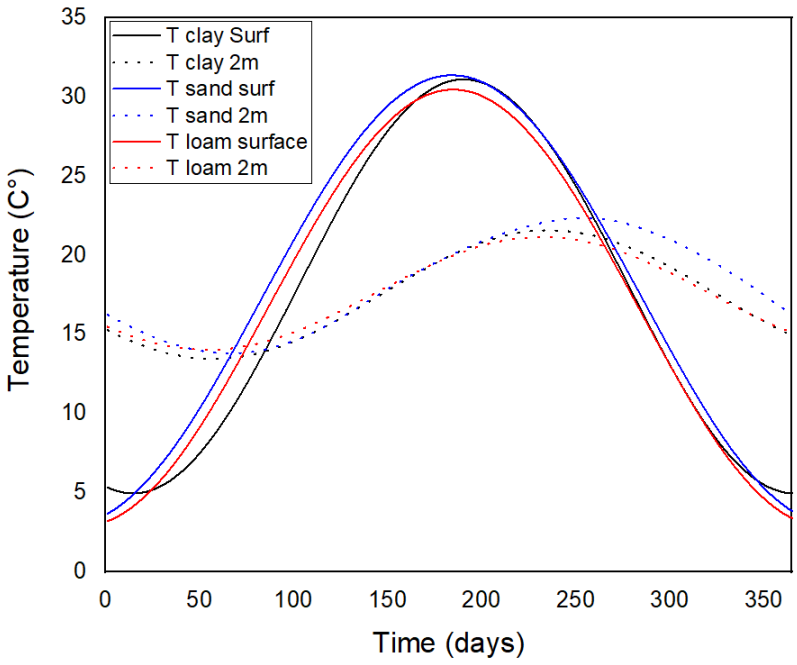

Figure V. 21. Seasonal Temperature Variations at the Surface and 2m Depth for Clay, Loam, and Sand

Figure V.22 shows the temperature variation in sandy soil at different depths for each month. The temperature is highest on the surface in June and July at 35°C and lowest at around 2°C in January and December. The range of the temperature is reduced with depth. At 2 meters depth, the maximum temperature is around 25°C in July and the minimum is around 10°C in January and December. At 5 meters depth, the temperature fluctuates less, with a maximum of around 18°C in late summer and a minimum of around 15°C in winter. At 8 meters, the variation is minimal, with temperatures staying close to 16°C year-round. Beyond this depth, the temperature remains almost constant throughout the year.

The soil temperature profile of loam is shown in Figure V.23. At the surface, there are significant seasonal variations in temperature, ranging from a minimum of 4°C in January to a maximum

of 30°C in July. More stable conditions predominate at deeper depths, while temperature fluctuation diminishes as depth increases.

The average annual temperature is nearly the same at about 6 meters, with a stable temperature of 16°C. The transition from a highly variable surface temperature to a stable subsurface environment takes place at this depth, demonstrating how the impact of seasonal variations diminishes with depth.

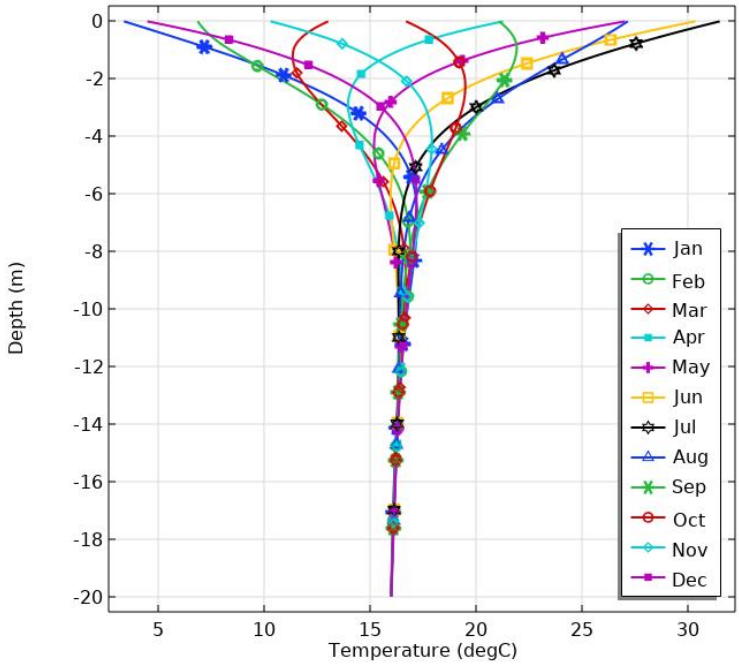

Figure V. 22. Temperature profile of Sand

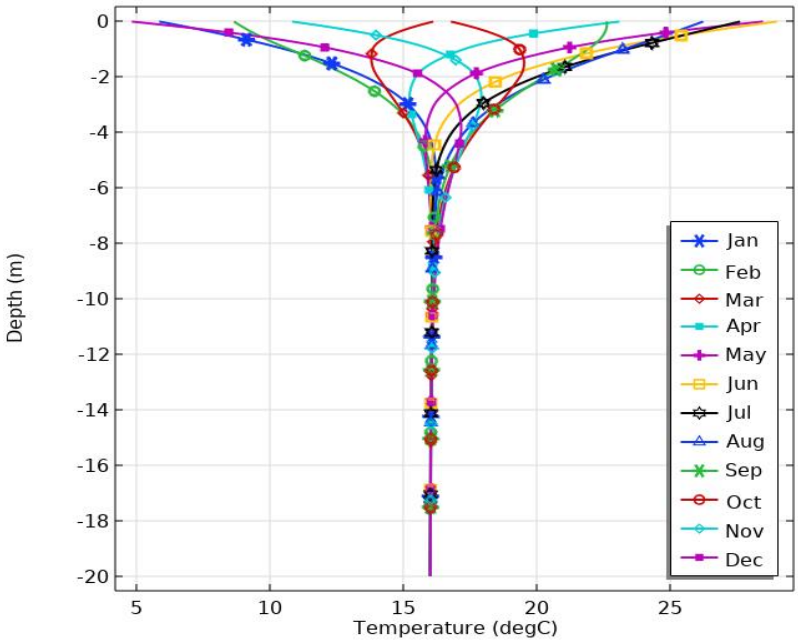

Figure V. 23. Temperature profile of Loam

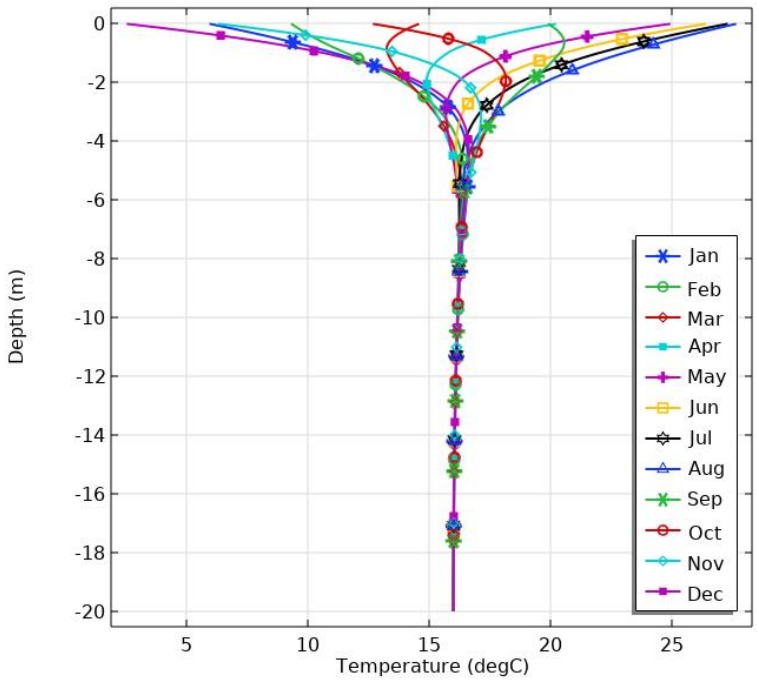

Figure V. 24. Temperature profile of Clay

The soil temperature profile variations for Clay are shown in Figure V.24. The upper surface experiences significant temperature fluctuations, attaining about 28°C during summer and dropping to about 3°C in winter. Temperature variations lessen with increasing depth, with deeper layers exhibiting greater stability. At 5 m, the temperature remains almost constant for the whole year at around 16°C, demonstrating the insulating properties of clay soil, which attenuate the effect of seasonal temperature variations at shallow depth.

d) Second conclusion

This study evaluated the thermal performance of three soil types in order to determine their suitability for geothermal energy applications. A numerical model was developed for the simulation of temperature variations influenced by the transient thermal conditions, meteorological data, and solar radiation cycles specific to the Oran region. The objective was to identify the soil type that provides optimal thermal efficiency for energy extraction at shallow depths, whereby limited drilling requirements and more energy gains from the soil maximize overall efficiency. It was found that clay soils perform better compared to the other two soils due to their high capacities for heat retention and moisture regulation, thereby rendering them most suitable for horizontal ground heat exchangers at shallow depths. Loam soils performed moderately well thermally, while sandy soils did have rapid temperature response but little

capacity to retain heat energy. Clay soils' natural ability to maintain thermal performance at lower depths suggests that they could be used efficiently, affordably, and to extract the most energy possible. Additionally, by incorporating site-specific soil and climatic conditions, the numerical model can be easily modified for use in other locations. In addition to ensuring economic and environmental sustainability, these results provide insight into how to optimize geothermal energy systems by installing efficient soils, like clay, at shallow depths. This could greatly improve energy output performance. Future research might look into different heat sources that could influence geothermal systems in one way or another and moderate the dynamics of soil temperature. Future research could examine how the performance and efficiency of geothermal energy applications are impacted by the variation in soil compositions within a single soil type. Assessing the necessary degree of soil compaction could be another area of focus in an attempt to determine the best compaction techniques that would improve soil performance and heat transfer efficiency of geothermal energy systems.

V.2.3. Influence of Salinity

Once the initial temperature profile has been established and the fluxes for each type of soil with different salinity levels have been determined, the study turns to examining soil temperatures at various depths. The seasonal variation in soil temperature at the surface of sandy soil with salinity levels of C = 0 M, C = 0.1 M, and C = 0.2 M is illustrated in Figure V.25. The highest peak temperature value was obtained on sand with C = 0.1 M in the summertime, followed by C = 0 M and then C = 0.2 M. In winter, the trend was the reverse, where sand at C = 0 M kept much of the heat. Therefore, it can be concluded that salinity affects the thermal behavior of sand divergently throughout the year, such that moderate salinity enhances heat retention during summer, while non-saline soils retain more heat in winter.

Figure V.26 reports the yearly variation in surface temperature for sandy loam soils of different salinity level C = 0 M, C = 0.1 M and C = 0.2 M. All soil types present a similar sinusoidal pattern in temperature peaking in the middle of the year and troughing at the beginning as well as at the end of the year. The highest summer peak was found in the saline soil (C = 0.2 M), which was just a little bit higher than moderate saline (C = 0.1) M and the non-saline (C = 0 M) types. This demonstrates that higher salinity causes the soil to retain more heat during the warmer months. Despite these variations, it is evident that the overall pattern of temperature change is similar, with salinity having a greater impact on sandy loam soils' summer peak temperatures.

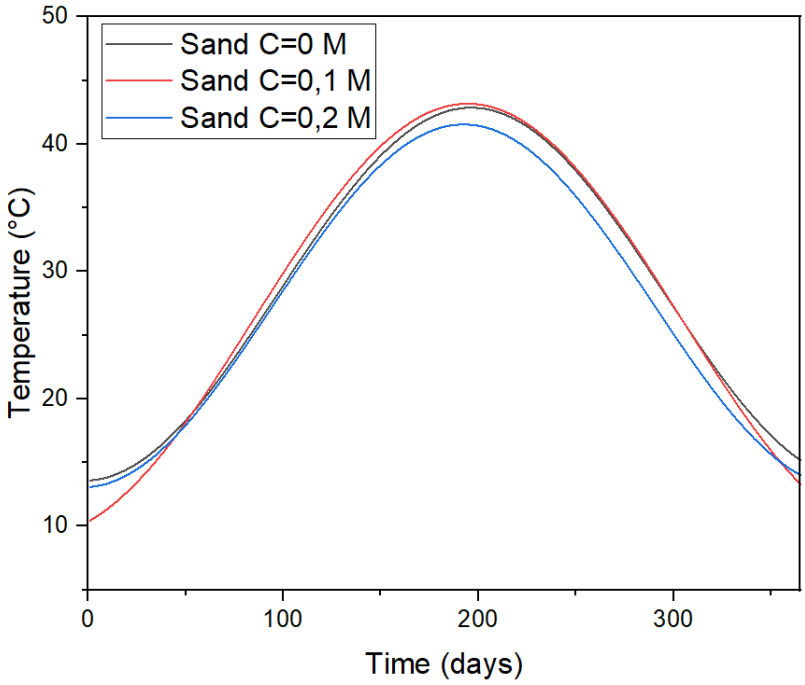

Figure V. 25. Seasonal Surface Temperature of Sand with Different Salinity Levels (C = 0 M, C = 0.1 M, C = 0.2 M)

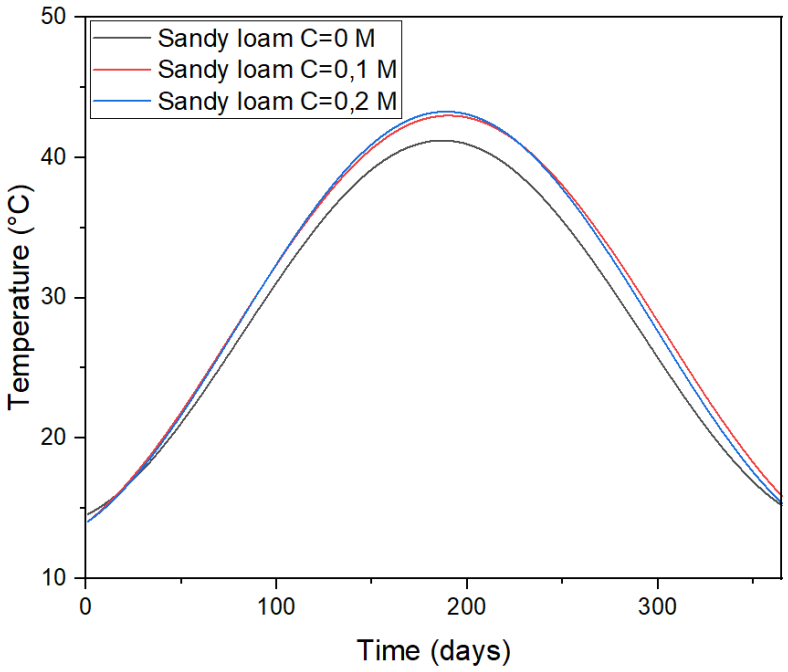

Figure V. 26. Seasonal Surface Temperature of Sandy loam with Different Salinity Levels (C = 0 M, C = 0.1 M, C = 0.2 M)

Figure V.27 presents the seasonal temperature variations at 20 cm depth in sandy soils under three salinity levels. During summer, the highest peak temperature is reached by soil with moderate salinity, corresponding to C = 0.1 M, next by the non-saline soil, corresponding to C = 0 M, while the last is the highly saline soil, corresponding to C = 0.2 M. In winter, in contrast,

the highest temperature appears in the non-saline soil C = 0 M, followed by that in the highly saline soil C = 0.2 M, while the minimum of the three will correspond to the soil with moderate salinity C = 0.1 M. From the variations, salinity level affects soil temperature in summer against that in winter; hence, in summer, moderately saline soil gets hotter, while in winter, the non-saline soil retains more heat.

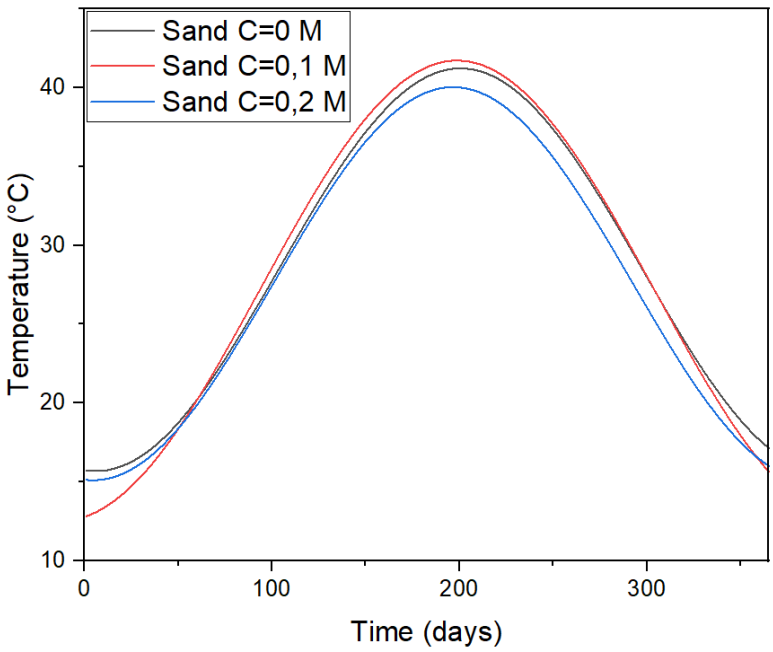

Figure V. 27. Seasonal Temperature Variations at 20 cm Depth in Sand with Different Salinity Levels (C = 0 M, C = 0.1 M, C = 0.2 M)

Figure V.28 illustrates the seasonal temperature variation in sandy loam soils at the same depth, comparing three salinity levels. In both summer and winter, the soil with the highest salinity C = 0.2 M had the highest temperature, demonstrating that increasing salinity improves the soil's ability to absorb heat; followed by moderately salinity soil C = 0.1 M, and non-saline soil C = 0 M having the lowest peak temperature. Therefore, salinity plays an important role in temperature variation of soils.

As shown in Figure V.29 below, similar to Figures V.25 and V.27, at a 40 cm depth, the seasonal variation of temperature over the year for three various salinities is described. The temperature rises to its summer maxima in the soils where C = 0.1 M, C = 0 M, and C = 0.2 M, respectively. In winter, however, the highest temperature is observed in soils where C = 0 M, followed by C = 0.2 M and C = 0.1 M.

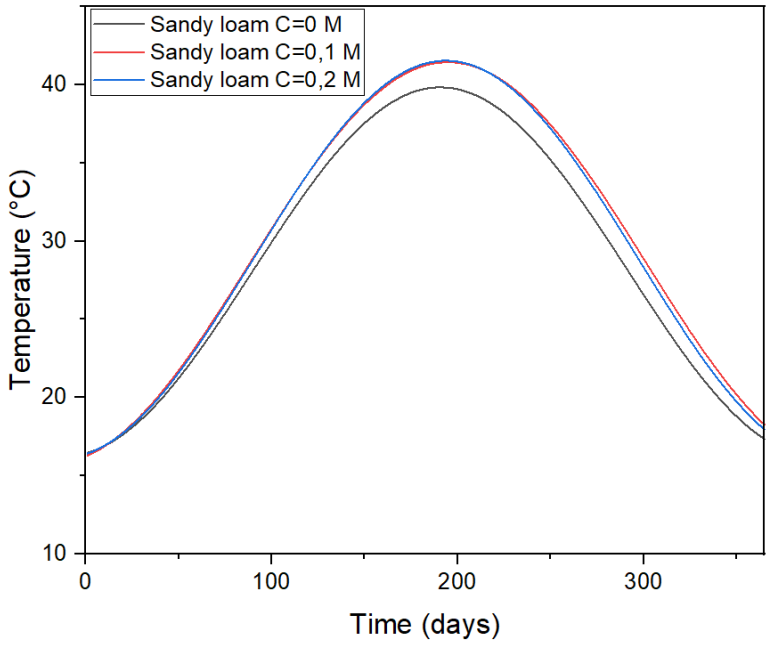

Figure V. 28. Seasonal Temperature Variations at 20 cm Depth in Sandy loam with Different Salinity Levels (C = 0 M, C = 0.1 M, C = 0.2 M)

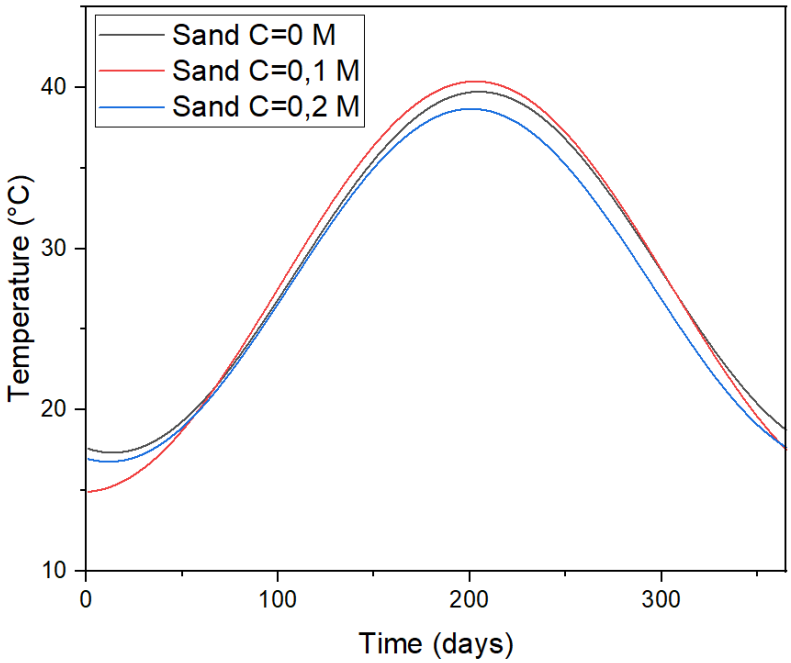

Figure V. 29. Seasonal Temperature Variations at 40 cm Depth in Sand with Different Salinity Levels (C = 0 M, C = 0.1 M, C = 0.2 M)

The annual temperature variation for three distinct salinity levels in sandy loam soil at a depth of 40 cm is depicted in Figure V.30. The findings support those in Figures V.26 and V.28, which demonstrate that temperature rises with salinity. The highest salinity of C = 0 was recorded

throughout the year, followed by C = 0.1 M and C = 0.2. The trend is most noticeable during the summer when heat retention causes temperature peaks to rise sharply with increased salinity.

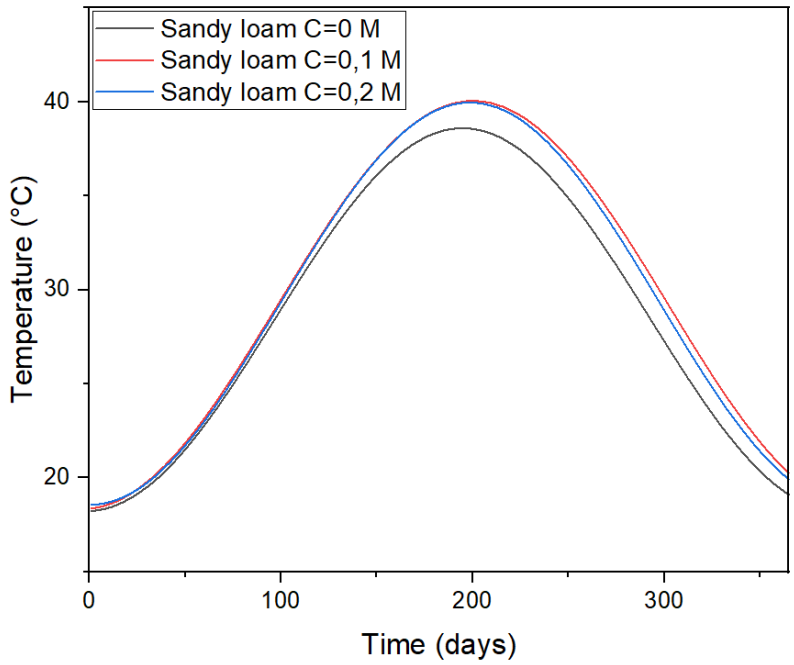

Figure V. 30. Seasonal Temperature Variations at 40 cm Depth in Sandy loam with Different Salinity Levels (C = 0 M, C = 0.1 M, C = 0.2 M)

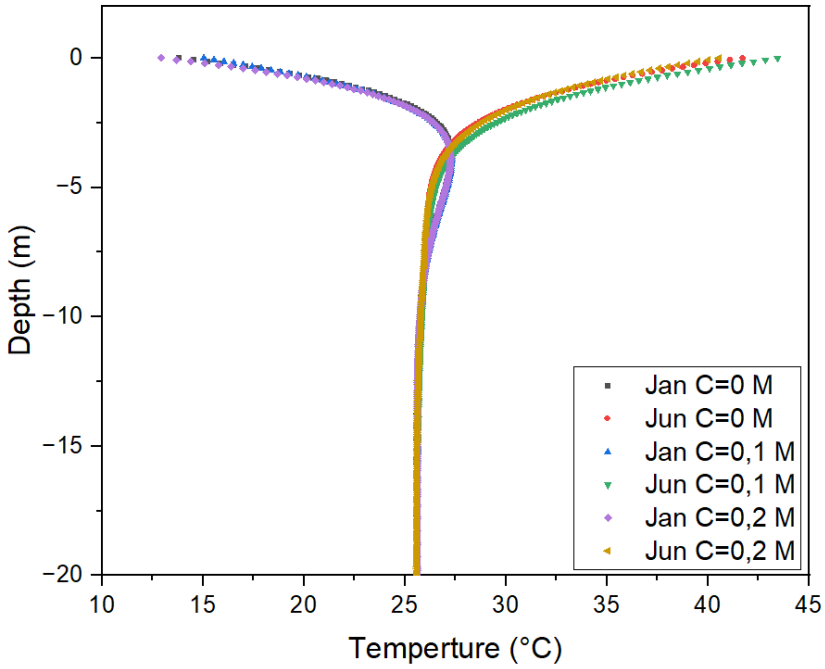

Figure V. 31.Temperature Profile in Sand for Varying Salinity Levels (C = 0 M, C = 0.1 M, C = 0.2 M)

Figure V.31 shows the temperature profile in sandy soil at various depths for different salinity levels during winter (January) and summer (June). Salinity was applied only at the surface down

to a depth of 40 cm in the model. Temperature variations are significant around the surface, especially in June, where salinity, C, equals 0.1 M, leading to a slight increase in temperature compared with salinity levels of C=0M and C=0.2M. In January, there are little differences in temperature due to salinity, which means that salinity has a more intense effect on the warmer period. Below the depth of 40 cm, the temperature, where salinity is not applied, stabilizes around 25°C. In general, salinity affects surface temperatures, particularly in summer. In winter, its impact is lesser.

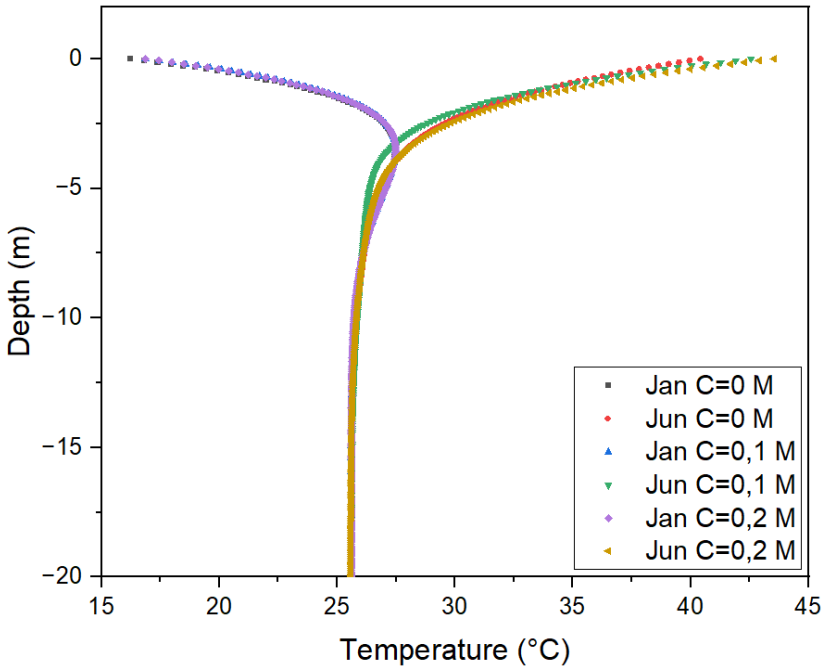

Figure V. 32. Temperature Profile in Sandy loam for Varying Salinity Levels (C = 0 M, C = 0.1 M, C = 0.2 M)

Figure V.32 demonstrates the temperature profile of sandy loam soil for different salinity in winter (January) and summer (June), with salinity applied only to the top 40 cm of the soil. Here in the upper layer, the temperature differences are most pronounced, particularly in the summer (June) when a higher salinity soil C = 0.2 M has higher temperatures. In winter (January), the temperature differences between salinity levels are less undetected, with non-saline soil C = 0 M slightly warmer. Below the depth of 40 cm, where salinity is not applied, the temperature stabilizes for all salinity and remains constant at around 25 ºC, with no considerable seasonal or salinity influence. This shows that salinity mainly affects the temperature surface and has more influence during hotter periods, while deep soil layers are stable and independent of salinity.

a) Third Conclusion

This study examined the effects of salinity levels on heat transfer through two distinct soil types—sand and sandy loam—in the Adrar region of Algeria, which is renowned for its extremely high temperatures, using COMSOL Multiphysics. Three salinity levels (C = 0 M, C = 0.1 M, and C = 0.2 M) were applied to the top 40 cm of the soil in order to examine the effects of these levels on heat absorption and retention over the course of the year. The findings demonstrated that different soil types react differently to variations in salt concentration and that salinity does not have an identical effect on all soil types. The optimal thermal performance for sandy soils was achieved at a moderate salinity level (C = 0.1 M). It provided a good balance between heat absorption and retention, allowing the soil to retain enough warmth in colder months while absorbing more heat during warmer ones. Conversely, sandy loam soils exhibited distinct behaviors. In summer, when surface temperatures were significantly higher, they retained the most heat when the highest salinity level (C = 0.2 M) was used. This shows that higher salinity improves heat storage, probably because it increases the soil's thermal conductivity, which increases its capacity to absorb and hold onto energy.

These results emphasize a crucial point: depending on the type of soil, salinity can have varying effects on soil temperature. Higher salinity in sandy loams helps the soil retain more heat, whereas too little or too much salinity can decrease the efficiency of heat absorption in sandy soils. Geothermal energy applications, agriculture, and climate adaptation all depend on an understanding of this relationship, particularly in arid areas where controlling soil temperature can significantly impact farming productivity and energy efficiency. To better optimize soil thermal behavior for applications, future studies could use ground heat exchangers to investigate how these effects change over time under real-world conditions.

V.2.4. Influence of physical properties

Our research spanned the entire year of 2023, with a focus on examining the data for a cold day in January and a hot day in July, as shown in Figure V.33. The graph (a) reveals large surface temperature variations between the two days, which decrease with depth, indicating that clay soil is thermally stable at a shallow depth of roughly 4 meters. The graph (b) depicts the temperature distribution in January, with the surface having the lowest temperatures and progressively increasing with depth due to limited heat penetration during the winter. In contrast, the graph (c) depicts the July distribution, which shows greater surface temperatures and a noticeable gradient as depth increases, influenced by summer conditions and thermal diffusion.

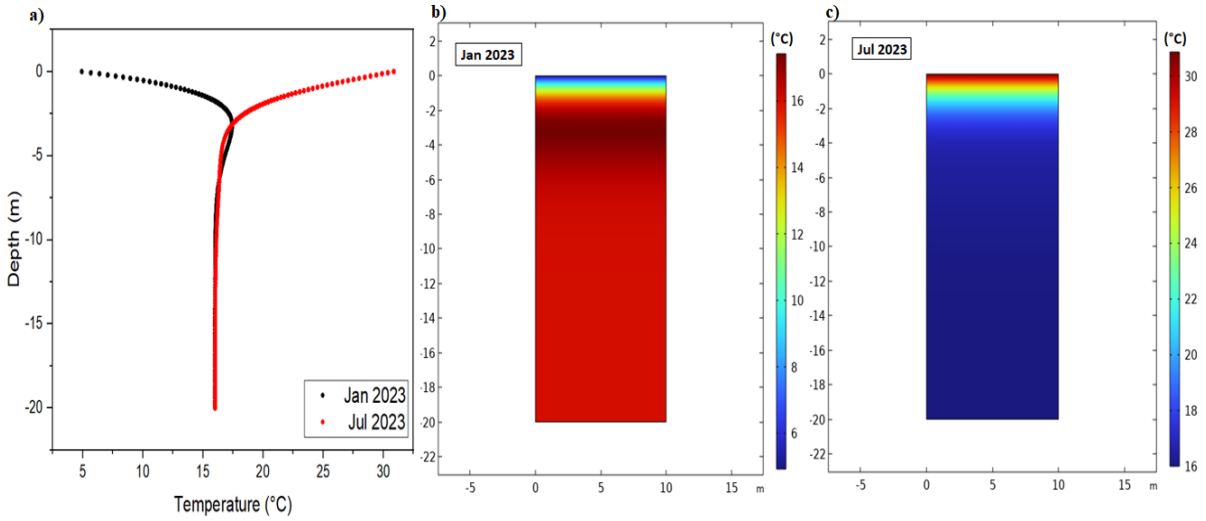

Figure V. 33. Temperature Profiles and Distributions of Clay on the Coldest Day in January and the Hottest Day in July 2023

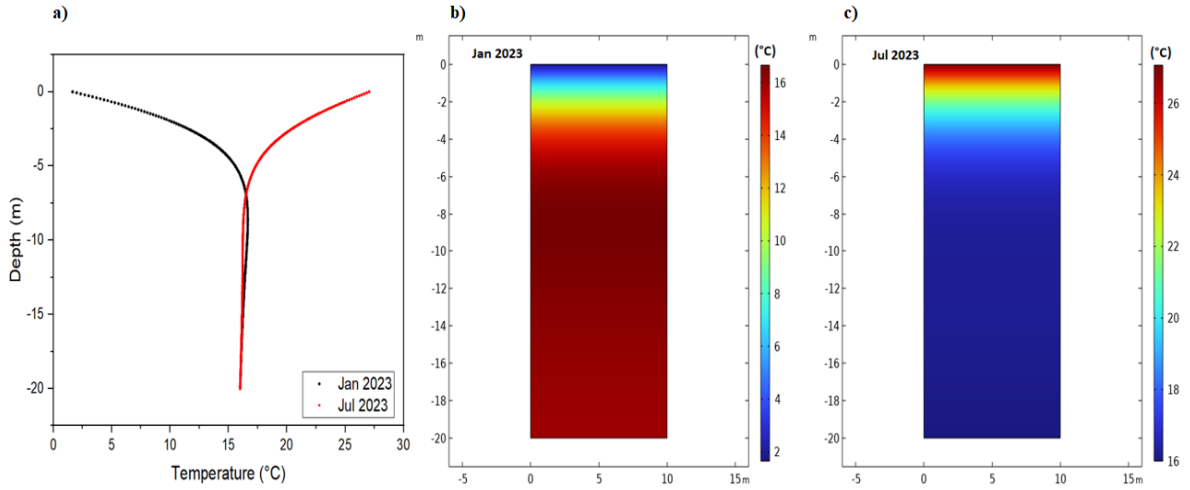

Figure V. 34.Temperature Profiles and Distributions of Sand on the Coldest Day in January and the Hottest Day in July 2023

The temperature distribution and profiles of sand soil for the coldest day in January and the warmest day in July of 2023 are shown in Figure V.34. Temperature changes with depth are depicted in graph (a), which highlights notable surface differences between winter and summer. These differences eventually diminish, with thermal stability being noted at around 6 m. January's temperature distribution is shown in graph (b), where limited heat transmission causes surface temperatures to be lower and progressively rise with depth. The distribution of July is shown in graph (c), which shows the impact of summer heat and thermal diffusion. There is a discernible gradient as depth increases and higher surface temperatures.

a) Effect of porosity

Figure V.35 illustrates how pressure head varies with depth in clay and sand at different porosity levels (n = 0.4, 0.6, 0.8). The graphs show that clay retains water effectively, especially at lower porosity (n = 0.4), where pressure head decreases gradually with depth. This characteristic makes clay particularly well-suited for geothermal systems, as lower porosity means less empty space, reducing both heat loss and water loss. In contrast, sand experiences a rapid drop in pressure head with depth, indicating poor water retention and quick drainage. However, when sand has a lower porosity (n = 0.4), it retains water slightly better, making it a more viable option. Yet, clay remains the superior choice. Overall, low porosity (n = 0.4) is the most efficient option for geothermal applications, as it minimizes heat loss and ensures stable energy retention. Clay with low porosity is particularly well-suited for these systems, while sand may be useful in scenarios requiring higher permeability and water movement.

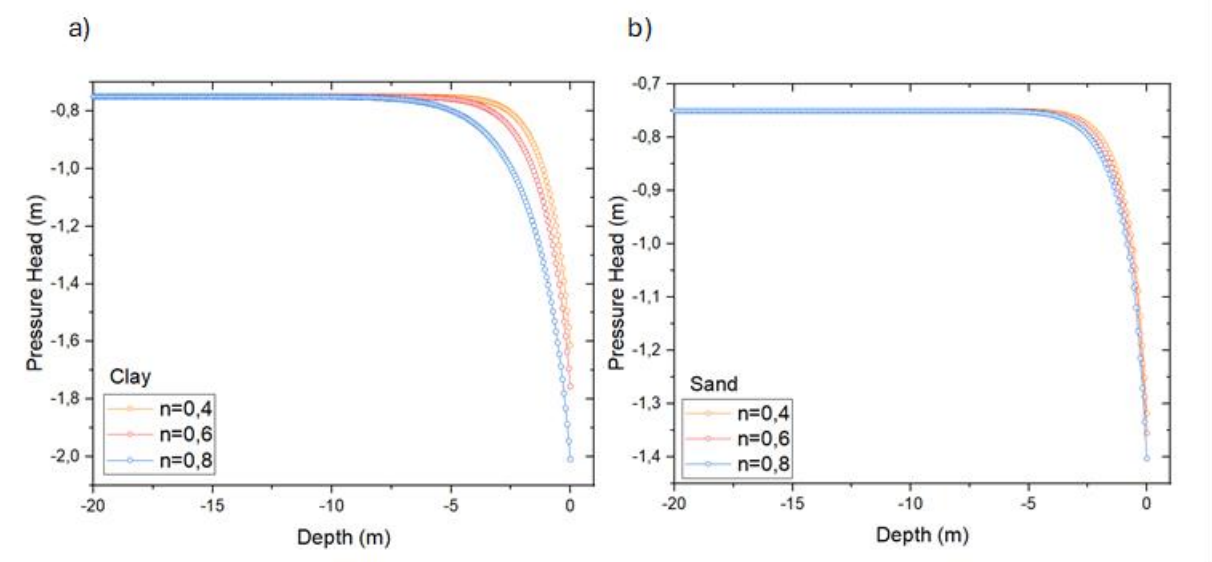

Figure V. 35. Impact of Porosity on Pressure Head Variation with Depth in (a) Clay and (b) Sand

Figure V.36 illustrates how temperature varies with depth in clay soil on a cold day, focusing on the influence of porosity (n = 0.4, 0.6, and 0.8) on heat transfer. As depth increases, temperature rises due to the Earth's natural heat. The efficiency of heat transfer depends on the soil's composition. Clay with low porosity (n = 0.4) heats up more quickly with depth, indicating better thermal conductivity since fewer air voids are present to delay heat flow. In contrast, clay with higher porosity (n = 0.6 and n = 0.8) heats up more slowly, as the increased air voids act as insulators, reducing heat transfer. For geothermal applications, clay with low porosity (n = 0.4) is the most effective option, as it facilitates efficient heat transfer, enhancing

system performance. In contrast, clay with higher porosity is less suitable due to its lower thermal conductivity.

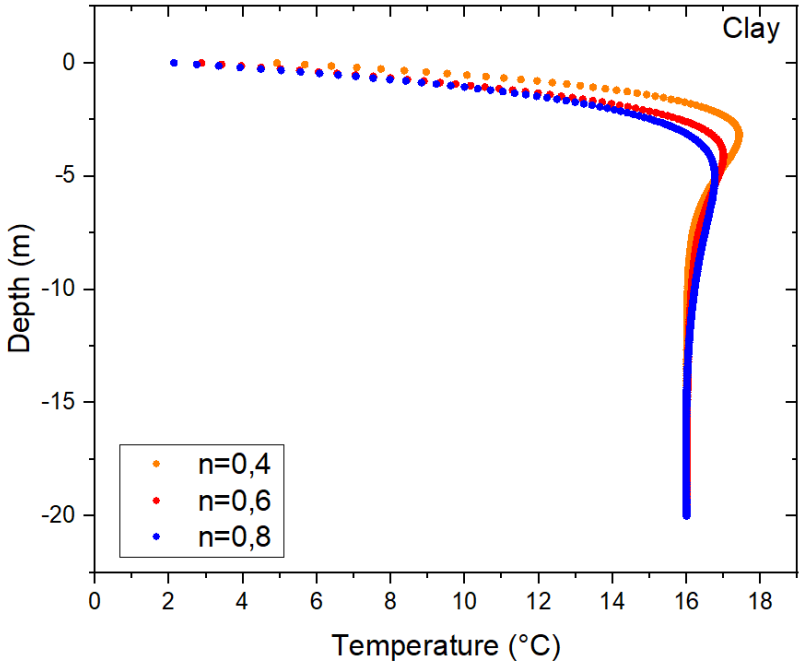

Figure V. 36. Effect of Porosity on Temperature profile in Clay (January 2023)

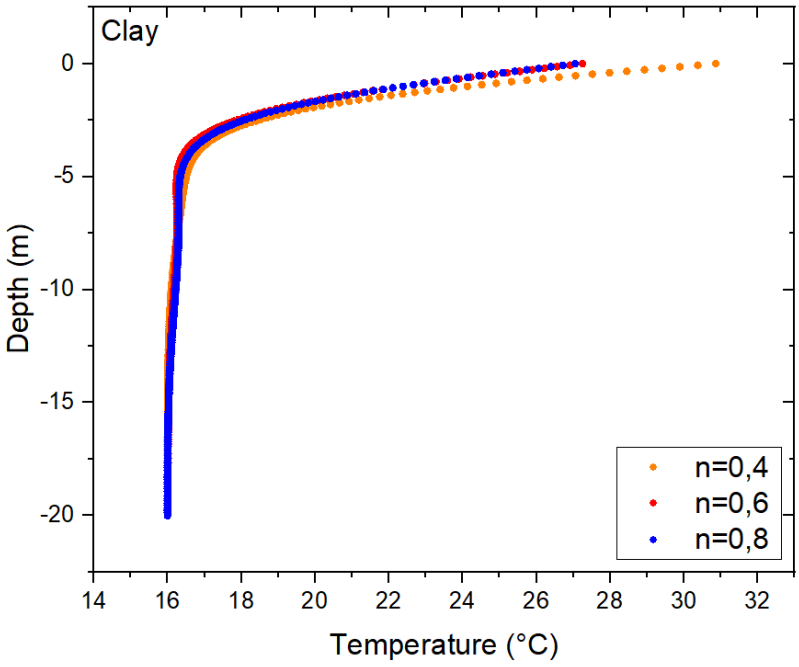

Figure V. 37. Effect of Porosity on Temperature profile in Clay (July 2023)

Figure V.37 illustrates the variation of temperature with depth in clay soil at different porosity levels (n = 0.4, 0.6, and 0.8) in July 2023. As depth increases, temperature gradually stabilizes. Clay with lower porosity (n = 0.4) exhibits a steeper temperature increase with depth, indicating

more efficient heat transfer due to its denser structure. In contrast, higher porosity levels (n = 0.6 and 0.8) slow down heat transfer, as the presence of more air voids reduces thermal conductivity and acts as an insulating barrier. For geothermal applications, clay soil with lower porosity (n = 0.4) is the most effective, as it allows for better heat transfer, making it more suitable for energy systems.

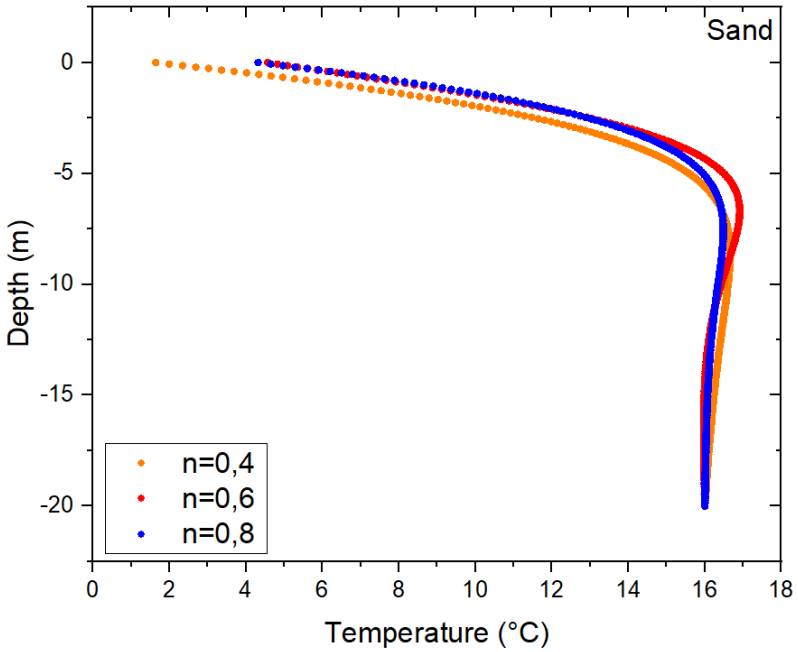

Figure V. 38.Effect of Porosity on Temperature profile in Sand (January 2023)

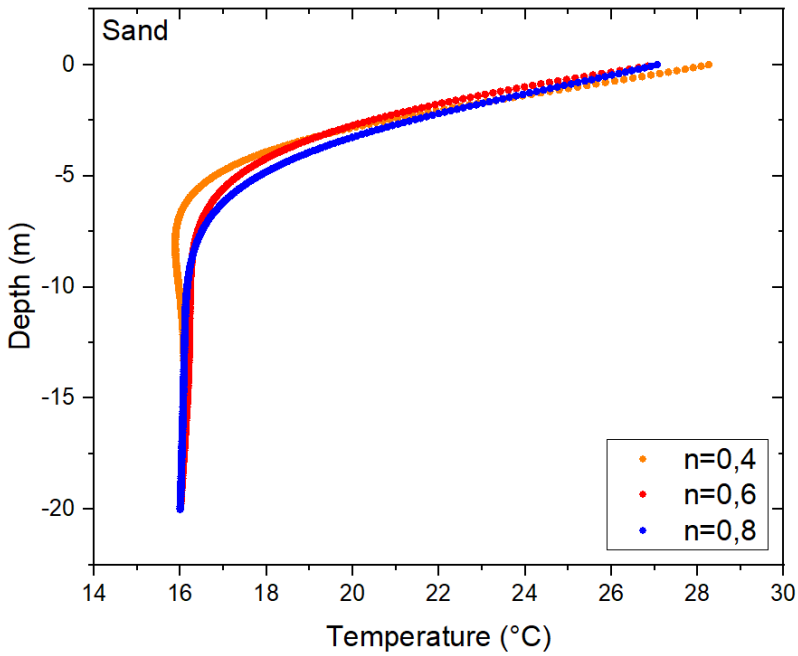

Figure V. 39. Effect of Porosity on Temperature profile in Sand (July 2023)

Figure V.38 illustrates how temperature changes with depth in sandy soil for different porosity levels (n = 0.4, 0.6, and 0.8). Unlike clay, the temperature increase with depth in sand is more gradual, showing a less pronounced thermal gradient. While all porosity levels follow the expected geothermal trend, the differences in temperature distribution due to porosity are less distinct. Sand with lower porosity (n = 0.4) shows a slightly sharper temperature rise, likely because it has fewer voids, allowing heat to move more easily. In contrast, higher porosity levels (n = 0.6 and 0.8) lead to a more gradual temperature increase, as the extra voids slow down heat transfer—but not as significantly as in clay. Overall, sand's thermal behavior is less affected by porosity compared to clay. This is likely due to sand's natural properties, such as larger grain size and lower water retention, which already play a key role in its heat conductivity.

Figure V.39 illustrates how temperature changes with depth in sandy soil during July for three different porosity levels (n = 0.4, 0.6, and 0.8). The results show that lower porosity (n = 0.4) leads to a steeper temperature increase with depth, suggesting better heat retention. In contrast, higher porosity (n = 0.8) results in a more gradual temperature transition, indicating that heat dissipates more easily. This is likely due to increased air or water circulation in the larger voids, which reduces heat conservation. Soil with lower porosity is more effective at retaining and transferring heat at greater depths, making it a potentially better choice for geothermal applications in similar conditions.

b) Effect of density

The density of the two soil types varies as follows:

aa) Clay: 1200, 1400, 1600, 1800 kg/m³

bb) Sand: 1400, 1600, 1800, 2000 kg/m³

Figure V.40 illustrates how volumetric heat capacity (J/m³K) changes with water content for clay and sand at different densities. In both soils, volumetric heat capacity increases linearly as water content rises, with denser soils storing more heat. For clay, higher densities (1600 and 1800 kg/m³) result in greater heat capacity, as more mass per unit volume allows for better heat storage. Sand follows the same trend, with higher densities (1800 and 2000 kg/m³) leading to increased heat capacity. However, at the same density, sand retains less heat than clay due to its coarser texture, which limits water retention and, consequently, reduces its ability to store heat. This makes clay a better option for thermal applications such as geothermal systems, where water retention and heat storage are crucial.

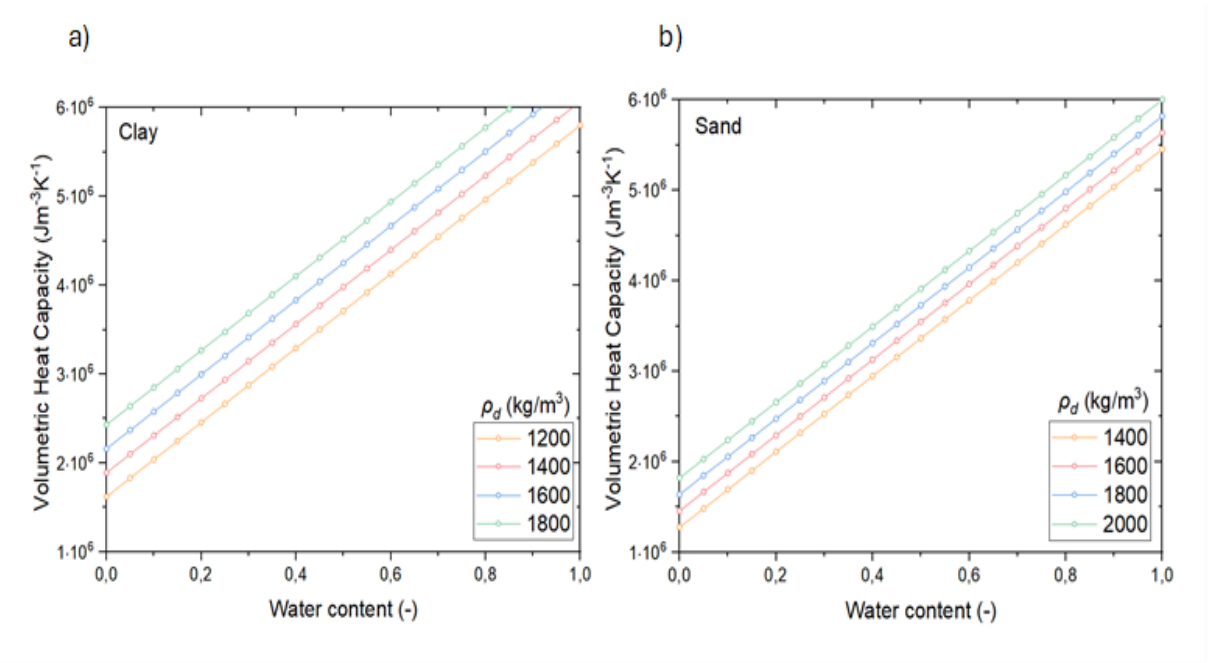

Figure V. 40. Volumetric Heat Capacity Variation with Water Content and Soil Density for (a) Clay and (b) Sand

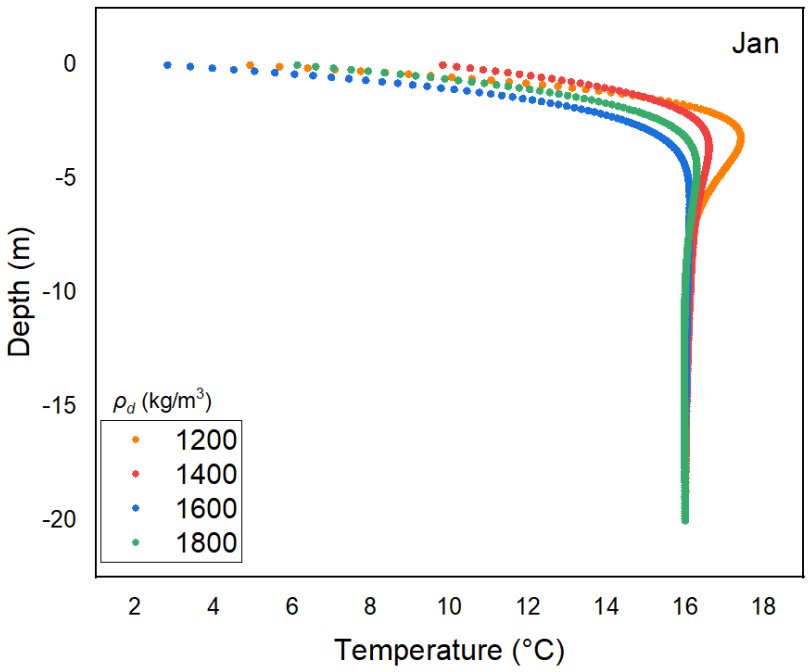

Figure V. 41. Temperature Distribution with Depth in Clay Soil at Different Densities (January 2023)

Figure V.41 illustrates the temperature changes in function of depth in clay soil at different densities during January. While seasonal variations cause surface temperatures to fluctuate, deeper layers stabilize at around 16°C. At the surface, density has the most noticeable impact: less dense soils show a more gradual temperature transition, while denser soils reach a stable

temperature more quickly due to faster heat transfer. However, as depth increases, all soil densities eventually converge to the same temperature, indicating that density mainly affects the surface layers influenced by seasonal changes. This pattern highlights the role of density in thermal dissipation near the surface, while deeper layers remain thermally stable, regardless of density.

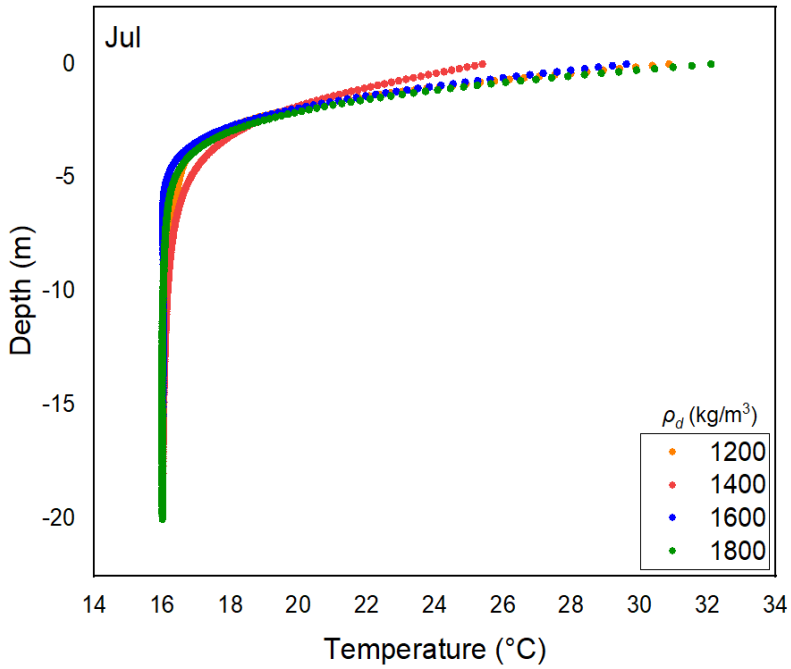

Figure V. 42. Temperature Distribution with Depth in Clay Soil at Different Densities (July 2023)

Figure V.42 illustrates how temperature varies with depth in clay soil at different densities (ρd = 1200, 1400, 1600, and 1800 kg/m³) during July. Near the surface, temperatures fluctuate significantly before stabilizing at deeper depths, with the most noticeable changes occurring within the first 5 meters, where surface heat has the strongest influence.

Denser clay soils (ρd = 1800 kg/m³) retain heat more effectively, allowing for slower heat dissipation at depth and better heat retention near the surface. In contrast, less dense clays (ρd = 1200 kg/m³) cool more quickly with depth, as their lower thermal capacity limits heat storage. Near the surface, low-density clay heats up more due to its greater sensitivity to atmospheric temperature changes, while denser soils distribute heat more evenly and reach slightly lower peak temperatures. This analysis highlights the important role of density in heat distribution within clay soils. Denser soils are better at storing and retaining heat, making them more suitable for thermal applications, such as geothermal energy systems.

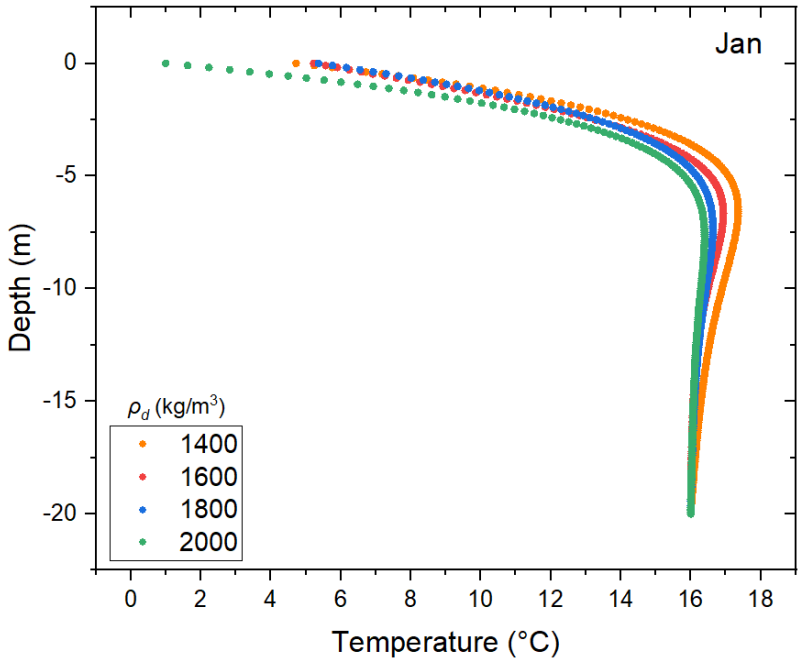

Figure V. 43. Temperature Distribution with Depth in Sand Soil at Different Densities (January 2023)

Figure V.43 illustrates the temperature variations with depth in sandy soil at different densities (ρd = 1400, 1600, 1800, and 2000 kg/m³) during January. In the upper layers, down to about 8 meters, temperatures increase rapidly due to the influence of winter conditions. However, at greater depths, temperatures gradually stabilize, forming a zone unaffected by seasonal changes. Denser sandy soils (ρd = 2000 kg/m³) retain more heat at depth due to their higher heat capacity, while less dense soils (ρd = 1400 kg/m³) heat up more quickly, indicating faster heat dissipation. These results highlight the important role of density in regulating heat distribution within sandy soil, which is particularly relevant for geothermal and thermal energy applications.

Figure V.44 illustrates how temperature changes with depth in sandy soil at different densities (ρd = 1400, 1600, 1800, and 2000 kg/m³) during July. In the upper layers, temperatures decrease rapidly down to about 8 meters, where the effects of summer heat are most pronounced. Beyond this point, temperatures gradually decrease and stabilize at greater depths, forming a zone unaffected by surface temperature fluctuations. Denser sandy soils (ρd = 2000 kg/m³) retain more heat at depth due to their higher thermal capacity, allowing for better heat storage and slower heat dissipation. In contrast, less dense soils (ρd = 1400 kg/m³) lose heat more quickly at depth, reflecting their lower heat retention capacity. Near the surface, low-density soils heat up faster but struggle to retain warmth at greater depths, whereas denser soils ensure a more

uniform heat distribution. These findings highlight the key role of density in influencing heat storage and transfer in sandy soils, making denser soils more suitable for thermal and geothermal applications where efficient heat retention is essential.

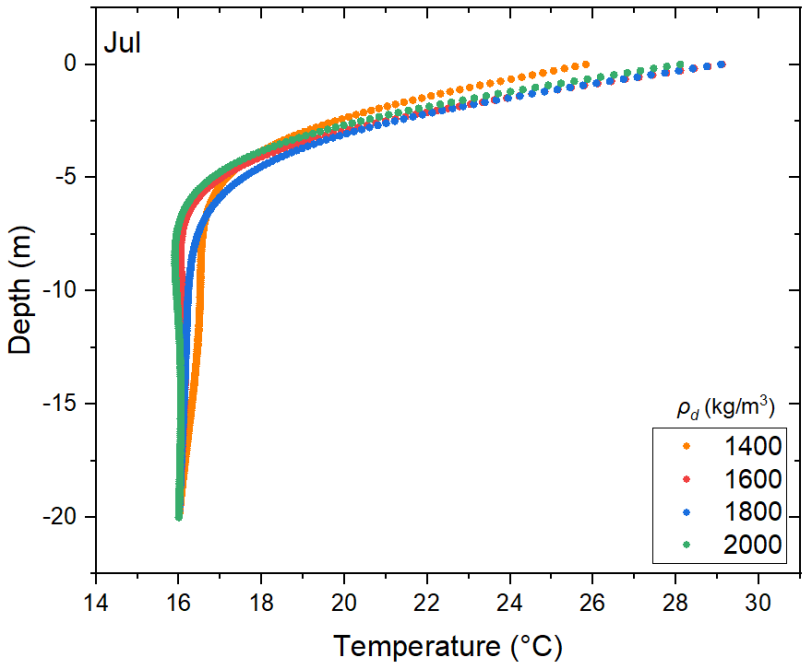

Figure V. 44. Temperature Distribution with Depth in Sand Soil at Different Densities (July 2023)

c) Fourth conclusion

The study established a numerical hydrothermal model between soil and atmosphere in the Oran region of Algeria, which analyzes effects caused by different soil characteristics on heat retention and stability. The model runs for different soil types (clay and sand), has different porosities (n = 0.4, 0.6, and 0.8), and uses different densities for clay (1200–1800 kg/m³) and sand (1400–2000 kg/m³). Additionally, it evaluates how these variables manifest in real-world conditions by comparing the warmest day in July and the coldest day in January 2023 in a model of more extreme climate scenarios in the region. It was discovered that density, porosity, and soil type all had a significant impact on temperature stability and heat retention. The best performance was shown by clay with low porosity (n = 0.4) and high density (1800 kg/m³), which retained heat with fewer losses. This makes it suitable for geothermal applications. Clay was able to efficiently store energy for a long time because it has a high heat capacity and retains more moisture. Sand has a high permeability that promotes rapid dissipation, which means it does not retain heat like clay does. However, because of its higher density, it showed better thermal performance after compaction. Therefore, in situations where clay is not available,

dense sand is a good alternative. When exposed to the extreme climatic conditions, clay has shown a much better performance than sand, especially at shallow depths where it behaved like a natural insulator for preventing fast temperature changes. Such usage therefore appears an efficient and economical solution for geothermal energy storage, whereby long-lasting heat retention could be achieved without constant energy supply. Clay with low porosity and high density is the best soil type for geothermal energy or effective heat storage since it retains heat, remains stable throughout the year, and is reasonably priced.

These findings demonstrate how crucial it is to take soil characteristics into account when developing geothermal systems, particularly in areas with sharp temperature swings. Future studies would look at additional physical characteristics and perhaps the use of horizontal ground heat exchangers to gain insight into their potential interactions.

Conclusion

Energy is one of the main basic needs of modern societies, and is essential to economic growth, industrialization and general quality of life. However, heavy dependence on fossil fuels has posed enormous problems in terms of resource depletion, environmental degradation and energy security in general. Despite its enormous hydrocarbon reserves, Algeria is being forced to reconsider its energy strategy due to the country's rising domestic energy demand. With more than 96% of its export revenue still coming from fossil fuels, Algeria must step up its energy diversification efforts to guarantee long-term, sustainable independence from oil and gas.

Among these alternative sources, the most promising appears to be geothermal energy, the most important abundant but underutilized resource for the country's transition to renewable energies. A thorough understanding of heat transfer processes in soils, especially in unsaturated conditions where density, porosity, salinity, and water content all have a significant impact on thermal conductivity and heat retention, is essential to the effective use of geothermal resources.

Therefore, this study used a numerical hydrothermal model applied to the Oran and Adrar regions of Algeria in order to examine the impact of different soil properties on geothermal heat transfer. The findings of this study shed light on the properties of the soil that control temperature stabilization, thermal performance, and energy storage capacity, all of which may be significant for the advancement of geothermal energy development techniques in Algeria. Here are the key Findings and Contributions of this study:

1. Temperature Stabilization in Multilayered Soils

One of the key insights from this study is that temperature stabilizes at shallow depths, even within multilayered soil formations. While the surface layers experience considerable temperature fluctuations due to seasonal changes, the deeper layers are largely insulated from atmospheric effects. This thermal stabilization occurs naturally because of the soil's thermal inertia, which allows it to absorb and gradually release heat over time. However, external energy sources, such as geothermal activity or human-induced heat emissions, can disrupt this balance, resulting in localized variations in underground temperature profiles. Understanding this thermal lag effect is essential for designing efficient geothermal systems, as stable subsurface temperatures offer a dependable and predictable energy source for heating, cooling, and other renewable applications.

2. Evaluation of Soil Types for Geothermal Applications

This study evaluated the thermal performance of three soil types: clay, loam, and sand, to assess their suitability for geothermal energy applications. A numerical model was created to simulate temperature variations under various environmental influences, including solar radiation cycles, transient thermal conditions, and meteorological data of the Oran region. The goal was to identify the soil type that offers optimal thermal efficiency for energy extraction at shallow depths, where lower drilling costs and improved heat transfer efficiency lead to greater overall energy output. The results show that clay soils perform the best due to their high heat retention and moisture regulation properties, making them the ideal choice for horizontal ground heat exchanger installations at shallow depths. Loam soils exhibited moderate performance, while sandy soils, despite their quick temperature response, were less effective overall.

3. Effect of Salinity on Thermal Performance

Salinity significantly influences the thermal properties of soil, but its effects vary based on soil type. In sandy soils, a moderate salinity level (C = 0.1 M) was found to improve heat absorption and retention, making it the ideal concentration for optimizing thermal performance. In contrast, sandy loam soils showed that the highest salinity level (C = 0.2 M) was most effective, especially during the summer months, where increased salinity led to higher surface temperatures and enhanced heat storage. This variability underscores the need to customize salinity levels according to specific soil types when designing geothermal energy systems. The findings indicate that controlled adjustments in salinity could serve as a practical approach to boost the thermal efficiency of geothermal transfer in arid and semi-arid regions like Algeria.

4. Soil Composition and Geothermal Suitability

The results indicate that soil composition plays a crucial role in geothermal energy storage and transfer. Clay-rich soils, especially those with low porosity (n = 0.4) and high density (ρd = 1800 kg/m^3), were found to be the most effective for geothermal applications. This effectiveness is due to clay's ability to minimize heat loss and retain thermal energy over extended periods. Its high heat capacity, low permeability, and excellent moisture retention properties contribute to reduced thermal dissipation and ensure long-term stability. On the other hand, sandy soils, which are more porous and less thermally conductive, showed lower heat retention capabilities. However, increasing the density of sand improved its thermal performance, making high-density sand formations (ρd = 2000 kg/m^3) a viable alternative when clay is not available. These

findings highlight the significance of selecting the right soil compositions for geothermal energy projects, as different soil types react differently to thermal stress and external heat sources.

The study's conclusions offer important new information for improving hydrothermal modeling by adding more physical processes, validating numerical models through experimental research, and optimizing geothermal energy applications, especially for the design and use of horizontal ground heat exchangers. To improve geothermal heat transfer efficiency and expand the usefulness of this renewable energy source, future research should concentrate on the following crucial areas.

- Investigation of Horizontal Ground Heat Exchangers for Efficient Energy Extraction

Given the study's findings on soil porosity, density, salinity, and soil type, the next step is to develop and optimize horizontal ground heat exchangers to effectively harness geothermal energy. Since clay soils with low porosity and high density have shown excellent heat retention, they should be prioritized for shallow geothermal systems where reduced drilling depths make geothermal energy extraction more cost-effective. Additionally, the study demonstrated that salinity influences heat transfer, meaning that controlling soil salinity levels could enhance the thermal performance of heat exchangers. By integrating these soil parameters into numerical models, future research can optimize the design of ground heat exchangers to improve energy extraction, making geothermal energy a more viable and sustainable alternative for heating, cooling, and industrial applications.

- Exploitation and Utilization of Geothermal Energy from Heat Exchangers

To fully utilize geothermal energy, it is essential to develop efficient systems to extract and exploit this stored heat for various applications. Future studies should explore the implementation of heat exchanger networks, which can transfer energy from the subsurface to residential, commercial, and industrial sectors. This involves investigating the best configurations, materials, and operating conditions to maximize heat transfer efficiency while minimizing thermal losses. Moreover, hybrid energy systems that combine geothermal energy with solar or other renewable sources could be developed to enhance reliability and efficiency in Algeria's diverse climate conditions.

- Incorporating Water Vapor Transport into Hydrothermal Transfer Models

While this study focused on heat and moisture transfer, the role of water vapor transport in geothermal heat exchange remains an essential factor in unsaturated soils. The presence of evaporation and condensation cycles significantly affects soil thermal properties, especially in arid and semi-arid regions. Future research should refine numerical models by incorporating water vapor dynamics, allowing for a more accurate representation of geothermal heat transfer.

- Experimental Validation of Numerical Findings

To strengthen the reliability of geothermal energy models, experimental validation is necessary. Future studies should involve on-site geothermal field tests, where real-time temperature, moisture, and salinity data are collected and compared with numerical simulations. Such experiments should include heat exchanger installations to evaluate actual heat transfer performance in various soil types, densities, and salinity levels. This will not only confirm the accuracy of numerical models but also provide essential insights for large-scale geothermal system implementation.

Algeria is currently at a turning point for its energy transition, and geothermal energy represents the golden opportunity to expand the energy mix away from the almost total reliance on fossil fuels. Using scientific research and advanced hydrothermal modeling, Algeria could take advantage of its geothermal potential while reducing its dependence on fossil fuels to promote access to cleaner and more sustainable energy.

References

1. BP p.l.c.: Statistical Review of World Energy 2022. BP p.l.c., London, United Kingdom (2022)
2. Harsh, G., Sukanta, R.: Geothermal energy: an alternative resource for the 21st century. Elsevier B.V. (2007)
3. Huang, Y.H., Shen, T.S.: An article on green firefighting equipment in Taiwan. Sustainability (Switzerland). 13, (2021). https://doi.org/10.3390/su132212421
4. Cano, N.A., Céspedes, S., Redondo, J., Foo, G., Jaramillo, D., Martinez, D., Gutiérrez, M., Pataquiba, J., Rojas, J., Cortés, F.B., Franco, C.A.: Power from Geothermal Resources as a Co-product of the Oil and Gas Industry: A Review. ACS Omega. 7, 40603–40624 (2022). https://doi.org/10.1021/acsomega.2c04374
5. Hebbal, B., Marif, Y., Hamdani, M., Belhadj, M.M., Bouguettaia, H., Bechki, D.: The geothermal potential of underground buildings in hot climates: Case of Southern Algeria. Case Studies in Thermal Engineering. 28, (2021). https://doi.org/10.1016/j.csite.2021.101422
6. Benmammar, I. abderrahime, Elhelli, A.: Enjeux de la transition énergitique en Algerie, (2021)
7. Ouali, S., Khellaf, A., Baddari, K.: Etude géothermique du Sud de l'Algérie. Revue des Energies Renouvelables. 9, 297–306 (2006)
8. Saibi, H., Elbarbary, S., Zaher, M.A.: Geothermal Signatures in North Africa: Examples from Egypt and Algeria. Presented at the (2024)
9. Aliouane, L., Ouadfeul, S.-A.: Geothermal Energy in Algeria and the Contribution of Geophysics. Presented at the March 27 (2023)
10. Kouider, M.H., Nezli, I.E.: The geothermal potentialities of Southern Algeria. Presented at the (2019)
11. Halim, R.A., Arentsen, M.J., Warbroek, B.: Geothermal Potency and Development, (2018)
12. Billewar, S.R., Londhe, G., Mane, P.S.: World Energy Demand. In: Integrated Green Energy Solutions Volume 2. pp. 275–316. Wiley (2023)

13. Saouter, E., Gibon, T.: A World Full of Energy. In: All You Need to Know About the Next Energy Revolution. pp. 1–29. Springer Nature Switzerland, Cham (2024)

14. koya79: earth core structure, https://parlonssciences.ca/sites/default/files/2020-07/earth-core-structure-with-geological-layers.jpg

15. Stober, I., Bucher, kurt: Geothermal Energy From Theoretical Models to Exploration and Development. Springer Nature Switzerland AG (2021)

16. Ouali, S.: Chauffage et rafraichissement par la géothermie. In: Bulletin des Energies Renouvelables (2019)

17. Aliouane, L.: La Géothermie en Algérie et la contribution de la Géophysique. In: The first International conference on physics of semicondutor devices, Renewable energies and Environment (2022)

18. Do Couto, D.: La géothermie : une énergie ubiquiste, sous différentes formes. Presented at the December 6 (2022)

19. Gudmundsson, J.S., Freeston, D.H., Lienau, P.J.: The Lindal Diagram. Transactions. 9, (1985)

20. Kirschstein, X., Ohagen, M., Reber, J., Vardon, P.J., Bishara, N.: Regeneration of shallow borehole heat exchanger fields: A literature review. Energy Build. 317, (2024). https://doi.org/10.1016/j.enbuild.2024.114381

21. Energy Institute: Statistical Review of World Energy. (2024)

22. Miklovicz, T.: Investigation on the potential of combined heat, power and metal extraction in Hungary, https://www.researchgate.net/publication/317388065, (2014)

23. Lund, J.W.: Direct utilization of geothermal energy. Energies (Basel). 3, 1443–1471 (2010). https://doi.org/10.3390/en3081443

24. Maps of Algeria, https://www.turkey-visit.com/algeria-map.asp

25. Algeria, https://en.m.wikipedia.org/wiki/File:Algeria_%28orthographic_projection%29.svg

26. IRENA (International Renewable Energy Agency): Renewable capacity statistics 2024. International Renewable Energy Agency, Abu Dhabi (2024)

27. Shortall, R., Davidsdottir, B., Axelsson, G.: Geothermal energy for sustainable development: A review of sustainability impacts and assessment frameworks. Renewable and Sustainable Energy Reviews. 44, 391–406 (2015). https://doi.org/10.1016/j.rser.2014.12.020

28. Aurélien, B.: Modélisation de la réflectance spectrale d'un sol nu en fonction de sa teneur en eau dans le domaine réflectif solaire (400 – 2500 nm), (2018)

29. Cuny, M.: Etude de l'impact des conditions géologiques et climatiques sur l'efficacité énergétique des systèmes géothermiques de surface, https://tel.archives-ouvertes.fr/tel-01716379, (2017)

30. Soil Mechanics, http://ecoursesonline.iasri.res.in/mod/page/view.php?id=125124

31. Baldwin, M., Kellogg, C.E., Thorp, J.: Soil Classification. (1938)

32. Soil Science Division Staff: Soil Survey Manual. United States Department of Agriculture (USDA), Washington, D.C. (2017)

33. Moreno-Maroto, J.M., Alonso-Azcárate, J.: Evaluation of the USDA soil texture triangle through Atterberg limits and an alternative classification system. Appl Clay Sci. 229, (2022). https://doi.org/10.1016/j.clay.2022.106689

34. Moreno-Maroto, J.M., Alonso-Azcárate, J.: What is clay? A new definition of "clay" based on plasticity and its impact on the most widespread soil classification systems. Appl Clay Sci. 161, 57–63 (2018). https://doi.org/10.1016/j.clay.2018.04.011

35. Chapitre : Classification des sols.

36. Cengiz, C., Konstantinou, M., Harkes, M., Boonstra, D., Piedrabuena, A.R., Talmon, A.: Application of concentration conductivity measurement (CCM) for porosity and density profiling in granular media. Measurement. 245, 116644 (2025). https://doi.org/10.1016/j.measurement.2025.116644

37. Ouoba, S., Cousin, B., Cherblanc, F., Koulidiati, J., Bénet, J.C.: Une méthode mécanique pour déterminer la porosité totale d'un sol. Comptes Rendus - Mecanique. 342, 732–738 (2014). https://doi.org/10.1016/j.crme.2014.07.003

38. André, M., Marc, S.: Physique du sol. (1991)

39. Laloui, L., Rotta Loria, A.F.: Heat and mass transfers in the context of energy geostructures. In: Analysis and Design of Energy Geostructures. pp. 69–135. Elsevier (2020)

40. M.R. Carter: Soil Sampling and Methods of Analysis. Taylor & Francis Group, Boca Raton, FL (2006)

41. Keramat, F., Zhong, L.: Technical Assessment of Frozen Soil on Geothermal Heat Pump Technology in Western Canada. In: E3S Web of Conferences. EDP Sciences (2023)

42. Wang, R., Yang, C., Ni, L., Yao, Y.: Experimental study on heat transfer of soil with different moisture contents and seepage for ground source heat pump. Indoor and Built Environment. 29, 1238–1248 (2020). https://doi.org/10.1177/1420326X19894037

43. Sedano, J.A.I., Evgin, E., Fu, Z.: A Coupled Analysis of Heat and Moisture Transfer in Soils. In: Comsol Conference. , Boston (2011)

44. Bigdelou, P., Pourfayaz, F., Noorollahi, Y.: Investigating the effect of soil type and moisture on the performance of a ground source heat pump system used for a greenhouse in Iran. J Therm Sci Eng Appl. 11, (2019). https://doi.org/10.1115/1.4041344

45. Bergman, T., Incropera, F., Lavine, A., DeWitt, D.: Fundamentals of Heat and Mass Transfer. Wiley, Hoboken, NJ (2011)

46. Zhu, X., Gao, Z., Chen, T., Wang, W., Lu, C., Zhang, Q.: Study on the Thermophysical Properties and Influencing Factors of Regional Surface Shallow Rock and Soil in China. Front Earth Sci (Lausanne). 10, (2022). https://doi.org/10.3389/feart.2022.864548

47. Chanchayanon, T., Chaiprakaikeow, S., Jotisankasa, A., Inazumi, S.: Optimization of Geothermal Heat Pump Systems for Sustainable Urban Development in Southeast Asia. Smart Cities. 7, 1390–1413 (2024). https://doi.org/10.3390/smartcities7030058

48. Umny Inc.: How do Ground Thermal Properties Change Geothermal Performance?

49. of Alberta, G.: Alberta Transportation Test Procedure ATT-48/2022 - Correction Factor-Nuclear Gauge.

50. Lérau, J.: GÉOTECHNIQUE 1. (2005)

51. Chapitre 1: Géotechnique: Les sols.

52. Rajomalahy, J., Andrianaivo, L., Andriamifidisoa, V., Ramamonjisoa, H., Nantenaina, &, Rarivoson, V.: Modélisation de flux de chaleur pour l'utilisation géothermique. MADA-HARY. 6, (2017)

53. Farouki, O.T.: Thermal properties of soils. (1981)

54. Yoshimoto, N., Rolando, O.P., Tanabe, F., Kikkawa, N., Hyodo, M., Nakata, Y.: measurement of degree of saturation on model ground by digital image processing. Soils and foundations. 51, 167–177 (2011)

55. Moevus-Dorvaux, M., Couvreur, L., Cloquet, B., Fontaine, L., Anger, R., Doat, P.: Béton D'Argile Environnemental Résultats d'un programme de recherche tourné vers l'application. , Villefontaine (2016)

56. Pahud, D.: Geothermal energy and heat storage. (2002)

57. Malek, K., Malek, K., Khanmohammadi, F.: Response of soil thermal conductivity to various soil properties. International Communications in Heat and Mass Transfer. 127, (2021). https://doi.org/10.1016/j.icheatmasstransfer.2021.105516

58. Zhang, N., Wang, Z.: Review of soil thermal conductivity and predictive models. International Journal of Thermal Sciences. 117, 172–183 (2017). https://doi.org/10.1016/j.ijthermalsci.2017.03.013

59. Kersten, M.S.: Thermal properties of soils associate professor of civil engineering, (1949)

60. Tian, Z., Lu, Y., Horton, R., Ren, T.: A simplified de Vries-based model to estimate thermal conductivity of unfrozen and frozen soil. Eur J Soil Sci. 67, 564–572 (2016). https://doi.org/10.1111/ejss.12366

61. Johansen, O.: Thermal Conductivity of Soils. (1977)

62. Donazzi, F., Occhini, M.A.I.C.A.E., Mem, S.I.E.E.E., Enq, C., Seppi, A.: Soil thermal and hydrological characteristics in designing underground cables. PROC. IEE. 126, 506–516 (1979)

63. Chen, S.X.: Thermal conductivity of sands. Heat and Mass Transfer/Waerme- und Stoffuebertragung. 44, 1241–1246 (2008). https://doi.org/10.1007/s00231-007-0357-1

64. Chung, S.-O., Horton, R.: Soil Heat and Water Flow With a Partial Surface Mulch. Water Resour Res. 23, 2175–2186 (1987)

65. Côté, J., Konrad, J.M.: A generalized thermal conductivity model for soils and construction materials. Canadian Geotechnical Journal. 42, 443–458 (2005). https://doi.org/10.1139/t04-106

66. Lu, S., Ren, T., Gong, Y., Horton, R.: An Improved Model for Predicting Soil Thermal Conductivity from Water Content at Room Temperature. Soil Science Society of America Journal. 71, 8–14 (2007). https://doi.org/10.2136/sssaj2006.0041

67. Lu, Y., Lu, S., Horton, R., Ren, T.: An Empirical Model for Estimating Soil Thermal Conductivity from Texture, Water Content, and Bulk Density. Soil Science Society of America Journal. 78, 1859–1868 (2014). https://doi.org/10.2136/sssaj2014.05.0218

68. Nikoosokhan, S., Nowamooz, H., Chazallon, C.: Effect of dry density, soil texture and time-spatial variable water content on the soil thermal conductivity. Geomechanics and Geoengineering. 11, 149–158 (2016). https://doi.org/10.1080/17486025.2015.1048313

69. Xiong, K., Feng, Y., Jin, H., Liang, S., Yu, K., Kuang, X., Wan, L.: A new model to predict soil thermal conductivity. Sci Rep. 13, (2023). https://doi.org/10.1038/s41598-023-37413-5

70. Nikolaev, I. V., Leong, W.H., Rosen, M.A.: Experimental investigation of soil thermal conductivity over a wide temperature range. Int J Thermophys. 34, 1110–1129 (2013). https://doi.org/10.1007/s10765-013-1456-5

71. Ochsner, T.E., Horton, R., Ren, T.: a new perspective on soil thermal properties a new perspective on soil thermal properties. Soil Sci. Soc. Am. J. 65, (2001)

72. Fricke, B.A., Misra, A., Beeker, B.R., Stewart, W.E.: Soil Thermal Conductivity: Effects of Saturation and Dry Density. In: Thermal Performance of the Exterior Envelopes of Whole Buildings V International Conference. pp. 158–165. , Clearwater Beach, Florida, USA (1992)

73. Wang, C., Yang, Y.L., Cai, G., Zhang, T.: Improvement of normalized prediction model of soil thermal conductivity. International Communications in Heat and Mass Transfer. 157, (2024). https://doi.org/10.1016/j.icheatmasstransfer.2024.107792

74. Tang, F., Nowamooz, H.: Hydro-Thermal Properties of the Unsaturated Soil. In: Sustainable Civil Infrastructures. pp. 18–26. Springer Science and Business Media B.V. (2018)

75. Kluitenberg, G.J., Ham, J.M., Bristow, K.L.: Error Analysis of the Heat Pulse Method for Measuring Soil Volumetric Heat Capacity.

76. De Vries, D.A.: Thermal Properties of Soils. In: van Wijk, W.R. (ed.) Physics of Plant Environment. pp. 210–234. North Holland Publishing, Amsterdam, The Netherlands (1963)

77. Wang, P., Firat, M.E., Lin, Y., Wang, T.: Predicting soil thermal properties in freeze-thaw cycles using EFAttNet: A comparative analysis. PLoS One. 19, (2024). https://doi.org/10.1371/journal.pone.0305529

78. Campbell, G.S.: Soil Physics with BASIC: Transport Models for Soil-Plant Systems. Elsevier, New York (1985)

79. Ghuman, B.S., Lau, R.: Thermal conductivity, thermal diffusivity, and thermal capacity of some nigerian soils. (1985)

80. Sikora E., K.J.: Thermal conductivity and diffusivity estimations of uncompacted and compacted soils using computing methods. Polish J. Soil Sci. 26, 19–26 (1993)

81. Abu-Hamdeh, N.H.: Thermal properties of soils as affected by density and water content. Biosyst Eng. 86, 97–102 (2003). https://doi.org/10.1016/S1537-5110(03)00112-0

82. Dysli, M.: Le gel et son action sur les sols et les fondations. PPUR presses polytechniques., Lausanne (1991)

83. Rubio, C.M., Josa, R., Ferrer, F.: Influence of the Hysteretic Behaviour on Silt Loam Soil Thermal Properties. Open Journal of Soil Science. 01, 77–85 (2011). https://doi.org/10.4236/ojss.2011.13011

84. Bals, Y., Gengel, A.: Thermodynamics: An Engineering Approach. McGraw-Hill (2008)

85. Yatish, T.S.: Thermal Energy: Sources, Recovery, and Applications. (2010)

86. Heat transfer modes, https://ena.our-dogs.info/pictures-2022.html

87. Alrtimi, A.A.: Experimental Investigation of Thermal Conductivity of Soils and Borehole Grouting Materials, (2014)

88. Holman, J.P.: Heat Transfer. McGraw-Hill (1997)

89. Saldana, M., Gallegos, S., Gálvez, E., Castillo, J., Salinas-Rodríguez, E., Cerecedo-Sáenz, E., Hernández-Ávila, J., Navarra, A., Toro, N.: The Reynolds Number: A Journey from Its Origin to Modern Applications, (2024)

90. Ke, J., Williamson, N., Armfield, S.W., Komiya, A., Norris, S.E.: High Grashof number turbulent natural convection on an infinite vertical wall. J Fluid Mech. 929, A15 (2021). https://doi.org/10.1017/jfm.2021.839

91. O'Malley, R.E.: Ludwig Prandtl's Boundary Layer Theory. In: Historical Developments in Singular Perturbations. pp. 1–26. Springer International Publishing, Cham (2014)

92. Marin, E., Calderon, A., Delgado-Vasallo, O.: Similarity theory and dimensionless numbers in heat transfer. Eur J Phys. 30, 439–445 (2009). https://doi.org/10.1088/0143-0807/30/3/001

93. Convection,https://www.techno-science.net/glossaire-definition/Convection.html#ref_2

94. Welty, J.R.: Engineering Heat Transfer. John Wiley & Sons, Inc, New York (1978)

95. Lienhard, J.H.I., Lienhard, J.H. V: A Heat Transfer Textbook. Phlogiston Press, Cambridge, Massachusetts, USA (2019)

96. Rees, S.W., Adjali, M.H., Zhou, Z., Davies, M., Thomas, H.R.: Ground heat transfer effects on the thermal performance of earth-contact structures. Renewable and Sustainable Energy Reviews. 4, 213–265 (2000)

97. Radiation budget, https://science.nasa.gov/ems/13_radiationbudget/

98. Versteeg, H.K., Malalasekera, W.: An Introduction to Computational Fluid Dynamics Second Edition.

99. Arbi, A. el ghani: Etude de la conduction de la chaleur, application de la méthode de volumes finis à la conduction thermique dans le sol. (2019)

100. Bear, J.: Hydraulics of Groundwater. Dover Publications, Inc., Mineola, NY, USA (1979)

101. Simmons, C.T.: Henry Darcy (1803-1858): Immortalised by his scientific legacy. Hydrogeol J. 16, 1023–1038 (2008). https://doi.org/10.1007/s10040-008-0304-3

102. Bouchemella, S., Alimi-ichola, I.: Détermination des paramètres des modèles empiriques des propriétes hydrauliques des sols non saturés. In: Journées Nationales de Géotechnique et de Géologie de l'Ingénieur. , Nancy (2016)

103. Šimůnek, J., van Genuchten, M.Th., Šejna, M.: Development and Applications of the HYDRUS and STANMOD Software Packages and Related Codes. Vadose Zone Journal. 7, 587–600 (2008). https://doi.org/10.2136/vzj2007.0077

104. Fan, Y., Gong, J., Wang, Y., Shao, X., Zhao, T.: Application of Philip infiltration model to film hole irrigation. Water Sci Technol Water Supply. 19, 978–985 (2019). https://doi.org/10.2166/ws.2018.185

105. Bennaceur, D., Laredj, N., Maliki, M., Missoum, H., Koten, H.: Study of Soil Temperature and Soil-Atmosphere Interaction for Three Soil Types in the Oran Region. Journal of Advanced Research in Fluid Mechanics and Thermal Sciences. 127, 175–192 (2025). https://doi.org/10.37934/arfmts.127.2.175192

106. Foken, T.: Micrometeorology. Springer, Berlin, Heidelberg (2008)

107. Oke, T.R.: Boundary Layer Climates. Routledge, London (1987)

108. Brutsaert, W.: Evaporation into the Atmosphere: Theory, History, and Applications. Springer, Dordrecht (1982)

109. Hillel, D.: Environmental Soil Physics. Academic Press, San Diego, CA, USA (1998)

110. Chalhoub, M., Bernier, M., Coquet, Y., Philippe, M.: A simple heat and moisture transfer model to predict ground temperature for shallow ground heat exchangers. Renew Energy. 103, 295–307 (2017). https://doi.org/10.1016/j.renene.2016.11.027

111. Tang, F., Nowamooz, H.: Outlet temperatures of a slinky-type Horizontal Ground Heat Exchanger with the atmosphere-soil interaction. Renew Energy. 146, 705–718 (2020). https://doi.org/10.1016/j.renene.2019.07.029

112. Idso, S.B., Jackson, R.D., Reginato, R.J., Kimball, B.A., Nakayama, F.S.: The dependence of bare soil albedo on soil water content. Journal of Applied Meteorology. 14, 109–113 (1975)

113. Khokhlov, V., Lukin, V., Khokhlov, S.: Modelling full-colour images of Earth: simulation of radiation brightness field of Earth's atmosphere and underlying surface. Ann GIS. 29, 143–161 (2023). https://doi.org/10.1080/19475683.2022.2064911

114. Garnacho Saucedo, G.M., Salido Vallejo, R., Moreno Giménez, J.C.: Effects of solar radiation and an update on photoprotection. An Pediatr (Engl Ed). 92, 377.e1-377.e9 (2020). https://doi.org/10.1016/j.anpedi.2020.04.014

115. Xia, X., Zong, X.: Shortwave versus longwave direct radiative forcing by Taklimakan dust aerosols. Geophys Res Lett. 36, (2009). https://doi.org/10.1029/2009GL037237

116. Möller, F.: Long-Wave Radiation. In: Compendium of Meteorology. pp. 34–49. American Meteorological Society, Boston, MA (1951)

117. Sun-Earth_Logarithmic_Spectrums, https://upload.wikimedia.org/wikipedia/commons/9/96/Sun-Earth_Logarithmic_Spectrums_with_Accurate_Scaling.svg

118. Pereira, L.S.: Crop evapotranspiration-Guidelines for computing crop water requirements-FAO Irrigation and drainage paper 56. (1998)

119. An, N., Hemmati, S., Cui, Y.J.: Assessment of the methods for determining net radiation at different time-scales of meteorological variables. Journal of Rock Mechanics and Geotechnical Engineering. 9, 239–246 (2017).

https://doi.org/10.1016/j.jrmge.2016.10.004

120. Fan, W., Ma, W., Hu, Z., Ma, Y.: Recovery of sensible heating and its elevation amplification over and around the Tibetan Plateau since 2000s. Theor Appl Climatol. 146, 617–630 (2021). https://doi.org/10.1007/s00704-021-03737-3

121. Duan, A., Liu, S., Hu, W., Hu, D., Peng, Y.: Long-term daily dataset of surface sensible heat flux and latent heat release over the Tibetan Plateau based on routine meteorological observations. Big Earth Data. 6, 480–491 (2022). https://doi.org/10.1080/20964471.2022.2037203

122. Li, M., Babel, W., Chen, X., Zhang, L., Sun, F., Wang, B., Ma, Y., Hu, Z., Foken, T.: A 3-year dataset of sensible and latent heat fluxes from the Tibetan Plateau, derived using eddy covariance measurements. Theor Appl Climatol. 122, 457–469 (2015). https://doi.org/10.1007/s00704-014-1302-0

123. Sun, G., Hu, Z., Sun, F., Wang, J., Xie, Z., Lin, Y., Huang, F.: An analysis on the influence of spatial scales on sensible heat fluxes in the north Tibetan Plateau based on Eddy covariance and large aperture scintillometer data. Theor Appl Climatol. 129, 965–976 (2017). https://doi.org/10.1007/s00704-016-1809-7

124. Choi, W., Ooka, R., Nam, Y.: Impact of long-term operation of ground-source heat pump on subsurface thermal state in urban areas. Sustain Cities Soc. 38, 429–439 (2018). https://doi.org/10.1016/j.scs.2017.12.036

125. R.G. Allen: A Penman for all seasons. (1986)

126. Dhungel, R., Allen, R.G., Trezza, R., Robison, C.W.: Comparison of latent heat flux using aerodynamic methods and using the penman-monteith method with satellite-based surface energy balance. Remote Sens (Basel). 6, 8844–8877 (2014). https://doi.org/10.3390/rs6098844

127. Saltzman, B.: Parameterization of the Vertical Flux of Latent Heat at the Earth's Surface for Use in Statistical-Dynamical Climate Models. (1980)

128. Černý, J., Pokorný, R., Haninec, P., Bednář, P.: Leaf Area Index Estimation Using Three Distinct Methods in Pure Deciduous Stands. Journal of Visualized Experiments. (2019). https://doi.org/10.3791/59757

129. Yang, J., Xing, M., Yang, Y., Tang, H., Lyu, H., Qian, J.: A Method for Estimating Effective Leaf Area Index Using UAV 3D Point Cloud Data. In: IGARSS 2024 - 2024 IEEE International Geoscience and Remote Sensing Symposium. pp. 5264–5267. IEEE (2024)

130. Wang, Y., Fang, H.: Estimation of LAI with the LiDAR technology: A review, (2020)

131. Allen, R.G., Jensen, M.E., Wright, J.L., Burman, R. DI, Allen, R., Burman, R., Agric Eng, D.: Operational Estimates of Reference Evapotranspiration. Agron J. 81, 650–662 (1989)

132. Celia, M.A., Bouloutas, E.T., Zarba, R.L.: A General Mass-Conservative Numerical Solution for the Unsaturated Flow Equation. Water Resour Res. 26, 1483–1496 (1990)

133. Mualem, Y.: Hydraulic Conductivity of Unsaturated Porous Media' Generalized Macroscopic Approach. Water Resour Res. 14, 325–334 (1978)

134. Van Genuchten, M.T.: A Closed-form Equation for Predicting the Hydraulic Conductivity of Unsaturated Soils 1. SOIL SCI. SOC. AM. J. 44, 892–898 (1980)

135. Bennaceur, D., Laredj, N., Maliki, M., Missoum, H.: Numerical investigation of heat and moisture migration in clayey and sandy soils, exploring seasonal fluctuations. Studies in engineering and exact sciences. 5, (2024). https://doi.org/10.54021/seesv5n2-234

136. Padilla, I.Y., Yeh, T.C.J., Conklin, M.H.: The effect of water content on solute transport in unsaturated porous media. Water Resour Res. 35, 3303–3313 (1999). https://doi.org/10.1029/1999WR900171

137. hikersbay: https://hikersbay.com/climate/algeria/oran?lang=fr, https://hikersbay.com/climate/algeria/oran?lang=fr

138. Climate-data: https://fr.climate-data.org/afrique/algerie/oran/oran-540/

139. Bennaceur, D., Laredj, N., Maliki, M., Missoum, H.: Effect of Soil Salinity on Thermal Behavior of Sandy Soils Under a Sahara Climate. Science, Engineering and Technology. 5, (2025). https://doi.org/10.54327/set2025/v5.i1.212

140. Yu, C., Cheng, J.J., Jones, L.G., Wang, Y.Y., Faillace, E., Loureiro, C., Chia, Y.P.: Data collection handbook to support modeling the impacts of radioactive material in soil. , Oak Ridge, TN (1993)

141. Alnefaie, K.A., H. Nidal, A.-H.: Specific Heat and Volumetric Heat Capacity of Some Saudian Soils as affected by Moisture and Density. International Journal of Materials. 7, 42–46 (2020). https://doi.org/10.46300/91018.2020.7.8

142. Busby, J.: Determination of Thermal Properties for Horizontal Ground Collector Loops. In: Proceedings World Geothermal Congress (2015)

143. Brum, R.D.S., Vaz, J., Rocha, L.A.O., Dos Santos, E.D., Isoldi, L.A.: A new computational modeling to predict the behavior of Earth-Air Heat Exchangers. Energy Build. 64, 395–402 (2013). https://doi.org/10.1016/j.enbuild.2013.05.032

144. Vaz, J.: estudo experimental e numérico sobre o uso do solo como reservatório de energia para o aquecimento e resfriamento de ambientes edificados," universidade federal do rio grande do sul, (2011)

145. Badache, M., Eslami-Nejad, P., Ouzzane, M., Aidoun, Z., Lamarche, L.: A new modeling approach for improved ground temperature profile determination. Renew Energy. 85, 436–444 (2016). https://doi.org/10.1016/j.renene.2015.06.020